A Flexible Wing Modeling and Physical Mass Estimation System for Early Aircraft Design Stages

Dem Promotionsausschuss der

Technischen Universität Hamburg-Harburg

zur Erlangung des akademischen Grades

Doktor-Ingenieur (Dr.-Ing.)

vorgelegte Dissertation

von

Felix Dorbath

aus

Müllheim (Baden)

2014

Übersicht der Gutachter

1. Gutachter:	Prof. Dr.-Ing. Volker Gollnick
2. Gutachter:	Prof. Dr.-Ing Peter Horst
Vorsitzender des Prüfungsausschusses:	Prof. Dr.-Ing. Frank Thielecke
1. zusätzlicher Gutachter:	Prof. Dr.-Ing. Frank Thielecke
2. zusätzlicher Gutachter:	Prof. Dr.-Ing. Otto von Estorff

Tag der mündlichen Prüfung: 10.01.2014

Danksagung

Diese Arbeit entstand während meiner Zeit als wissenschaftlicher Mitarbeiter in der Abteilung Integrierter Luftfahrzeugenwurf am Institut für Lufttransportsysteme des Deutschen Zentrums für Luft- und Raumfahrt (DLR) in Hamburg. An dieser Stelle möchte ich mich bei allen bedanken, die zum Gelingen dieser Arbeit beigetragen haben.

Vielen Dank meinem Doktorvater Prof. Dr.-Ing. Volker Gollnick für die Betreuung meiner Arbeit. Herrn Prof. Dr.-Ing. Peter Horst danke ich für die Prüfung meiner Arbeit und Prof. Dr.-Ing. Frank Thielecke für die Übernahme des Vorsitzes des Promotionsausschusses. Mein besonderer Dank gilt auch Dipl.-Ing. Björn Nagel der mir die zielgerichtete Arbeit an meinem Forschungsthema ermöglichte.

Des Weiteren möchte ich mich bei allen Kollegen bedanken, die zum gelingen dieser Arbeit beigetragen haben: Daniel Böhnke, Pier Davide Ciampa, Jörg Fuchte, Jonas Jepsen, Erwin Moerland und Till Pfeiffer sowie bei allen weiteren Kollegen der Abteilung und des Institutes. Dank gilt auch Leigh Glasgow und Eva Hoogh für das Korrekturlesen der Arbeit.

Meiner Familie gilt der besondere Dank, vor allem meinen Eltern für die bedingungslose Unterstützung in allen Lebenslagen. Ein ganz besonderer Dank gilt meiner Freundin Carina für ihre große Unterstützung und den Halt den sie mir während der gesamten Promotionszeit gegeben hat.

Hamburg, im Februar 2014

Felix Dorbath

Abstract

A new developed extended physics-based wing mass estimation system is presented in this study. The tool chain is highly flexible in terms of geometries and therefore applicable for conventional and unconventional wings and novel structural layouts. Compared to state-off-the-art wing mass estimation tools, the physical modeling and therefore the physics-based mass estimation is extended beyond the wing primary structure. The developed mass estimation system includes the masses of the heaviest secondary structures, which are the flaps including flap tracks and carriages as well as the ailerons including their wing attachment. Additionally, the load-carrying structure of the engine pylon and the landing gear is included in the structural model, to take their influence on the wing structure into account.

Besides the structural analysis and sizing capability, the tool chain consist of the load calculation modules for the aerodynamic loads, the distributed fuel pressure loads, the landing gear loads and the engine thrust loads. The tool chain includes a static aeroelastic loop, which updates the aerodynamic, fuel and engine loads with respect to the wing deformation.

The structural wing model is based on finite element shell models. The load carrying structures of the flap tracks is modeled in detail. This enables the deflection of the flaps in the FE model and ensures realistic load paths in the tracks, which is mandatory for a realistic sizing.

The aerodynamic load estimation is based on the vortex-lattice theory. The vortex-lattice model includes a representation of the slats and flaps that takes the fowler motion of the flaps into account. The validation of the vortex-lattice results is performed by comparing the vortex-lattice results with RANS results and shows a high accuracy.

The estimation of the fuel loads on the wing is performed by a detailed modeling of the fuel in the wing, which allows the accurate computation of the distributed fuel pressure on the wing skins, ribs and spars. The ground forces on the landing gear and the engine thrust are considered as force vectors in the finite element model, while the engine itself is modeled as a mass point that is attached to the engine pylon.

Beside the analysis tools, the developed multi-model generator ELWIS is the core element of the mass estimation system. The generation of complex analysis models, as in the WINGmass tool chain, usually requires a huge amount of user-defined input parameters. This makes such models infeasible for preliminary aircraft design. Therefore, a knowledge-based approach is chosen for the ELWIS model generator. This means, that a large amount of engineering rules are implemented in ELWIS, wherefore the model generation process is performed automatically based on few user-friendly input parameters. The data model CPACS is chosen as input format. Therefore, the WINGmass tool chain is easy to integrate in a wider aircraft design environment, which is favorable for analysis tools of the preliminary design phase.

The mass output of the WINGmass tool chain is calibrated with respect to two reference aircraft: the Airbus A320 and the Airbus A340-200. The calibration shows very small differences between the calibrated results and the reference aircraft, which shows the high accuracy of the tool chain.

To demonstrate the required flexibility of the wing mass estimation system, exemplary studies on five different configurations are performed. The configurations include a strut braced wing, a box wing, a blended wing body, a conventional wing with a double slotted flap and a conventional wing with a multi-spar flap.

Finally, the benefits of the extended physics-based modeling and the application of the WINGmass system in an interdisciplinary aircraft design environment are shown in an aircraft design study. The objective of this study is to compute the optimal wing shape in terms of mission fuel as a function of the take-off field length. Therefore, a parameter variation on the wing and flap geometry is performed, the engine scaled correspondingly and the mission fuel evaluated.

Contents

x

List of Figures

List of Tables

Nomenclature

Roman Letters

a	Longer edge of buckling field or unloaded edge [m]
a	Non-optimum mass factor [-]
A	Cross section area [m^2]
b	Shorter edge of buckling field or loaded edge [m]
b	Span [ft]
b	Exponent to compute total mass from modeled FE mass [-]
c	Constant
d	Degree of freedom [-]
E	Young's modulus/elastic modulus [N/m^2]
E_T	Tangent modulus [N/m^2]
F	Force [N]
g	Gravity acceleration [N/m^2]
G	Shear modulus [N/m^2]
I	Second moment of inertia [m^4]
I$_w$	Wing weight index [10^{-6} lb/ft]
k	Buckling coefficient [-]
k_{flap}	Flap type factor [-]
k_{red}	Reduction factor [-]
K	Coefficient in Ramberg-Osgood equation [-]
l	Length [m]
L	Reference length [m]
m	Mass [kg]
m	Moment per unit length [Nm/m]
m	Ramber-Osgood coefficeint [-]
M	Moment [Nm]
MLM	Maximum landing mass [kg]
MRM	Maximum ramp mass [kg]
$MTOM$	Maximum take-off mass [lb], [kg]
$MZFM$	Maximum zero fuel mass [lb], [kg]
n_{ult}	Ultimate load factor [-]
$\vec{n}$	Normal vector [m]
N	Normal force [N]
N	Shape function [-]
p	Pressure [Pa]
r	Radius, distance [m]
S	Surface area [m^2]
S	Component area [ft^2]

t	Time [t]
t	Layer thickness [m]
t/c	Thickness to chord ratio [-]
t_{root}	Wing thickness at the root [ft]
TR	Taper ratio [-]
u	Displacement [m]
u	Velocity in x-direction [m/s]
v	Velocity [m/s]
v	Velocity in y-direction [m/s]
V_A	Design speed for maneuver [m/s]
V_C	Design cruise speed [m/s]
V_D	Design dive speed [m/s]
V_F	Flap design speed [m/s]
V	Volume [m³], Velocity [m/s]
w	Velocity in z-direction [m/s]
U	Potential energy [Nm]
x	Generalized coordinates
$\vec{x}$	Position vector [m]
x, y, z	x-, y-, z-coordinates [m]

Greek Letters

δ	Flap deflection angle in landing configuration [°]
Γ	Vortex strength [-]
ε	Strain [-]
θ	Theta angle [°]
ϑ	Rotation [rad]
ν	Poisson's ratio [-]
σ	Longitudinal stress [N/m²]
σ_2	Proportional limit stress [N/m²]
σ_{acutal}	Actual stress [N/m²]
σ_{crit}	Critical stress/maximum allowed stress [N/m²]
τ	Shear stress [N/m²]
$\varphi_{0.5}$	Sweep at 50% chord line [°]
φ_{EA}	Sweep at the elastic axis [°]

Tensors

$\bar{\bar{C}}$	$\bar{\bar{C}}$-matrix of the constitutive equation (CE)
$\bar{\bar{K}}$	Stiffness matrix
$\bar{\bar{L}}$	$\bar{\bar{L}}$-matrix of the kinematic equation (KE)

Subscripts

$1,2,3,\dots,6$	Position in vectors and tensors
$appr$	Approach
d	Degree of freedom
eq	Equivalent
$flap$	Flap
i	Iteration index
$wing$	Wing
x,y,z	x-, y-, z-coordinate directions
∞	Value of the parameter in an infinite distance from point of interest

Abbreviations

3D	Three Dimensional
ACSYNT	AirCraft SYNThesis
AI	Artificial Intelligence
ANSYS	ANalysis SYStem
APD	Air Passenger Duty
APDL	ANSYS Parametric Design Language
APM	Aerodynamic Performance Map
AVL	Athena Vortex Lattice
BWB	Blended Wing Body
CAD	Computer Aided Design
CE	Constitutive Equation
CEASIOM	Computerized Environment for Aircraft Synthesis and Integrated Optimization Methods
CFD	Computation Fluid Dynamics
CFRP	Carbon Fiber Reinforced Plastic
CMU	Cpacs Mass Updater
CO_2	Carbon Dioxide
CPACS	Common Parametric Aircraft Configuration Scheme
CS-25	Certification Specifications 25
DC	Deflection Case
DEE	Design and Engineering Engine
DLR	Deutsches Zentrum für Luft- und Raumfahrt e. V. (German Aerospace Center)
DOF	Degree of Freedom
ELWIS	finite ELement WIng Structure model generator
ES	Expert System
ESEL	finite Element SEcondary Loads
EU	European Union
FAME-ACSS	Fast and Advanced Mass Estimation of Aircraft Secondary Structures
FAME-W	Fast and Advanced Mass Estimation of Wings
FBS	Frame Based System
FE	Finite Element
FEM	Finite Element Method
FEMMAS	Finite Element Method for Mass Estimation
FLOPS	FLight OPtimization System
FRP	Fiber Reinfoced Plastic
FSD	Fully Stressed Design
FSMS	Fast and Simple Mission Simulator

FWD	Forward
GDL	General-purpose Declarative Language
GFEM	Global Finite Element Method
HTP	Horizontal Tail Plane
ICARE	Illustrations, Constraints, Activities, Rules and Entities
KB	Knowledge Base
KBE	Knowledge-Based Engineering
KBS	Knowledge-Based System
KE	Kinematic Equation
LISP	LISt Processing
LTH	LuftfahrtTechnisches Handbuch
MATLAB	MATrix LABoratory
MDCAD	Multi-Disciplinary Concept Assessment and Design
MDO	Multidisciplinary Design Optimization
MLG	Main Landing Gear
MMG	Multi Model Generator
MML	MOKA Modeling Language
MOKA	Methodology and software tools Oriented to Knowledge-Based Engineering Applications
MTOM	Maximum Take-Off Mass
NASA	National Aeronautics and Space Administration
NeoCASS	Next gEneratiOn Conceptual Aero-structural Sizing Suite
OME	Operating Mass Empty
P2	Post-Processing
PARA_MAM	PARAmetric simple and fast Mesh based Aircraft Modeling tool
PrADO	Preliminary Aircraft Design and Optimization Program
PESTsewi	Preliminary mass ESTimation of SEcondary WIng structures
RANS	Reynolds-Averaged Navier-Stokes
RCE	Remote Control Environment
RBS	Rule Based Systems
RTT	Reynolds Transport Theorem
S_BOT	Sizing Robot
SimSAC	Simulating Aircraft Stability and Control Characteristics for Use in Conceptual Design
TRIM_VL	TRIMming with Vortex-Lattice
TsAGI	Central Aerohydrodynamic Institute
TU	Technical University/Technische Universität
TWdat	TriebWerks DATenbasis
uID	Unique IDentifier
UK	United Kingdom
USAF	United States Air Force

VAMP   Virtual Aircraft Multidisciplinary analysis and design Processes

VCP   Vehicle Sketch Pad
VTP   Vertical Tail Plane
XML   Extensible Markup Language

Chapter 1

INTRODUCTION

The international aviation industry is facing significant economic and environmental challenges. On the economics side, the aviation industry needs to manage considerable increases in fuel prices [1] as well as diverse new taxes and duties, like the emission trading scheme of the European Union [2], the German air passenger taxes [3, 4], the Air Passenger Duty (APD) in the UK [5] or the different airport improvement fees, such as the passenger facility charge (PFC) in the United States [6].

On the environmental side, the aviation industry is responsible for a growing proportion of the worldwide CO_2 emissions. The public awareness of the aviation industry's CO_2 emissions is growing even faster, which has led to strong pressure from the public to reduce aircraft emissions. Additionally, the growing public awareness on aircraft noise has led to increasing pressure on the aviation industry, as shown for example by the protests against new runways in Frankfurt and Munich [7].

These challenges have to be addressed by all participants of the air transportation system. One group of these participants are the aircraft manufacturers, who are expected to develop new aircraft meeting the increased economic and environmental demands. In the design offices of the manufacturers and research institutions, a large collection of different suggestions exist, how future aircraft could be designed. The different concepts and technologies range from completely new aircraft configurations, like blended wing body (BWB) [8, 9, 10] or box wing aircraft [11, 12, 13], to the implementation of new technologies in more conventional aircraft designs. Examples are advanced materials, like CFRP, laminar flow wings [14, 15] or configurations employing powered lift concepts for quieter takeoff and landing procedures [16, 17]. Additionally, more detailed technologies, such as integrated CFRP multi-spar torsion boxes [18] must be considered for new aircraft generations.

Most of the aforementioned concepts require new wing designs, including new designs of the high-lift system. In the majority of studies on preliminary wing design, models are used which employ physics-based methods, making use of the beam or shell theory for primary structural wing components. Secondary structures are captured via empirical correlations (see chapter 1.2).

However, most of the proposed novel concepts exceed the knowledge base of the empirical methods as materials, construction principals, wing geometry or loads are fundamentally changed compared to the knowledge base. Therefore, the accuracy of these methods in terms of absolute values and sensitivities has to be seen critical, if they should be used for the proposed novel concepts. Additionally, the separate and independent models for primary and secondary wing structures do not necessarily lead the optimizer to the optimal design as the interaction between the wing primary structure and its subcomponents is not considered.

With the developed multidisciplinary physics-based wing mass estimation process, a contribution towards the development of integrated design tools, meeting the challenges of the future, is presented.

1.1 Wing Mass Estimation as Part of Preliminary Aircraft Design

During the development of a new aircraft, the development process is split in several phases, starting with the product idea and ending with

Fig. 1.1: Innovative wing concepts requiring integrated physics-based design capabilities.

the entry into service of the aircraft. One of the early phases is the preliminary aircraft design, in which the new configuration is optimized as a whole in order to minimize fuel burn and costs. During this design phase, various methods with different level of fidelity are used to predict the properties of the aircraft.

Beside the efficiency of the engine and the aerodynamic properties of the aircraft, the aircraft mass is one of the key performance indicators. Therefore, the estimation of the aircraft mass is one of the most important challenges during the early design stages. With a share of 35-50% of the structural mass of modern passenger aircraft [19], the wing is the heaviest structural component. Therefore a special focus has to lay on the accurate mass estimation of the wing.

1.1.1 The Aircraft Design Process

The overall aircraft design process is described by various authors in the main aircraft design text books [20, 21]. Within these text books, the aircraft design is divided in three major phases:

the conceptual design phase, the preliminary design phase and the detailed design phase (see Fig. 1.2). The Airbus milestone model [22, 23] is similar, but more detailed. In particular, the Airbus model not only considers the engineering part of the aircraft design, but also focuses on economic, management and manufacturing aspects of the project. Note, that the aircraft design is never a straight forward process, rather than a highly iterative process inside and between the different phases of aircraft design.

During the conceptual design phase a very wide design space is considered for the new aircraft design in order to find the optimal design meeting the requirements. During this phase the configuration of the aircraft is defined, e.g. wing and tail configurations. To make the complexity manageable, typically simpler methods and tools (e.g. analytical methods) are used. These methods require only a few input parameters and are therefore well suited for this design phase.
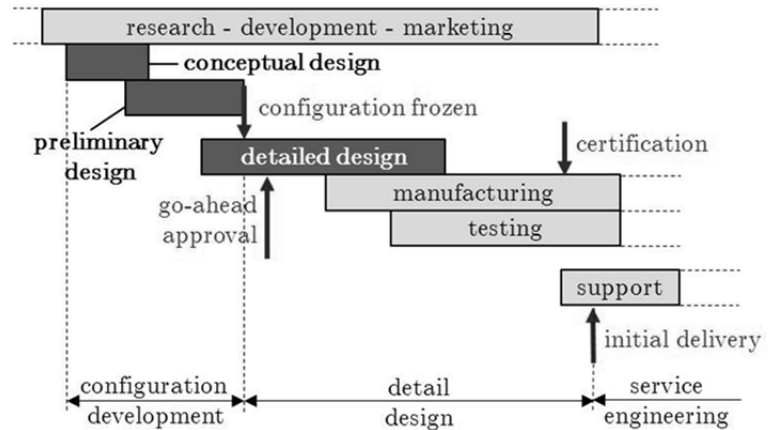
Fig. 1.2: Development phases of the conventional aircraft design process (based on [21]).

During the preliminary design phase the conceptual design from the previous phase is analyzed more in detail. The specialists from the various disciplines, such as structures, landing gear and aerodynamics, perform analyses and optimizations for their portion of the new aircraft. During this phase, the aircraft concept remains unchanged, but on a more detailed level the aircraft is modified. For example the exact wing planform or the spanwise thickness distribution of the wing is optimized. In the preliminary design phase, physics-based methods and tools with analytical extensions are used (see chapter 1.1.2).

The detailed design phase is the last phase of the aircraft design process. During this phase all individual parts of the aircraft are designed and the production is prepared, while the outer geometry and the structural layout are not changed. During this phase the most detailed methods are used, such as non-linear finite element analysis of structural parts and assemblies.

The above described design approach has been sufficient for aircraft design over the last decades. However, the question arises, if this approach is nowadays still sufficient enough. La Rocca [25] described several weaknesses of the conventional design approach:

- The conceptual design phase is far too short, if one considers the enormous impact of this phase on the development program. 70% of lifecycle costs are committed during this phase, while only 1% of the total costs are incurred (see Fig. 1.3).
- The baseline concept after the conceptual design phase is only modified in detail during the later phases. But this concept is mostly based on extremely simplified methods and engineers experience. These analytical methods become inadequate as soon as new requirements or technologies are to be considered. Additionally, the number of new

aircraft programs is declining, while aircraft become much more complex. Therefore, the engineers experience is less available as the main guide for design decisions.

- The conventional design approach leads to the 'knowledge paradox'. This means, that the designers increase their knowledge about the design, but at the same time lose their design freedom, which may lead to suboptimal designs.

To overcome these weaknesses, considerable research efforts have been undertaken during the last years. One focus of this research is to increase the product knowledge in the early design phases, while slowing down the decreasing design freedom in later design phases. A second focus lies on the coupling of different disciplines to enable the designers to find the real optimal solution, which might differ from the sum of disciplinary optima.

The increasing computational power of today's computers provides the basis for the development of numerous new aircraft design tools. The goal of these tools is to support the designer, as much as possible, in designing the optimal aircraft. Therefore, these tools provide capabilities such as multidisciplinary analysis and (partly-) automated model generation that are often based on knowledge-based engineering techniques.
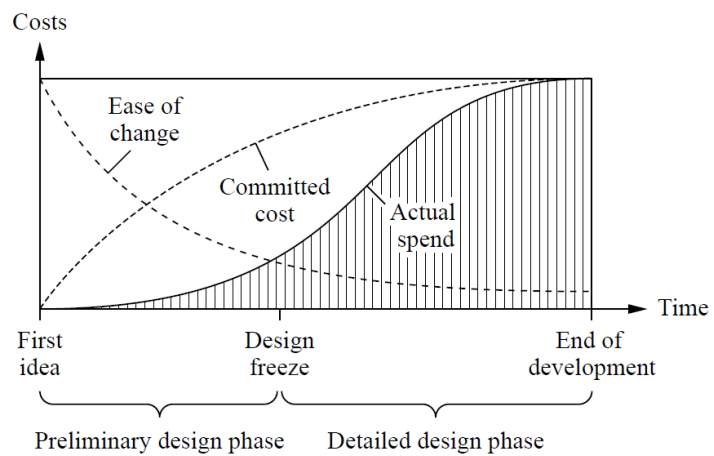
Fig. 1.3: Costs during aircraft development [24].

1.1.2 Classification of Methods for Wing Mass Estimation

In principal, analysis methods for wing mass estimation (as well as for all other disciplines) can be classified as either empirical or physics-based.

Empirical methods are derived from statistical analysis of existing aircraft. For wing mass estimation, the wing mass is e.g. correlated with the wing area and the maximum take-off mass (MTOM) of the aircraft. These methods can be applied for the total wing mass, but also for smaller subsystems such as the flap body, spoilers or fairings. The advantage of these analytical methods is the high computational speed, as these methods offer a direct correlation between the input parameters and the mass of the component. Additionally, these methods require only few input parameters, wherefore they can be used easily. The disadvantage of these methods is that they are only valid for aircraft which are similar to the aircraft of the underlying database. If new technologies or new requirements need to be considered such methods lose their validity.

Physics-based methods are derived from physical relations. Methods for wing mass estimation are mostly based on beam or shell models. These methods can be used for a wider design space as they are not based on a statistical database. Therefore, also unconventional configurations can be analyzed. Compared to empirical methods, physics-based methods have higher computa-

tional cost and require more input parameters, e.g. describing the detailed wing geometry and the wing loading.

Several current wing mass estimation tools are not based only on either empirical or physics-based methods, but on a combination of both methods. An often seen approach is to determine the mass of the wing box with physics-based methods, while the wing secondary structures, such as flaps and slats, are captured via analytical correlations. With this approach the flexibility of the physics-based methods is used for the part of the wing that accounts for most of the mass and which is relatively simple to model while the parts of the wing that are lighter and more complex to model are handled via empirical methods.

1.1.3 Multidisciplinary Wing Mass Estimation Process

A physics-based wing mass estimation cannot be performed as a mono-disciplinary analysis, as the interaction with other disciplines is too strong. The wing structure needs to withstand all static and dynamic loads that act on the wing. These loads are aerodynamic loads, loads resulting from the fuel mass, the wing mounted engines and the wing mounted landing gear as well as inertia loads. In a wing mass estimation process the response of the wing structure on these loads has to be analyzed and the structural components have to be dimensioned accordingly to ensure a safe

Fig. 1.4: Characteristics of an autonomous physics-based wing mass estimation process [24].

aircraft operation. Finally, the wing mass can be derived from the wing geometry, the results from the wing sizing and the material properties.

A typical wing mass estimation process needs the aircraft geometry, a definition of the load cases and parameters describing the sizing criteria as input. The output is at least the structural mass. In addition, the results from the sizing (e.g. skin thickness), wing stiffness properties and the wing deformation under the applied loads are often obtained.

Hürlimann [24] defines six characteristics that are necessary for an autonomous physics-based wing mass estimation process (see Fig. 1.4):

- *Multi-model generation capability:* Automatic generation of all models that are used for the analysis. These models are the structural model as well as the models for the load generation. To ensure the consistency between the models, all models should be based on the same geometrical description and this description should be interpreted by the same model generator.

- *Load generation capability:* Computation of all loads that act on the wing. These loads are aerodynamic loads, loads from the fuel that is stored in the wing, inertia loads, loads from the engine pylon and loads from the landing gear.
- *Load application capability:* All loads have to be applied on the wing structure in an adequate way. This function is crucial, as different ways of load applications can influence the result of the structural analysis.
- *Structural analysis capability:* The structural analysis is mostly either performed with beam or shell models, depending on the level of accuracy of the wing mass estimation process. Results of the structural analysis are the deformation of the wing as well as the stress and strain distribution, which is the input for the structural sizing.
- *Structural sizing capability:* The structural sizing algorithm determines the material thicknesses with respect to the stresses and/or strains of all load cases according to one or more sizing criteria. The sizing algorithm should include methods for isotropic (e.g. metals) and anisotropic (e.g. CFRP) materials.
- *Aeroelastic feedback capability:* The wing of an aircraft deforms due to the applied loads. This deformation results in considerable changes to the aerodynamic loads, wherefore the loads need to be recomputed and the wing dimensioning has to be repeated. Therefore, a wing mass estimation process is always an iterative process.

1.2   State-of-the-Art in Wing Mass Estimation

In the following chapter the state-of-the-art in wing mass estimation during preliminary aircraft design is presented.

Due to the high number of methods and tools for wing mass estimation, it is impossible to mention all of the available methods within this chapter. Therefore, the focus is placed on the most important methods to provide an overview of past and current developments.

In most wing mass estimation methods and tools, the mass estimation of primary and secondary structures is separated. The main load-carrying structures, such as skins, ribs and spars belong to the primary structures, while the other wing components, such as flaps, slats, winglets and flap tracks belong to secondary structures. Therefore, this chapter is divided in subchapters for primary and secondary masses, wherefore some methods and tools are mention in more than one chapter. Additionally, for each major physics-based or non-physics-based method one subchapter is introduced.

1.2.1   Empirical Methods for Primary Structures and Total Wings

Empirical methods for the total wing mass have been used as first guess estimations for more than half a century. Early in the 1950's, several empirical methods containing one or more parameters were already available [26, 27].

During the following decades numerous empirical methods were developed by most aircraft manufacturers, research institutions and universities. These methods can roughly be split in two groups: The first group of methods are based on pure statistical analysis that correlate the total wing weight with parameters such as sweep, wing area, thickness to chord ratio or maximum takeoff weight. A good example of these methods is the wing mass estimation formula of Torenbeek [28]:

$$
m_{wing} = 0.0017 \cdot MZFM \left(\frac{b_{wing}}{\cos(\varphi_{0.5})} \right)^{0.75} \left[1 + \left(\frac{6.3 \cdot \cos(\varphi_{0.5})}{b_{wing}} \right)^{0.5} \right] \cdot
$$
$$
\cdot n_{ult}^{0.55} \cdot \left(\frac{b_{wing} \cdot S_{wing}}{t_{root} \cdot MZFM \cdot \cos(\varphi_{0.5})} \right)^{0.3}
$$

(1.1)

with m_{wing} being the wing mass, $MZFM$ the maximum zero fuel mass, b_{wing} the wing span, $\varphi_{0.5}$ the sweep at the 50% line, n_{ult} the ultimate load factor and S_{wing} the wing area.

Similar methods utilizing differing amounts of parameters have been developed, e.g. the USAF [28], General Dynamics [28], Howe [29], Jenkinson [30] and Raymer [20]. The latest version of the equation from Sellner [31] was presented in 2002 and is based on an impressive database that contains characteristics of more than 100 different aircraft, ranging from World War II to current aircraft. Sellner's equation is highly flexible and can be used for a wide range of different wing shapes and aircraft types. However, the flexibility and the large number of aircraft lead to a relatively low accuracy of a root mean square of 14.3%.

The second group of methods is based on some basic physical relations for the correlation of the primary wing mass with the wing geometry, material properties and loads. These methods are, generally, more flexible. A good example of these formulas is the formula developed by Shevell [32], who computes the wing mass with respect to two factors, the wing area S_{wing} and a so called wing weight index I_w. The wing weight index includes the wing geometry and can (almost) be derived if one considers the wing as an equivalent straight beam:

$$
I_w = \frac{n_{ult} \cdot b_{wing}^3 \cdot \sqrt{MTOM \cdot MZFM}(1 + 2 \cdot TR)}{(t/c)_{eq} \cdot \cos^2(\varphi_{EA}) S_{wing}^2 (1 + TR)} \cdot
$$

(1.2)

with $MTOM$ being the maximum take-off mass, TR being the taper ratio, $(t/c)_{eq}$ the equivalent thickness to chord ratio and φ_{EA} the sweep of the elastic axis.

Other equations that are based on basic physical relations have been developed by Howe [29] and Torenbeek [21]. The NASA development FLOPS (Flight Optimization System) [33] also utilizes these kinds of equations for the wing mass estimation [34]. Perhaps the longest formula has been developed by Udin [35], whose formula can barely fit on one journal page. The complexity of his formal results in a very high accuracy, with a root mean square error of 5.9% for his 13 reference transport aircraft. However, his formula is only applicable for wings having maximal one kink. Additionally his formula includes seven manufacturing coefficients, for which the aircraft designer has to choose a value from a given bandwidth, which requires a high degree of expert knowledge.

In Germany, the "Luftfahrtechnisches Handbuch" (LTH) should be mentioned, which is produced by a consortium of several industrial partners and research institutions. The LTH publishes mass estimation methods for all aircraft components over the last decades. The latest wing mass estimation formula was published in 2013 and is based on more than 50 aircraft, including most state-of-the-art large civil jet transport aircraft [36]. This relatively simple formula provides a standard deviation of 6.2%.

Comparisons of the different methods show, that none of the methods are accurately applicable for a wide range of aircraft configurations. All methods strongly depend on their underlying database. As the structural weights of most aircraft are not published, these databases often include only a relatively low number of aircraft. Therefore, one needs to consider the origin of the methods and the underlying database before one should make use of these methods.

Most of the empirical methods are based only on few parameters and simplified geometries. This makes the methods simple to use, but limits the range of different geometries that can be computed. If these methods are to be used for an optimization of the wing, the optimization is limited to these parameters. Additionally, the sensitivity behavior of these methods is often worse, when compared to physics-based methods.

1.2.2 Primary Wing Structures using Beam Theory

In principle, methods that are based on the beam theory attempt to determine the locally required amount of wing box material within the wing's cross sections and subsequently to integrate these cross sections over the wing span. The usage of this method for wing mass estimation started in the early 1950's as Ripley [37] introduced his new method. This method was developed for wings of spar-type construction, in which the bending strength is provided by the spars, while the torsional stiffness is provided by the wing box. Ripley's method already included several additional masses for undercarriage attachment, engine attachment, different kind of fuel tanks, joints, etc.

This method was further developed by Burt [38] in 1955 for the application of wings of box construction, in which both bending strength and torsional stiffness are provided by a single structural box, as is the case in all of today's commercial airliners. His method is applicable for wings of skin-stringer-rib, multi-spar, honeycomb sandwich and corrugated core sandwich construction. In addition to the mass estimation due to bending loads, his method already includes the mass estimation due to torsional loads, such as subsonic and transonic flutter, aileron reversal and wing divergence at all speeds.

In parallel, Shanley [39] developed methods for mass estimation and structural design for a wide range of aircraft structures. His approach was primary based on optimal design principles and buckling/stability analysis.

The method of Ripley and Burt was further developed by Schneider [40], who expanded the loads assumptions that were used for the computation. In his calculation procedure, he used a wide range of different types of load cases, such as gust, maneuvers, landing, taxiing, flap and

aileron load cases. Additional standardized loading spectra are introduced, to take the effects of fatigue for the required service life of the aircraft into account.

In the 1990's Torenbeek [41] and Macci [42] developed two approaches for wing mass estimation that are based on simplified beam theory. In addition several practical consideration and empirical corrections led to methods which are relatively simple to handle, but still deliver good results.

Fig. 1.5: PrADO aircraft model [44].

Due to the development in computing power during the last decades, a large number of wing mass estimation tools that are based on beam theory have been developed. PrADO (Preliminary Aircraft Design and Optimisation Program) (see Fig. 1.5) is an overall aircraft design tool that was developed by Heinze [43] at the TU Braunschweig in the early 1990's. Since then, PrADO has been continuously developed and refined. The wing mass estimation process can base on a beam model, if specified by the user. The sizing of the beam model is based on fully stressed design principles and handbook methods for buckling. The beam-based wing mass estimation in PrADO is still used in the actual research activities, such as [44] where a more climate friendly air transportation system is investigated.

One of the most advanced beam-based wing mass estimation tools is the Airbus in-house development FAME-W (Fast and Advanced Mass Estimation of Wings) [45, 46, 47]. FAME-W fulfills all of the characteristics of an autonomous physics-based wing mass estimation process including the capability for aeroelastic analysis (see Fig. 1.6). In contrast to other tools, FAME-W considers several physical effects (such as buckling and warping) as well as non-optimum masses (e.g. mass due to cut-outs, joints etc.). FAME-W is continuously refined with new features being added, such as the capability for CFRP sizing [48]. FAME-W is regularly revalidated against weight book data of existing aircraft configurations in order to assess and improve the accuracy of the results [49].

In 1996, Ardema et al. [50] published a method for wing mass estimation, which is implemented in the AirCraft SYNThesis (ACSYNT) computer program. This method is based on a simplified geometry model, an assumed load distribution and a simplified beam model. In their report, the method is described in detail step by step, which makes reprograming of the method easy. Therefore, refined and extended versions of this method are widely used. A good example

is the CEASIOM framework which was developed within the EU project SimSAC [51]. Within this framework the NeoCASS [52, 53] module performs the aero-structural sizing. Before the sizing with a dynamic aeroelastic non-linear finite element (FE) beam model is performed, a modified Ardema method is used to generate the starting solution. The finite element formulation of beam models has several advantages, for example that the model can also be used for statically over-determined wings (e.g. box wings) and dynamic aeroelastic computations are much easier to implement. The disadvantage of the CEASIOM framework is that the wing geometry is limited to two straight segments, which reduces the design space for aircraft optimization.
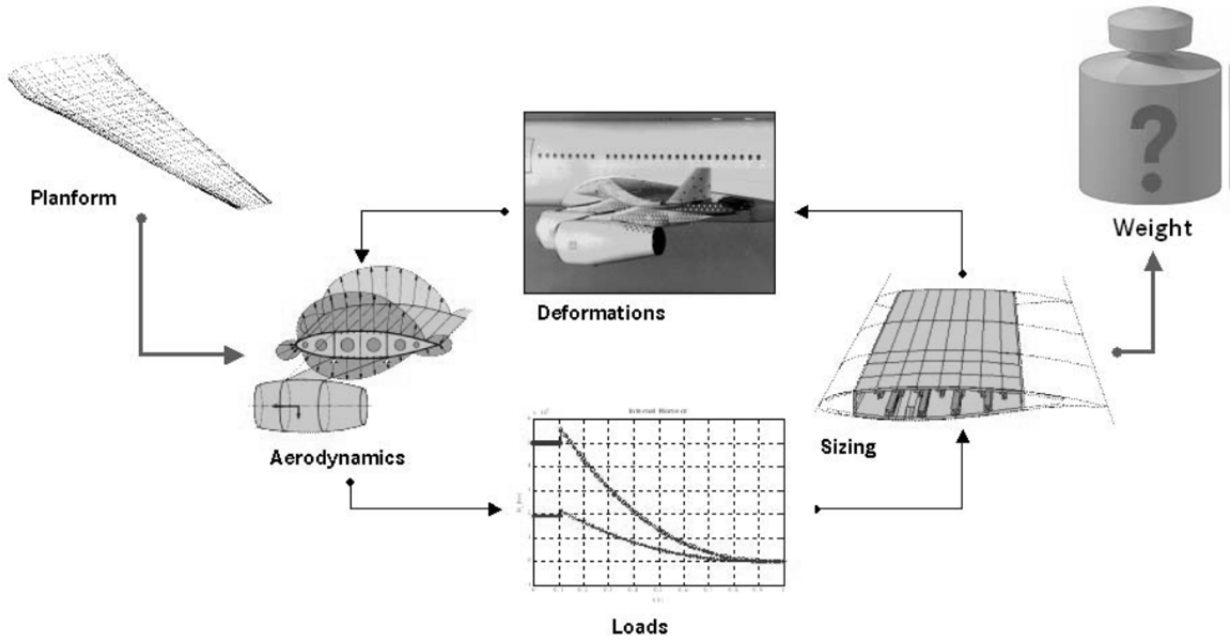
Fig. 1.6: Iterative multi-disciplinary calculation process for mass prediction in FAME-W [47].

Bindolino [54] developed a multilevel structural optimization tool for the preliminary weight estimation of wing boxes based on beam theory. This tool uses a finite element formulation of the beam, which enables the tool to be applicable for statically indeterminate configurations, such as box wings. It includes a static aeroelastic loop for the load estimation and sizes the wing with respect to stresses, aileron effectiveness, stiffener and panel instabilities and flutter constraints. It is planned to include a finite element shell model at the high-level end of the multilevel structural optimization environment.

Beam-based methods and tools can deliver very accurate results for higher aspect ratio wings, if they are adjusted on real aircraft as is shown in [49, 50 and 55]. In addition, the sensitivity behavior of the primary wing mass is quite good for several global wing parameters [56]. However er beam models produce worse results when local effects need to be taken into account, such as kinks of the structural box [56]. This needs to be considered at all swept wings as they have a kink of the wing box at the wing root. Additionally, local load introductions are not well captured by beam models, due to the cross-section based approach.

1.2.3 Primary Wing Structures using Shell Theory

Methods that are based on finite element shell elements are developed to solve several of the issues existing in beam-based methods. As for beam-based methods, a large number of shell-based tools have been developed by different institutions. The most important methods and tools are highlighted in the following paragraphs. These tools range from very simple approaches, where results can be produced within minutes, to highly complex methods.

In the latest version of the NASA conceptual design tool Vehicle Sketch Pad (VSP), shell based wing mass estimation is included [57]. In VSP the user can create the wing interactively with a graphical user interface. The structural model includes skin, ribs and spars. Compared to other tools, the chosen approach is very simple, e.g. the whole wing consists of only one straight segment, only one material can be defined (incl. leading and trailing edges), only one load case can be analyzed, no aeroelastic coupling is included and the final material thicknesses are directly derived from the initial solution (no iterations). However, the advantage is that results can be produced within minutes.
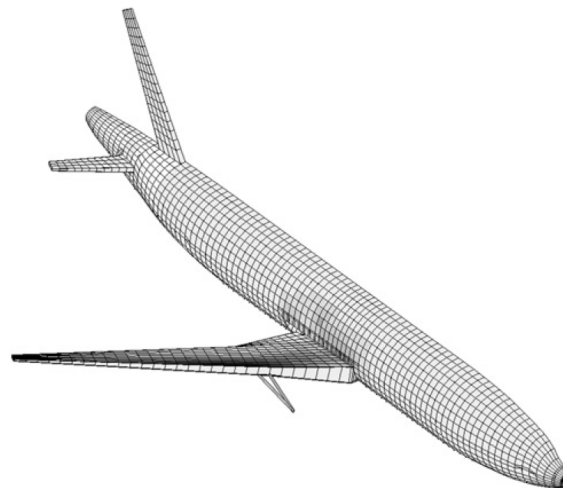
Fig. 1.7: PrADO finite element shell model [59].

Österheld [58] developed a FEM (Finite Element Method) module for mass estimation of primary structural components for the preliminary aircraft design tool PrADO (see Fig. 1.7). In addition to the wing, the model includes the fuselage, the horizontal tail and the vertical tail. The mass estimation process is integrated in the PrADO framework and includes a static aeroelastic loop. The structural sizing is based on fully stressed design (FSD) principals. To derive the total mass of the primary structure, analytical methods are implemented, which correct the mass of the pure FEM computation, which leads to an accurate method for wing mass estimation. The FEM module was further develped by Rieke [60, 61], who extended the module for fiber reinfoced plastic (FRP) structures and buckling criteria.

Nagel et al. [62] developed a method which focusses on the multidisciplinary analysis of aircraft wings. In Nagel's method, the structural model is directly derived from the CFD mesh from a previous aerodynamic analysis. In the input file for his model generator PARA_MAM (PARAmetric simple and fast Mesh based Aircraft Modeling tool) only the positions of the ribs and spars as well as the material properties need to be specified. In PARA_MAM the wing's internal structure is defined in one step for the whole wing rather than separately for each wing segment, as is the case in several other model generators. With PARA_MAM complex internal structures can be realized. However, the tool input is quite complex. This is due to the fact, that the input must be written as MATLAB source code and all real and virtual ribs and spars are required to be explicitly defined by the user in large matrices. Together with the sizing routine S_BOT (Sizing Robot) and CFD calculations, a static aeroelastic loop can be implemented. The

sizing in S_BOT is based on fully stressed design (FSD) principles for metal and composite materials.

More than 10 years ago, the Delft University of Technology started to develop a distributed computational design system concept, called the Design and Engineering Engine (DEE) [63, 64 and 65]. The DEE consists of a wide collection of design and analysis tools. The core of the DEE is the Multi-Model Generator (MMG), which creates the input files for all of the DEE's analysis tools. The MMG is based on knowledge-based engineering principles.
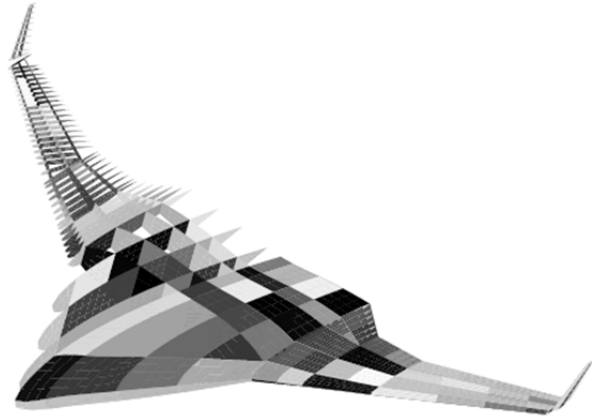
Fig. 1.8: Finite element shell model, created by the MMG [63].

The MMG can generate a wide range of different wing configurations, such as wings, tails and blended wing bodies (see Fig. 1.8). This is realized by using the concept of wing trunks. A wing trunk represents one very simple segment of the wing, with one root and one tip airfoil. The wing structure is defined within one wing trunk and only simple structural layouts can be defined within a single wing trunk. By combining any number of wing trunks, complex wings and structures can be realized. Due to the knowledge-based approach, the MMG automatically generates finite element models of wings having structured finite element (FE) meshes. Within the DEE, the finite element model is coupled with aerodynamic loads models. The sizing is based on the stress distribution of one single load case. Additionally, flutter constraints can be applied.

At Airbus, large research effort was undertaken to develop an FEM-based mass estimation tool [24, 66 - 72]. The work began under the project name FEMMAS (Finite Element Method for Mass Estimation) in cooperation with several research institutions and the development is still ongoing. Within this work, a multidisciplinary tool chain for mass estimation of primary structural components is developed. The core of the chain is a parametric-associative CAD surface model, where the geometry is defined (see Fig. 1.9). This model is partly generated automatically, by using knowledge-based features that are implemented in Catia V5. The sizing of the model is done with respect to several different criteria, such as FSD, buckling and manufacturing constraints. The last point is particularly important for CFRP wings, where the additional mass due to manufacturing constrains plays an increasing role. The aerodynamic load estimation is based on potential flow theory while the fuel load is estimated via a detailed representation in Catia. For better estimation of the loads, a static aeroelastic loop is implemented.

A highly advanced structural analysis and sizing tool is the program LAGRANGE, developped by Cassidian [73]. LAGRAGNE is a tool for multidisciplinary structural design optimization and was developped since 1984. LAGRANGE can be used for different fidelity models, ranging from the total aircraft, to assamblies or parts. If the total aircraft or the wing structure is analyzed, only the wing primary structure is included in the structural model. LAGRANGE includes static and dynamic aeroelasticity, flutter analysis, various sizing criteria

for metal and composite materials, including manufacturing constraints, blucking analysis, displacement constraints and several strength failure critera. LAGRANGE has been used in several aircraft projcts, including the Eurofighter Typhoon, the Airbus A350 and the Talarion.

Beside the methods and tools described above, several commercial software tools exist, that can be used for wing mass estimation. An example is the MDCAD (Multi-Disciplinary Concept Assessment and Design) framework developed by QinetiQ. This framework is similar to the Airbus FEMMAS approach, but simpler in several aspects [71, 74]. The HyperSizer from the Collier Research Corporation [75] and OptiStruct from Altair Engineering [76] are examples for highly developed structural sizing and optimization tools that can be used for all kinds of structures. Both tools can be applied for wing structural design

Fig. 1.9: Virtual engineering model, developed within the FEMMAS project [67].

and wing mass estimation purposes. However, these tools are usually not used during conceptual or preliminary design, but in later development phases.

In summary, shell based mass estimation methods can be seen as state-of-the-art in preliminary wing design. However, the different methods differ strongly in their approach. All of the discussed scientific approaches are based on basic FSD principles and only PrADO considers buckling criteria. The FEMMAS project from Airbus includes a higher level sizing. However the FEMMAS project is based on CAD-Software, which has some disadvantages that are discussed in chapter 2.2.2.

1.2.4 Secondary Wing Structures using Empirical Methods

The majority of empirical methods for secondary structural components are based on area weights. This area weight is either constant or depends on parameters representing the loads. Such parameters might be the design diving speed, the maximum take-off weight or the flap loads.
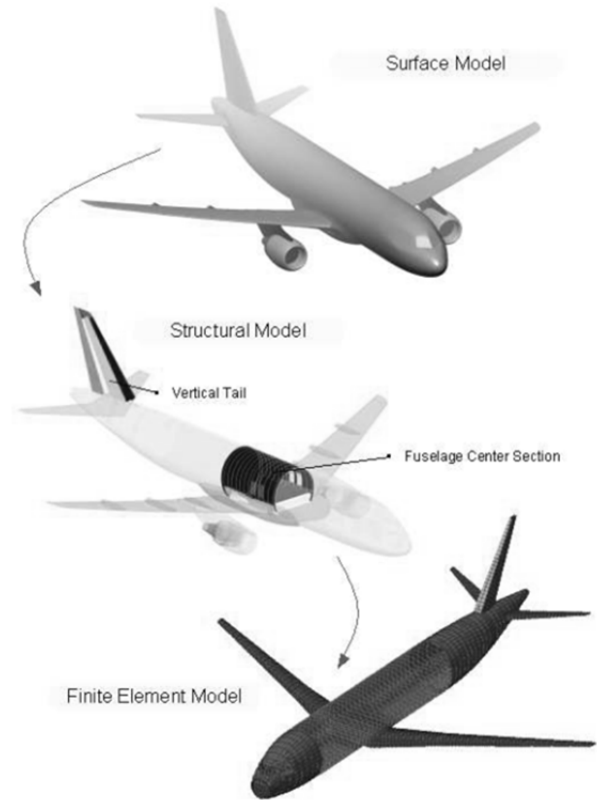
Fig. 1.10: Flap mass estimation according to Ripley in 1951 [37].

One of the first methods for empirical mass estimation of secondary structures was published by Ripley [37] in 1951. Using his graphics based method (see Fig. 1.10), it is possible to estimate the flap and aileron mass with respect to the surface area and the design diving speed. A similar approach was chosen by Burt [38] in 1955 for the total leading and trailing edge masses. Sanders [77] used the same approach in 1969, but with separate formulae for different types of leading and trailing edge flaps based on a wide range of aircraft – ranging from the Messerschmitt 109 to the Boeing 707.

Shanley [39] used constant area weights for the leading edge, flaps and ailerons. The same approach was used by Rudolph [78]. He published area masses of 6 different flap types, in 1996, which are split in 4 components: flap body, supports, actuation and fairings.

Torenbeek [21, 41] developed equations for many different kinds of fixed and movable leading and trailing edge devices, including the support structure. His method is also mainly based on area weights that depend on the maximum take-off mass (MTOM). A similar approach was chosen by Schneider [40]. The method of Torenbeek was developed further by Jenkinson [30], who developed a flap mass estimation formula that depends on more detailed parameters and covers different types of flaps:

$$m_{flap} = 2.706 \cdot k_{flap} \cdot S_{flap} \cdot \left(b_{flap} \cdot S_{flap}\right)^{0.1875} \cdot \left[\frac{0.002 \cdot v_{appr}^2 \cdot \sin(\delta)}{(t/c)_{flap}}\right]^{0.75} \qquad (1.3)$$

with m_{flap} being the flap mass, k_{flap} the flap type factor ($k_{flap} = 1 \ldots 1.3$), S_{flap} the flap area, b_{flap} the flap span, v_{appr} the approach speed, δ the flap deflection angle in landing configuration and $(t/c)_{flap}$ the flap thickness to chord ratio.

A formula of similar complexity was developed by Patterson [79] and led to good results for a wide range of civil and military transport aircraft. The method of Macci [42] computes the secondary wing masses with one formula that can be applied for different types of high-lift devices. The formula is based on the area of the devices, design diving speed, MTOM and the type of device.

The NASA tool FLOPS [33] uses an MTOM based area weight for all secondary structures including the wing ribs and spars [34]. Here, the underlying assumption is that the mass of shear material (ribs and spars) directly depends on the control surfaces [34]. FLOPS was used for ex-

ample by Gur et. al. [80] to compute the wing secondary masses of strut braced wings. The overall aircraft design tool PrADO [43] of TU Braunschweig employs one user-defined area weight for the leading edge and one for the trailing edge.

In contrast to the area-based methods, Howe [29] developed a method, in which all secondary structures are expressed as a share of the MTOM. If the detailed wing layout is unknown in early design stages this method can be very useful for the designer.

Another simpler approach is to derive the total wing mass from the primary structural masses. For example Kessler et al. [81] multiplies the wing box weight by 1.5 to estimate the total wing weight, while Perez et al. [82, 83] multiplies the weight of the load-carrying structure by 1.85. A similar approach was chosen by Ardema et al. [50], who multiplied the primary structure mass with 1.7372. As an alternative, Ardema made use of an exponential function instead of the constant factor, as also done by Elham [55].

The methods which are implemented in the Airbus in-house development FAME-ACSS, are primary based on area weights, but also take into account the flap loads [84]. The underlying database consists of most of the Airbus aircraft. In total 22 different formulas have been developed for the different components that belong to the wing secondary structures (flaps bodies, flap tracks, slats, spoilers etc.). FAME-ACSS was also used by Hürlimann [71] in combination with higher fidelity analysis of the wing primary structure.

The German mass analysis working group of the "Luftfahrttechnisches Handbuch" (LTH) recently developed a formula for all secondary wing masses of civil transport aircraft [85]. The secondary structures are split in 18 different categories, allowing a detailed analysis of the wing secondary structures. The methods in the LTH are primary based on the area of the component, but also other parameters, which are available during preliminary design. The final validation of the LTH formulas shows a high degree of accuracy for state-of-the-art aircraft.

1.2.5 Secondary Wing Structures using Physics-Based Models

In 1969, Sanders [77] developed a method for flap mass estimation based on beam theory. Sanders simplified the flap to a straight non-tapered beam, which is a valid assumption for most flap configurations. The beam is loaded by a uniformly distributed load over the flap. Using this load and the material limits, the required amount of bending material is computed. All other loads (e.g. torsion) are neglected, but a statistical factor, covering the ratio of the bending mass to the total mass, is introduced to compute the total weight.

Van der Laan [86, 87] extended the Multi Model Generator (MMG) of the TU Delft, in a way that finite element models of trailing edge devices can be created (see Fig. 1.11). The model includes the body of the device and the hinge, where the model is clamped. However, more complex track types cannot be created. Van der Laan's application case is a small general aviation aircraft. Therefore, the aerodynamic pressure load is a generic pressure distribution computed according to JAR 23 requirements and is not based on a aerodynamic analysis. The developed process includes the model generation, loads computation and the structural analysis in the fi-
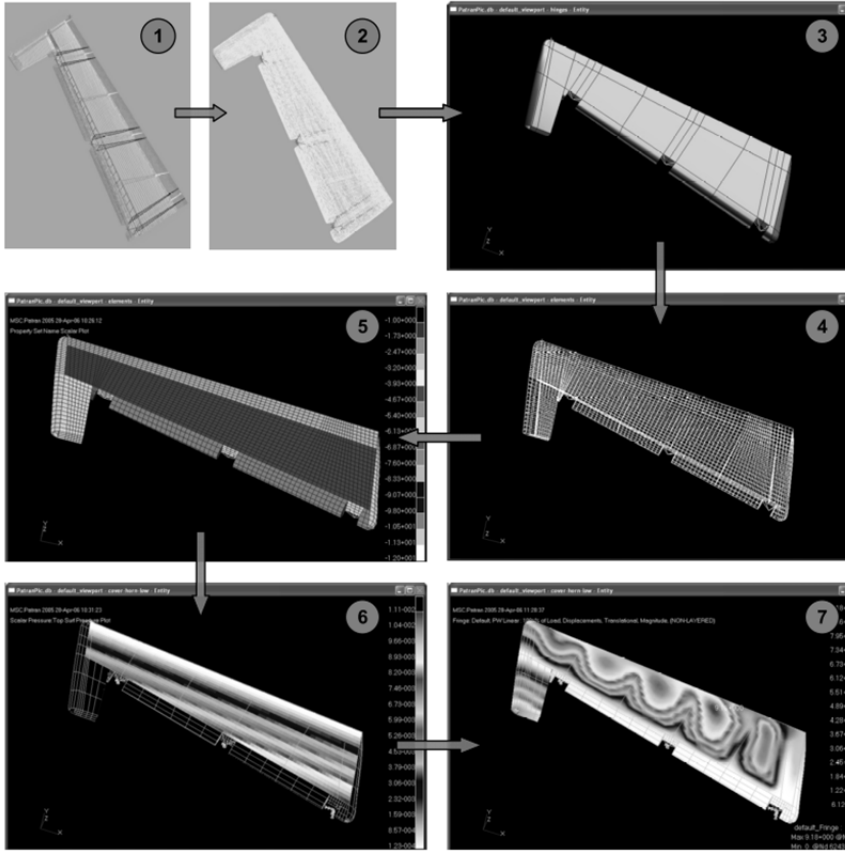
Fig. 1.11: Process for structural analysis of trailing edge devices, developed by van der Laan [87].

nite element solver NASTRAN. The outputs of the process are the results from the FE computation (e.g. stress, strain or displacement). A structural sizing is not performed.

Bayandor et al. [88] developed an ANSYS based process to optimize the mass of a composite Krueger flap. To accomplish this, two representative load cases are defined which are used to perform the sizing. First, a topology optimization on the ribs and spars is performed, which is followed by an optimization of the total composite thickness as well as the layup sequence. A significant weight saving could be achieved, compared to the original flap. However, for this study, the outer shape of the flap was given and fixed. Therefore, this process is not intended to be used for aircraft preliminary design aspects.

Anhalt [89] conducted a study on a transport aircraft flap. The background of his study was an attempt to reduce the number of tracks on the A340 outer flap from three to two. As such, he analyzed the two remaining track positions and the structural layout of the flap with both, a beam and a finite element shell model. He used four load cases and performed the structural sizing with respect to deformation and strength requirements. With his approach, it was possible to compute the material properties of a composite flap meeting all requirements of the design. However, no aircraft design aspects were considered, as the geometry of the flap was given and only the internal structure redesigned.

All methods described above can only be used for the specific design of a flap or slat body without considering the interactions with the wing. Additionally, all of the discussed methods focus on the flap and slat body, while none of the described methods considers the attachment of the device to the wing (e.g. flap tracks).

1.2.6 Physics-Based Models for Primary and Secondary Structures

For the development of the Dornier 728 family a new multidisciplinary optimization (MDO) process was develop at Dornier [90]. The core of the process was a finite element NASTRAN model of the wing, including wing box, engine pylons, engine (modeled as point mass) and ailerons (see Fig. 1.12). The aerodynamics were covered via a double-lattice method and the structural sizing was performed with respect to stress, buckling, aileron reversal and flutter constraints. The aim of the process was to size the wing box and not the aileron or the pylon. However, the aileron was needed for the aileron reversal load cases, in order to fully capture the effect of the aileron on the wing box. Similarly, the engine and the engine pylon are needed for the flutter computation.
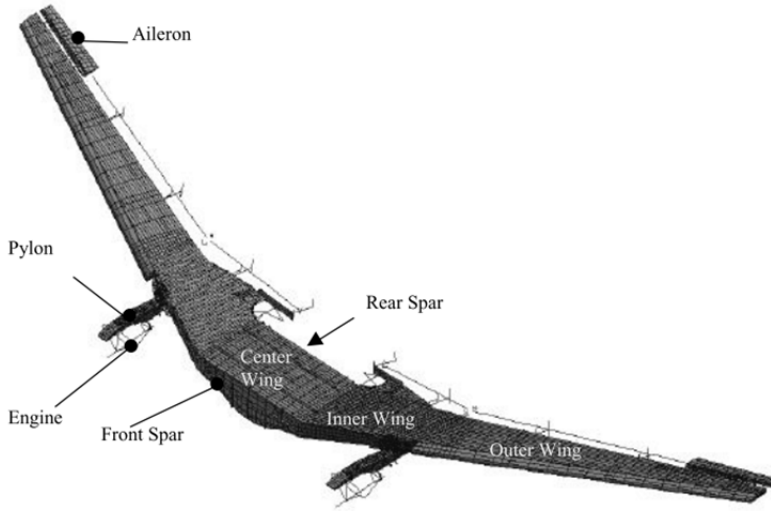
Fig. 1.12: Finite element model including pylons and ailerons [90].

Nagel et al. [91] performed a study on aeroelastic design of winglets. In order to decrease loads and to increase the aerodynamic efficiency of the wing, the addition of a tab (similar to an aileron) to the winglet was considered. To accomplish this, the model generator PARA_MAM (see chapter 1.2.3) was extended to be able to generate a tab, which was connected via hinges to the winglet. The sizing of the wing, the winglet and the tab was performed by S_BOT for aluminum as well as CFRP. In this study, the wing box and the tab were sized and their masses estimated. Additionally, the interaction of both components was considered. However, the definition of the tab in the PARA_MAM input was complex and therefore unfriendly for the user. More complex track kinematics could not be generated.

Finite element models of the whole aircraft, including the wing with its leading and trailing edge devices are used in several studies on fluid-structure coupled analysis, for example in [92, 93] (see Fig. 1.13). However, for these studies, the focus is the differences in the high-fidelity CFD results with coupled and uncoupled CFD computations. The finite element model is only used to compute the wing deformation and not for structural design or wing mass estimation purposes. Additionally, these studies are not related to the early design stages, where the wing geometry and internal structural layout is defined.
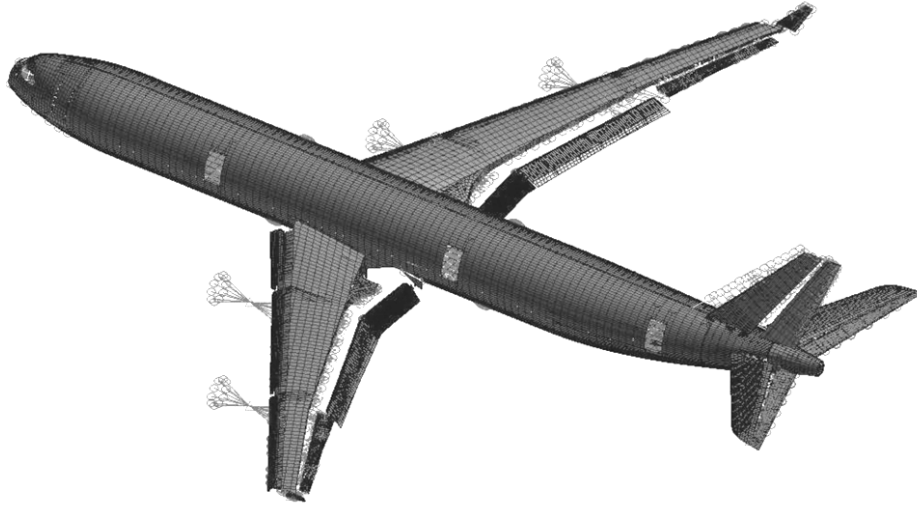
Fig. 1.13: Finite element of A340 in landing configuration [92].

1.3   Contributions of the Study

The performed literature review of wing mass estimation methods shows that there is a wide range of different methods and approaches available. Pure empirical methods can deliver accurate results for conventional configurations. However, the quality of the formulae strongly depend on the underlying database and the sensitivity behavior is limited to a few input parameters.

As described in [49, 50, 55 and 58], beam- or shell-based methods can lead to very good results for primary wing structures. Therefore the methods need to be well validated and good empirical correlations for non-optimum masses need to be derived to compute the total primary structural mass from the physics-based mass. The sensitivity behavior for global wing parameters is good for both, beam and shell-based methods. Shell-based methods have the additional advantage that local effects can be reflected, whereas beam-based methods cannot. The most important local effects in wing mass estimation are kinks of the wing box, engine attachments or landing gear attachments.

Secondary wing structures can only be covered effectively using empirical methods, as all of the previously discussed physics-based methods are unable to be used for mass estimation in early design stages. Only the method of Sanders [77] may be used for physics-based mass estimation of flaps. But this method is limited to the body of the flap and the interactions between the wing and the flaps are not covered. The empirical methods for secondary structures have the same disadvantages as the empirical methods for total wing masses. They can only be used for conventional configurations within a small design space and the sensitivity behavior is highly limited, as most of the methods are based on very few parameters.

For novel aircraft configurations and technologies, meeting the demands of future air transportation, reliable methods for calculating the total wing mass are required. Therefore, the research question of this study is:

How can the wing mass estimation process for novel configurations or structural concepts be advanced, in order to make, already in early design stages, reliable predictions for the total wing mass, including the major secondary structures?

The aim of this study is the development of a method for wing mass estimation that covers the wing primary structures as well as the most important parts of the secondary structures. The method should be able to deliver accurate results for conventional and unconventional configurations as well as varying structural concepts. On the unconventional side the method should be able to analyze all of the concepts, which current research is focusing on.

It should be possible to use the method in a wing optimization process. Therefore, the method should deliver both, accurate results as well as good sensitivities for a wide range of different parameters. Additionally, the interactions between the different components should be represented by the developed method.

Chapter 2

FUNDAMENTALS AND APPROACH

The physical theories and mathematical principles, which this study is based on, are introduced in the Fundamentals subchapter. In the Approach subchapter, a description of the approach that was chosen to create the user-friendly, extended physics-based wing mass estimation tool chain is explained.

2.1 Fundamentals

Within this chapter the most important physical theories that are used in this study are derived and described. These fundamental theories are: the vortex-lattice method that is used for aerodynamic load estimation; the beam and shell theory as well as the finite element method (FEM), upon which the structural analysis is based. These structural fundamentals are described in the following order: first the beam theory is derived and the underlying assumptions explained, next the finite element method is introduced on the example of a bending beam and finally the fundamentals of the used shell element are described.

2.1.1 Vortex-Lattice Method

The load estimation of the aerodynamic forces in this study is performed by using the tool AVL (Athena Vortex Lattice) [94], which is based on the vortex-lattice theory. The vortex-lattice method is a method that is well suited for the estimation of the lift distribution and the induced drag of lifting surfaces. However, other drag components cannot be estimated with the vortex-lattice method. The following explanations are based on references [95 - 99].

Vortex Filament

The influence of a small segment $\overrightarrow{dl}$ of a three-dimensional general vortex filament (straight or curved) on the velocity increment $\overrightarrow{dV}$ at point P in the flow field can be described by the *Biot-Savart law*:

$$\overrightarrow{dV} = \frac{\Gamma}{4\pi} \frac{\overrightarrow{dl} \times \vec{r}}{|\vec{r}|^3} \qquad (2.1)$$

with Γ being the vortex strength and $\vec{r}$ being the vector from $\overrightarrow{dl}$ to the point P (see Fig. 2.1). The derivation of the Biot-Savart is beyond the scope of this description, but can be found in advanced aerodynamic text books, such as [100].
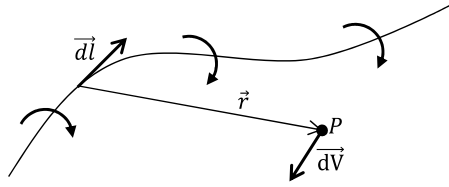
Fig. 2.1: Vortex filament and illustration of the Biot-Savart low (based on [96]).

According to the *Helmholtz's vortex theorems* such vortex filaments:

- have a constant strength over their length.
- cannot end in a fluid. It must extend to the boundaries of the fluid (which can be $\pm\infty$) or form a closed path.

Prandtl's Classical Lifting-Line Theory

The first practical theory for the prediction of aerodynamic properties of a wing was developed by Ludwig Prandtl and his colleagues in Göttingen during the period of 1911 to 1918.

In Prandtl's method (see Fig. 2.2), a bounded vortex filament of the strength Γ is placed from tip to tip of the wing. According to the *Kutta-Joukowski theorem*, this bound vortex will lead to a lift force of $L = \rho_\infty V_\infty \Gamma$. In contrast to a free vortex, which moves with the fluid elements through the flow, this bounded vortex has a fixed location. According to *Helmholz's vortex theorems*, this vortex cannot end at the wing tip. Therefore, the vortex filament is continued as a
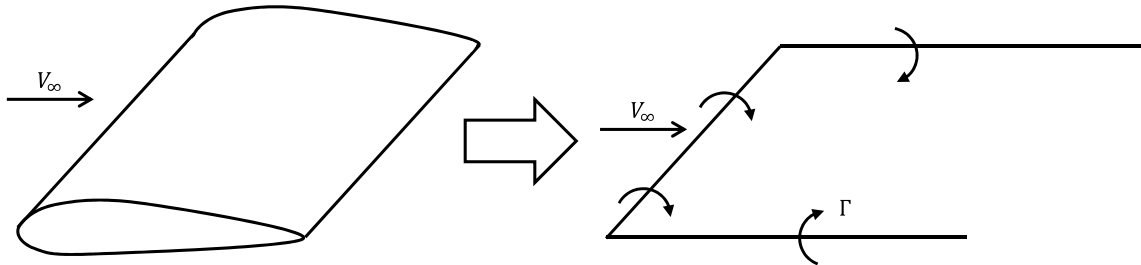
Fig. 2.2: Replacement of the wing with a horseshoe vortex (based on [96]).

free vortex at the wing tips downstream to infinity. These two free vortex filaments lead to an induced downwards oriented velocity along the wing. Due to their shape, these vortex filaments (the bounded plus the two free vortices) are called horseshoe vortex.

As the downwash as well as the lift distribution due to one single horseshoe vortex does not realistically simulate a real wing, this approach can be refined by distributing several horseshoe vortices along a line between the two wing tips. This line is called *lifting-line*, which gives this approach its name.

Lifting-Surface Theory and Vortex-Lattice Method

Prandtl's classical lifting-line theory delivers reasonable results for straight wings with moderate to high aspect ratios. But for low aspect ratios, swept and delta wings the classical lifting-line theory is inapplicable.

Therefore, the vortex filaments along a single lifting line are replaced by several parallel lifting lines spread over the chord of the wing. This leads to a system of horseshoe vortices laying on the wing planform. This means that each horseshoe vortex represents the lift of one small part of the wing surface – the so called *lifting surface*. Such a system of horseshoe vortices is shown in Fig. 2.3. Please note that the free vortices between two neighboring lifting surfaces lay exactly on each other. They are shown separately for better understanding in Fig. 2.3.
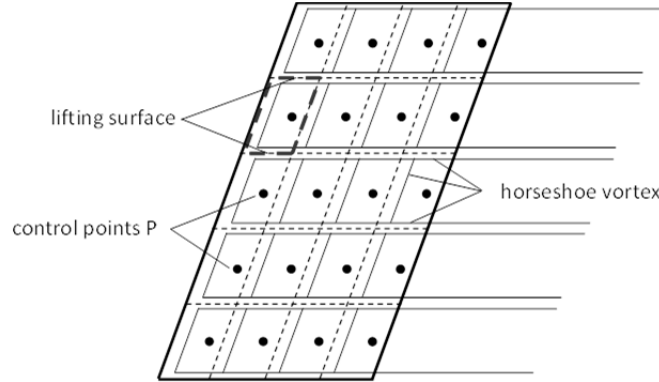
Fig. 2.3: Vortex-lattice system on a finite wing (based on [96]).

The induced velocity at any arbitrary point P on the wing planform can be computed by using the *Biot-Savart law*, which is mentioned above. By summing up all of the induced velocities from all bounded and free vortices, the total induced velocity can be computed. As there is no flow through the wing planform, the sum of the induced velocity and the normal component of the free stream velocity at an arbitrary point P on the wing planform must be zero. This is called the flow-tangency condition. The central problem of the lifting-surface theory is to set the individual vortex strengths Γ such that flow-tangency conditions on each point P are fulfilled.

To handle this numerically, one vortex and one control point P is placed on each lifting surface. The bounded vortex is placed at 25% of the surface chord, while P is placed at 75% of the surface chord (see Fig. 2.3). One equation for the flow-tangency condition is applied on each

control point P, which results in a system of simultaneous algebraic equations that can be solved numerically. This numerical approach is the *vortex-lattice method*.

2.1.2 Beam Theory

The beam theory is a simplified method for the structural computation of beam-like structures. It has to be noted, that there is not one single beam theory, rather several different theories based on different assumptions and simplifications. Dependent on the physics of the problem (e.g. the shape of the beam cross section) it must be decided which theory is applicable. In the following subchapter, the equations that are used in this study, including their basic assumptions, are derived. The equations and derivations are based on reference [101].

The basic assumption of all beam theories is, that the structural member has one dimension that is much larger ($>$ factor 5-10) than its other two dimensions. This kind of shape allows reducing the point of view to a cross section based view. Therefore, the structural computation of a beam is done cross section by cross section, depending on the section properties and the loads acting at this section. This implies that the behavior of the beam at one cross section is independent from the neighboring one.

In the following, the equations for axial, bending and torsion loads are explained separately. The total deformation of the beam can be derived by adding these deformations.

Tension and Compression

The relation between the stress along the bar σ_y and the strain ε_y for a bar, loaded under tension or compression is:

$$\sigma_y = \mathrm{E} \cdot \varepsilon_y \qquad\qquad (\ 2.2 \ )$$

with E being the Young's Modulus which represents the material stiffness. Equation 2.2 can be transformed to the correlation between the applied force F_y, the stiffness of the beam EA (A equals the cross section area) and the displacement field u_y:

$$\sigma_y = \frac{\mathrm{F}_y}{A} = \mathrm{E} \cdot \varepsilon_y \quad \Leftrightarrow \quad \mathrm{F}_y = \mathrm{EA}\varepsilon_y = \mathrm{EA}\frac{\delta u_y}{\delta y} \quad \Leftrightarrow \quad \frac{\delta u_y}{\delta y} = \frac{\mathrm{F}_y}{\mathrm{EA}} \qquad (\ 2.3 \ )$$

Bending

The equations for computing bending beams as described below are based on the following assumptions:

- The beam coordinate system is the principal coordinate system of the beam.
- The strain distribution in z-direction varies linearly with z and is zero at the neutral axis.

- A cross section that is perpendicular on the neutral axis before bending, remains perpendicular during bending.
- The cross section remains undeformed during bending.
- Maximal strain is small, thus linear elastic material behavior can be applied.

The last three assumptions are the so called *Bernoulli assumptions*. With the Bernoulli assumptions, the shear fixed beam assumption is included implicitly.
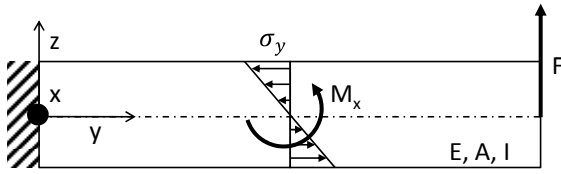
Fig. 2.4: Beam under bending load.   Fig. 2.5: Bending line of a beam (based on [101]).
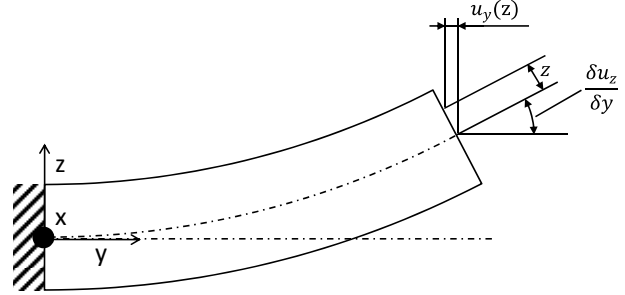
The moment M_x around x at one specific cross section can be computed by the integral of the stress σ_y multiplied with the lever arm z over the cross section area A (Fig. 2.4):

$$M_x = \int_A \sigma_y z \, dA \qquad (2.4)$$

With the assumption of a linear stress distribution, σ_y can be replaced by $\sigma_y = cz$ with c being a constant value, which results in:

$$M_x = \int_A cz^2 \, dA = c \int_A z^2 \, dA = cI_x \quad \Leftrightarrow \quad c = \frac{M_x}{I_x} \qquad (2.5)$$

with I_x being the second moment of inertia. Equation 2.5 can be inserted in the original expression for the stress σ_y, which leads to the stress equation for bending beams:

$$\sigma_y = cz = \frac{M_x}{I_x} z \qquad (2.6)$$

From the geometry of the bending beam in Fig. 2.5, it can be seen that at any point of the beam cross section, the first derivation of the bending displacement u_z equals the negative displacement in y-direction u_y divided by the z-coordinate of the point:

$$\frac{\delta u_z}{\delta y} = \frac{-u_y}{z} \quad \Leftrightarrow \quad u_y = -z \frac{\delta u_z}{\delta y} \qquad (2.7)$$

If one considers that $\varepsilon_y = \delta u_y / \delta y$, the expression for the strain of a bending beam results in:

$$\varepsilon_y = \frac{\delta}{\delta y} \left(-z \frac{\delta u_z}{\delta y} \right) = -z \frac{\delta^2 u_z}{\delta y^2} \qquad (2.8)$$

Equations 2.6 and 2.8 can be combined by using the definition of the Young's modulus E in equation 2.2, which leads to the differential equation of the bending beam:

$$\frac{\delta^2 u_z}{\delta y^2} = -\frac{M_x}{I_x E} \qquad (\,2.9\,)$$

Torsion

The torsion of a beam according to the theory of Saint-Vénant is valid, when no stresses in beam direction appears during pure torsion around the shear center and when the cross section of the beam remains undeformed in the x-z-plane. As no stresses along the beam axis appears, the cross section can deform along the beam axis, which means that the cross section is non-planar after torsion. The shear stress distribution is assumed to be linear within the cross section, with the stress being zero at the shear center. This theory is valid for beams having free ends, but is not valid close to the clamping of the beam.

The rotation ϑ at any position L of the beam can be computed by integrating the twist $\delta\vartheta/\delta y$ along the beam axis, starting at the clamping at x=0:

$$\vartheta = \int_0^L \left(\frac{\delta\vartheta}{\delta y}\right) dy \qquad (\,2.10\,)$$

For the special case of a beam with constant cylindrical cross section and constant torsion moment, the twist $\delta\vartheta/\delta y$ is constant and can be written as:

$$\frac{\delta\vartheta}{\delta y} = \frac{M_y}{I_y G} \qquad (\,2.11\,)$$

with M_y being the torsion moment, I_y the polar moment of inertia and G the shear modulus. By comparing equation 2.11 with the corresponding equations for bending 2.9 and tension/compression 2.3 the identical shape of the equations can be seen.

2.1.3 Finite Element Method

In this chapter, the basics of the finite element method (FEM) are explained and the approach is derived on the example of a bending Euler-Bernoulli beam. The chapter is based on references [102 - 104].
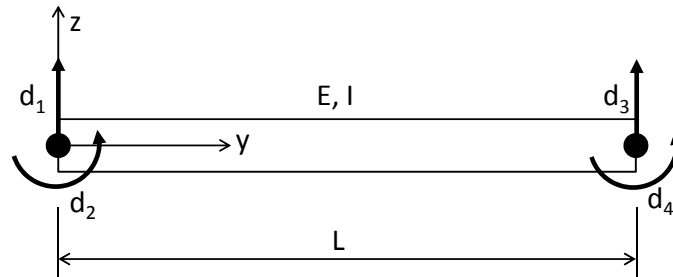
Fig. 2.6: Euler-Bernoulli beam with two nodes and four degrees of freedom (based on [102]).

The finite element method is a method for the numerical solution of field problems. In a field problem, the spatial distribution of one or more dependent variables is determined. Although FEM is very popular for structural analysis, it can also be used for different problems, such as computing temperature distributions or fluid dynamics. In the following, the focus is laid purely on the structural use of FEM, as it is only used for structural analysis in this study.

The basic idea of FEM is to split the analysis in several small regions, the so called *finite elements*. On each finite element, the field variable, such as e.g. the displacement, is approximated by simple interpolation functions, the so called *shape functions*. In FEM, each element has several specific points that are called *nodes*. Nodes are used to connect the different elements and to apply loads on the elements. Additionally, the field variable is computed at these discrete points. Each node has several degrees of freedom (DOFs), such as translational or rotatory degrees of freedom. For the solution, a linear system of equation is assembled, having one line for each DOF. This system is solved for the DOFs, while the other properties, such as stress or strain, are computed from the displacement field in the post-processing.

For a static analysis this linear equation has the form:

$$\bar{\bar{\mathrm{K}}}\vec{d} = \vec{F} \qquad (\,2.12\,)$$

with $\vec{d}$ being the vector of all DOFs, $\vec{F}$ the vector of all forces acting on the nodes in the direction of the DOFs and $\bar{\bar{\mathrm{K}}}$ the stiffness matrix that includes the relation between the DOFs and the forces. For a translational DOF, the entity in $\vec{F}$ is a force, while for a rotational DOF, the entity in $\vec{F}$ represents a moment.

The derivation of the stiffness matrix $\bar{\bar{\mathrm{K}}}$ is presented in the following on the example of a bending Euler-Bernoulli beam. The beam (see Fig. 2.6) has one node at each of its ends and four degrees of freedom (DOFs) $\mathrm{d}_1 - \mathrm{d}_4$. The continuous displacement of the beam is described by the four shape functions $\mathrm{N}_1 - \mathrm{N}_4$ in beam coordinates.

Each of the shape functions equals 1 at one of the DOFs, while being 0 for all other DOFs. The shape functions are used to compute the continuous beam displacement from the discrete displacement of the nodes. Depending on the physics of the problem, the shape functions can be simple (e.g. linear) or more complex. The continuous displacement of the whole beam can be described by the discreet DOFs multiplied with the shape functions according to:

$$u_z(\mathrm{y}) = N_1 d_1 + N_2 d_2 + N_3 d_3 + N_4 d_4 = \vec{N}^T \vec{d} \qquad (\,2.13\,)$$

To derive the stiffness matrix of this beam, the *Lagrange energy formulation* for a static mechanical system is the starting point:

$$\frac{\delta U}{\delta x} = F_x \qquad (\,2.14\,)$$

with $\delta U/\delta x$ being the derivation of the potential energy U in the direction of the generalized coordinates x that equals the generalized forces F_x. For the generalized coordinates x the four DOFs d are used in the following calculations. The potential energy in the beam example is the *strain energy U*, which is the energy that is stored in a body due to its deformation. The strain

energy per unit volume is called *strain energy density* and equals the area underneath the stress-strain curve. For the linear elastic range, where the correlation between stress σ and strain ε can be described using the Young's modulus E, the strain energy can be written as:

$$U = \int\limits_V \int\limits_0^\varepsilon \sigma d\varepsilon \, dV = \int\limits_V \int\limits_0^\varepsilon E\varepsilon d\varepsilon \, dV = \int\limits_V \frac{E\varepsilon^2}{2} \, dV \qquad (\ 2.15\ )$$

In the case of a bending beam, the strain can be computed from the second derivation of the bending line (equation 2.8). If equation 2.8 is inserted in equation 2.15 and the volume integral is split in one integral over the beam cross-sectional area A and one integral over the beam length, equation 2.15 results in:

$$U = \int\limits_0^L \left[\int\limits_A \frac{E}{2}\left(z\frac{d^2 u_z}{dy^2}\right)^2 dA \right] dy = \int\limits_0^L \left[\frac{E}{2}\left(\frac{d^2 u_z}{dy^2}\right)^2 \int\limits_A z^2 dA \right] dy = \frac{1}{2}\int\limits_0^L EI_x \left(\frac{d^2 u_z}{dy^2}\right)^2 dy \qquad (\ 2.16\ )$$

In equation 2.13, the correlation between the discrete DOFs and the bending line of the beam is expressed which can be inserted in equation 2.16, giving:

$$U = \frac{1}{2}\int\limits_0^L EI_x \left(\vec{N}''^T \vec{d}\right)^2 dy = \frac{1}{2}\int\limits_0^L EI_x \left(\vec{d}^T \vec{N}''\right)\left(\vec{N}''^T \vec{d}\right) dy = \frac{1}{2}\vec{d}^T \left[\int\limits_0^L EI_x \vec{N}'' \vec{N}''^T dy \right]\vec{d} \qquad (\ 2.17\ )$$

with $\vec{N}''$ representing the second derivation of $\vec{N}$. This expression for the strain energy of a bending beam is inserted in the Lagrange's equation (equation 2.14), which results in:

$$\int\limits_0^L EI_x \vec{N}'' \vec{N}''^T dy \vec{d} = \vec{F}_d \qquad (\ 2.18\ )$$

By comparing equation 2.12 and 2.18, it can be seen that the integral represents the searched stiffness matrix $\overline{\overline{K}}$:

$$\overline{\overline{K}} = \int\limits_0^L EI_x \vec{N}'' \vec{N}''^T dy \qquad (\ 2.19\ )$$

Equation 2.19 represents the specific stiffness matrix for a bending Euler-Bernoulli beam. This expression can be transformed in the general expression of the FE stiffness matrix, if the second derivation of the shape functions $\vec{N}''$ is replaced by the matrix $\overline{\overline{L}}$, multiplied with the shape functions $\vec{N}$:

$$\vec{N}'' = \overline{\overline{L}}\vec{N} \qquad (\ 2.20\ )$$

This means that the two derivation operators d/dy are written in the $\overline{\overline{L}}$ matrix. In general, the matrix $\overline{\overline{L}}$ contains the mathematical operator that is needed to compute the strain respectively the curvature from the displacement field. This correlation is the so called *kinematic equation* (KE). In the example of the bending beam, the kinematic equation is the second derivation. For a beam under tension/compression or torsion this would be the first derivation. In

the next step, the stiffness of the beam EI_x can be replaced by the general matrix $\bar{\bar{C}}$. $\bar{\bar{C}}$ contains the stiffness of the element, against deformation along the degree of freedoms due to the loads. This correlation is the so called *constitutive equation* (CE). For a beam, bending around the x axis, the entity is EI_x, while the entity for a beam under tension or compression is EA and GI_y for a beam under torsion. Finally, the integral over y has to be extended to the general 3-dimensional case, which leads to a volume integral over V. This results in the general expression for the stiffness matrix:

$$\bar{\bar{K}} = \int_V \left(\bar{\bar{L}}\vec{N}\right)^T \bar{\bar{C}}\left(\bar{\bar{L}}\vec{N}\right) dV \qquad (\ 2.21\ )$$

2.1.4 Shell Elements

In all structural analysis in this study the ANSYS shell element SHELL181 is used. In the following the basic assumptions and properties of the element are described. The following explanations are based on reference [105].

The used shell element is a 4-node structure shell element for thin to moderate shell structures. The shell element has 6 degrees of freedom at each node – 3 translational DOFs and 3 rotational DOFs. It is also possible to use the element in a triangular shape. In this case two nodes are coincident. The shell element is suitable for linear and non-linear analysis.

The shell element can be used to model composite shells or sandwich constructions. The accuracy in modeling composite shells is governed by the first-order shear-deformation theory (Mindlin-Reissner shell theory).

The shell element employs linear shape functions for all DOFs. To avoid shear locking, the basic functions for the transvers shear strain are changed according to Dvorkin [106].

The assumptions for the shell element in the used condition with homogeneous linear-elastic materials are:

- The thickness of the shell is much smaller than its next larger dimension (length, width or curvature).
- The thickness of the shell is constant.
- The strain distribution during bending in height direction is linear and symmetric to the shell's middle plane.
- For pure bending, the stress and strain is 0 at the middle plane.
- For longitudinal loads, stress and strain are constant over the thickness.
- The normal to the middle plane remains straight during bending, but not necessarily normal to the middle plane.

2.2 Approach

In the following, the approach used to develop the new method for the estimation of the wing mass, is explained. The different aspects of the approach are directly derived from the requirements formulated in the research question in chapter 1.3.

2.2.1 Extended Physics-Based Modeling

In the research question, a *reliable prediction* of the wing mass of *novel configurations or structural concepts* is demanded. As shown in the literature review in chapter 1.2, reliable prediction of a wider design space can only be achieved with physics-based methods, rather with statistical methods. Additionally, it is shown that beam-based methods cannot effectively cover multiple local effects, which is required for the evaluation of new structural concepts and novel wing configurations. Therefore, the mass estimation process needs to be based on finite element shell methods, as only these methods combine the needed flexibility, accuracy and acceptable computational costs.

According to the research question, the *wing mass including its major secondary structures* should be estimated accurately. Therefore, physics-based methods are also required for the secondary structures. Each wing contains a wide range of different secondary structures, of which most are very lightweight. Therefore, the physics-based mass estimation in this approach is limited to the heaviest parts

Fig. 2.7: Extended modeling of the wing structure including flaps, flap tracks, a pylon and a landing gear.

of the high-lift system, which are the flaps, including flap tracks, as well as the ailerons, including their attachment (see Fig. 2.7).

As the wing, the flaps and the ailerons have a very similar structural buildup (skins, ribs and spars) they can by modeled using the same approach based on shell elements. To capture the interactions between the main wing and the movable structures, it is necessary to include both parts of the wing in one common model, including a realistic modeling of the connection parts (e.g. flap tracks). Therefore, one finite element model is used for the whole wing, including flaps and ailerons.

To achieve the required accuracy of the new method, all characteristic capabilities of a state-of-the-art multidisciplinary wing mass estimation process according to the description in chapter 1.1.3 need to be fulfilled. These characteristic capabilities clearly describe the need for a multidisciplinary analysis including the computation of all loads, the need for an aeroelastic feedback

loop and the capability for structural analysis and sizing. Therefore, the so called WINGmass tool chain is developed, that includes methods and tools for each of these capabilities.

The WINGmass tool chain must include a physics-based estimation of the aerodynamic loads that is able to capture the loads on the wing as well as on the high-lift systems. Only the pressure distribution over the wing and the movable structures is of interest, while further aerodynamic properties such as drag or maximum lift are not needed for the load estimation. Therefore, a vortex-lattice method, such as described in chapter 2.1.1, is chosen for the loads computation.

After the aerodynamic loads, the loads resulting from the fuel inside the wing are the second largest contributor to the wing loads. Therefore, these loads need to be captured by a reliable and detailed representation. For the fuel loads, a module is developed, that computes the static fuel pressure on each area of the finite element model. Using this approach, the total fuel mass as well as the fuel distribution along the wing can be captured accurately.

Other important loads, are the loads due to the wing mounted landing gear and the engines. The landing gear loads consist of inertia loads and of the ground forces that are transferred over the landing gear in the wing structure. The engine loads consist of inertia loads and of the engine thrust force. To capture these loads, a module is implemented to compute these loads for each load case. To achieve a realistic load introduction in the wing, the primary structural components of the landing gear and the engine pylon in the finite element wing model are included.

The next element of the tool chain is the structural analysis and sizing routine. Here, the loads are applied on the structural model, the model is analyzed and new material thicknesses are computed with respect to stresses and deformations. A wide range of load cases are required to be used for the analysis, as the most critical loads for the wing primary structure as well as the movable structures need to be taken into account.

The aerodynamic load distribution, the loads due to the fuel distribution and the orientation of the engine thrust vector change due to wing deformation. Therefore, a loop is implemented, iterating between the structural analysis and sizing routine and the loads computation modules.

2.2.2 CPACS Parameterization

The wing mass estimation process should be usable *already in early design stages*, according to the demand of the research question. Early design stages can be characterized by their multidisciplinary nature, where several disciplines are used in parallel. These disciplines include aerodynamics, costs, flight physics, performance, wing mass estimation and several others. Therefore, a wing mass estimation
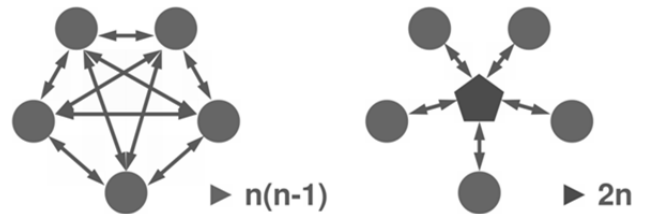
Fig. 2.8: Number of interfaces for multidisciplinary tool chains without (right) and with (left) central data model (n = number of tools) [109].

process must be easily integrable in a multidisciplinary aircraft design environment. Additionally, a disciplinary study on only the wing mass must be possible.

To fulfill these requirements, the whole wing mass estimation process uses the data model CPACS (Common Parametric Aircraft Configuration Scheme) as input and output format. The xml-based CPACS format has been under development since 2005 and is used as a common language for several disciplinary aircraft design tools [107, 108]. The CPACS data model acts as a central data model, where all tools in the tool chain get their inputs from and where they store their outputs. Therefore, tools that run later in the chain can use the previously computed results, independent of the specific tool that has produced these results. For example an aerodynamic spanwise load distribution can be used by a structural model as load input, without the need of a direct coupling between the aerodynamic tool and the structural tool. Using the central data model approach, each tool only needs one CPACS input and output to communicate with all other tools in the tool chain, which clearly reduces the necessary interfaces between the tools (see Fig. 2.8).

Additionally, the demand of the research question for the ability to analyze *novel configurations or structural concepts* can be fulfilled with the CPACS parameterization. From the beginning of the CPACS development, a special focus was led on the flexibility of the parameterization that allows the definition of nearly all thinkable aircraft configurations or structural layouts.

As the CPACS data model is used for this study, the chosen approach is CAD-free. For wing mass estimations processes that are based on CAD systems, the CAD system is primary used as user interface and model generator (such as in [24]). However, tools that are coupled to CPACS do not have a user interface, as all required information is stored within the CPACS database. If a CAD system is desired to be used to define the aircraft geometry or to control the tool chain, it would be possible to write a module that translates the CAD data in the CPACS parameterization or that derives a CAD model from CPACS. Then, the whole chain could be seen as CAD-based, whilst the tools of the tool chain are not related to the CAD system. For the tools in the chain, the CAD system would simply act as another CPACS-coupled tool.

2.2.3 Central Multi-Model Generation

The WINGmass tool chain consists of several analysis modules that get their inputs from the CPACS parameterization. Most of the CPACS coupled tools existed before the CPACS data model was developed. Therefore, these tools have their own tool specific input and output. To translate between the CPACS parameterization and the tool specific parameterization so called *wrappers* are used. These wrappers are normally small modules, transforming one parameterization in another. In case of complex wing models, these 'small modules' can become quite complex tools. The wrappers that are computing the tool inputs can also be called model generators.

Instead of implementing one wrapper (or model generator) for each tool input, it has been decided to implement only one central model generator in this study (see Fig. 2.9). This model generator is called ELWIS, which stands for Finite Element Wing Structure. The name reflects that the core of the model generator is the generation of the finite element wing models, but is extended to create other tool specific inputs. The use of one central model generator instead of several different wrappers has several advantages:

Fig. 2.9: Concept of a multi model generator to reduce CPACS interfaces.

- *Saving implementation time:* A model generator always works as follows: first the input (here: CPACS) is read, then an internal model is computed and finally the tool specific output is derived from the internal model.

  The functions of a model generator for one tool can be reused for the model generation of another tool in two different ways: on the one hand, some computations need to be done for most models and therefore these functions can be reused. E. g. the wings outer shape is required for almost all analysis tools.

  On the other hand, several functions that are implemented in a general manner can be used for the computation of different models. An example is the function computing the structured mesh of a finite element model, which can also compute the structured mesh of a vortex-lattice model, if the input of the function is modified correspondingly.

  The saving of implementation time can nicely be seen at a comparison of lines of code that are needed for the generation of the different tool specific outputs. The ELWIS model generator consists of roughly 37000 code lines and can currently create tool inputs for 10 different tools (including tools that are not part of this study). For the model generation of the structural FE model around 32000 of the 37000 lines are needed. For the generation of the vortex-lattice model around 10000 code lines are needed, of which only 2600 lines are added specifically for the vortex-lattice model, while the other 7400 lines are reused code from the FE model generation. For the input of the model computing the fuel, engine and landing gear loads only 650 code lines are implemented additionally, while in total around 14000 lines are used for that computation.

- *Easier maintenance of the model generator:* The CPACS parameterization is constantly developed further, wherefore new releases are published on a regular basis. Each time, a new release is published, all wrappers must be adapted to the new CPACS version. In the case of the ELWIS central model generator, this work needs to be done once, instead of once per CPACS coupled tool.
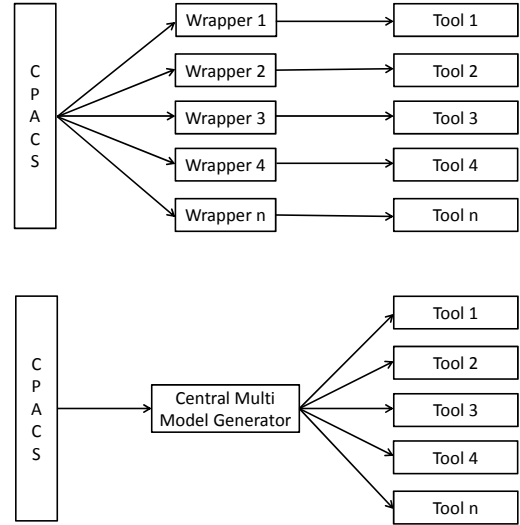
- *Saving computation time:* As mentioned above, some computations are required for several models, wherefore computation time can be saved if these computations are performed once, instead of once per tool. Examples are the computation of the wings outer geometry or the pure loading of the CPACS input file, which is one of the slowest parts of the whole model generation.

- *Better consistency between models:* In a multidisciplinary tool chain, the consistency between the single models is crucial. A good example is the outer shape of the aerodynamic and the structural model. For the interpolation of the aerodynamic load distribution on the structural model, both geometries need to be the same. This consistency can be reached, if all analysis models are derived from the same master geometry. This is the case, if one central model generator is used.

  In addition, the central model generator can make an interpolation unnecessary, which leads to the best possible consistency. In the WINGmass tool chain, the structural gird is also used as grid for the fuel load computation. This means, that the fuel pressure load is directly computed on the structural grid, allowing it to be directly applied on the structural model without any interpolation.

2.2.4 Knowledge-Based Approach for Model Generation

This chapter is structured in four parts: First an overview of knowledge-based engineering systems, which are the software applications of knowledge-based engineering (KBE), is given. Next the state-of-the-art of formalized approaches for the development of such systems is described. This is followed by the description of the approach that is chosen in this study and finally some basic considerations related to the implementation of the ELWIS model generator are described.

It should be noted, that various different terms and definitions exist in the field of KBE. The following descriptions are primary based on the research that is performed at TU Delft by La Rocca et al., as their work represents a good state-of-the-art of knowledge-based engineering techniques in aeronautics.

Knowledge-Based Engineering Systems

In a traditional engineering design cycle, 80% of the development time that is spent by the engineers can be characterized by repetitive non-creative work, while only 20% of the time is spent on creative engineering [25]. By applying the knowledge-based engineering (KBE) approach, these shares can be switched to 80% creative work and 20% repetitive work including a considerable time saving for the total design cycle (see Fig. 2.10) [25]. The main advantages of KBE are [25]:

- Enhancement of productivity levels: more designs in shorter time due to design automation.

- Improvement of product quality levels: better designs, due to multidisciplinary analysis and optimization approach.
- Improved confidence in generated designs.
- Improved level of workers' satisfaction and more space for innovation due to less repetitive work and more time for real creative design.
- Capability to capture, retain and re-use the knowledge of the engineers due to the implementation of the knowledge.

These advantages can be realized by the application of software tools, the so called KBE systems that capture the design knowledge from the engineer and can therefore support the engineer in repetitive non-creative parts of the design. This automation is reached by the implementation of rules in the software, describing the engineers' knowledge in a formalized way. The KBE systems are knowledge-based systems (KBS), extended with capabilities for geometry handling to provide engineering design solutions. Therefore, KBE systems can be seen as a cross point of KBS and CAD-systems [25].
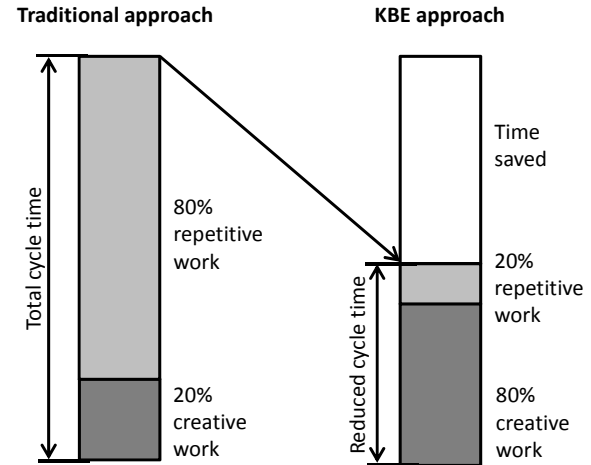
Fig. 2.10: Impact of KBE on design cycle time (based on [25]).

The roots of knowledge-based systems can be found in the field of artificial intelligence, where the basic methods and techniques of KBS have been developed. Knowledge-based systems (or expert systems (ES)) are computer programs that use stored knowledge for solving problems [25]. Compared to 'conventional' computer programs, in KBS the knowledge base (KB) is strictly separated from its processing respectively the problem solving strategies [25]. This means that in the knowledge base, the whole knowledge is stored in the form of rules that are laid down in an arbitrary order. The processing component of the KBS decides which rules respectively functions are 'fired' (or called) and in which order this occurs. This has the advantage that the rules in a KBS can easily be modified or extended, as the implementer does not need to be concerned about its integration in the system.

The knowledge rules in the knowledge base need to be structured and formalized by means of a symbolic representation. In knowledge-based systems, so called rules and frames are the two most common types of structure for the knowledge representation. The systems that are based on rules are called rule based systems (RBS). These rules are codified in the form of if-then statements. Systems that are based on frames are called frame based systems (FBS) and their rules and parameter values are stored in frames. A frame represents a single data structure where everything is stored in. From the view of an implementer, FBS can be seen as RBS implemented in an object oriented way [25].

To define the sequence, in which the functions (or rules) are fired, two different approaches can be identified [25] (see Tab. 2.1):

- *Forward chaining* is an iterative approach. In the first loop all functions, of which all needed inputs are available, are fired. In the next loop additional functions can be fired, as in the meanwhile more parameters are computed. A function that is fired once is never fired again. This requires, that a parameter that is once computed, is never changed by any other function. The iteration stops, if no additional function can be fired.

- *Backward chaining* first checks, which parameter is requested by the user. If this parameter is not available in the database, the function that computes this parameter is searched and it is checked, which parameters are additional needed to run this function. Then, these functions are searched to compute the required parameters and so on. In the end, only these functions are fired, that are necessary for the solution of the problem.

For the implementation of KBE systems, special software languages are developed, that have different properties, compared to non-KBE languages. KBE languages, like GDL (General-purpose Declarative Language), that is used by La Rocca can be characterized by [25, 110 and 111]:

- *Based on LISP:* KBE languages are very often based on object oriented dialects of the programming language LISP (LISt Processing). LISP is based on lists as its major data structure. LISP source code itself is made up of lists. Therefore, LISP programs can manipulate their own source code as a data structure. By using macros that are written in LISP, it is possible to provide the implementer with a higher-level and more user–friendly language construct.

- *Object oriented paradigm:* As already described above, object oriented software languages are needed for frame based systems.

- *Declarative coding style:* The order of functions or rules is arbitrary. The order in which the functions are called is decided by the processing part during runtime, dependent on the actual problem (see description above).

- *Functional coding style:* Each function returns a new parameter instead of modifying already existing parameters. This means, that a parameter that is once computed, will never change. The functional coding style is a precondition for declarative coding.

- *Runtime value caching and dependency tracking:* The system computes and stores only these parameters that are needed. Each value is only computed once (compare backward chaining described above).

- *Dynamic data types:* parameters and objects do not have a predefined data type. The data type is set automatically and can change during runtime.

- *Automatic memory management:* Memory is automatically allocated and de-allocated.

The way of working of declarative and functional coding is shown in the example in Tab. 2.1. Here the order of fired rules/functions is shown in cases of forward and backwards chaining. It can be seen that for the two different cases, different functions are called in a different sequence, depending on the given input and the required output.

Tab. 2.1: Sequence of fired rules with forward and backward chaining, for a simple mathematical example that is implemented in declarative and functional coding style.

Rule/Function	Case1: D given, C searched		Case 2: A given, B searched	
	Forward chaining	Backward chaining	Forward chaining.	Backward chaining
A = B	2	2	3	-
B = D + 1	1	1	2	2
C = A + B	3	3	3	-
D = A - 1	3	-	1	1
E = D - B	2	-	3	-

Implementation of a KBE System

Beside the software aspect of KBE systems, another research focus in KBE lies on the implementation of the KBE systems. A number of different methodologies are available for the development of KBE applications and systems. The most popular of these methods is the 'Methodology and Software Tools Oriented to Knowledge-Based Engineering Applications' (MOKA) method [112]. According to the MOKA methodology the knowledge elements are stored in so called ICARE (Illustrations, Constraints, Activities, Rules and Entities) forms. This knowledge is then formalized by using MML (Moka Modelling Language, an adaption of UML) to classify and structure the ICARE informal model elements. The MML model can finally be translated in product and process models (see Fig. 2.11) [112].

A shortcoming of MOKA is that MOKA is focused on the development of the KBE application, but not on the end user or the usage of the application [112]. In addition, MOKA does not provide a methodology how the KBE application can be integrated in a multidisciplinary design optimization (MDO). Because of this, the concept of the Design and Engineering Engine (DEE) is under development at the TU Delft. The DEE consists of three main parts. The first part operates the design process, including the multidisciplinary optimization and the first initialization of the product model parameter values. The next major element is the Multi-Model Generator (MMG), which is a modeling framework that uses the product model parameters and formalized knowledge to generate the inputs for the various analysis modules, which make up the third major part of the DEE. The MMG contains a fully formalized KBE application that could result from the MOKA approach. But the DEE does not include a methodological, formalized approach for knowledge capture,
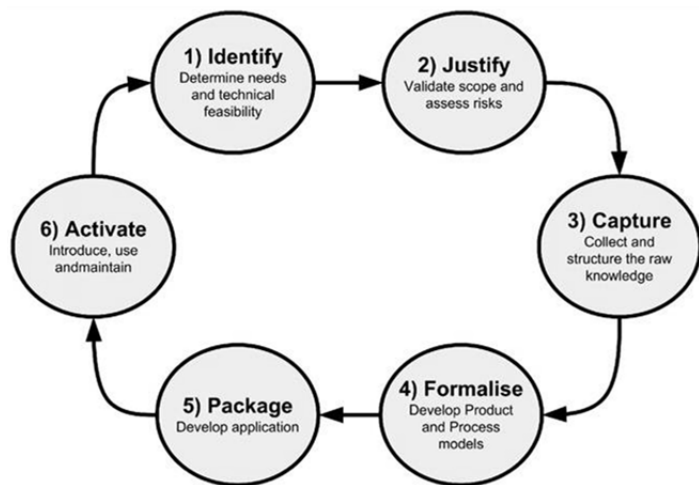
Fig. 2.11: MOKA methodology elements [112].

knowledge formalization and knowledge delivery which is provided by the MOKA approach [113].

To overcome this shortcoming of the DEE, the concept has been further developed in the KNOMAD ('Knowledge Nurture for Optimal Multidisciplinary Analysis and Design' respectively 'Knowledge capture, Normalization, Organization, Modeling, Analysis and Delivery') approach. The KNOMAD approach includes the MMG and the analysis modules from the DEE but is extended with a formalized description for the knowledge capture, formalization and delivery processes. From a global point of view, the KNOMAD and the MOKA approaches are similar, with the difference that the KNOMAD approach is focused on MDO application. Therefore, the 'develop application' phase of MOKA is split in the development of the MMG and the disciplinary analysis modules. From a more detailed point of view, it can be seen that the KNOMAD approach puts emphasis on the second phases of knowledge formalization and defines this phase in more detail [113].

Knowledge-Based Approach in this Study

As already mentioned above, a shortcoming of the MOKA approach is the lack of end-user orientation [112]. Besides other aspects, such as the MDO orientation, the KNOMAD also improves the end-user orientation [112, 113], whilst the main focus is still on the various other phases. This is the major difference between these approaches and the knowledge-based approach in this study.

The research question demands the usage of the tool chain in *early design stages*. Therefore, the developed wing mass estimation method must be manageable by a single aircraft design engineer, without the assistance of e.g. a wing-structural specialist. Additionally, it must be possible to set up a simulation run within very few hours and as such the user input, demanded by the WINGmass tool chain, must be limited. However, the required level of detail of the physical analysis tools is high, compared to the state-of-the-art methods that are currently used in aircraft pre-design (see chapter 2.2.1). Such detailed models, usually require large quantities of input parameters which are not manageable during early design stages.

Therefore, the challenge of this study is, to uncouple the quantity of input parameters from the increasing level of detail. In the development of a new tool, usually the capabilities of the new tool are described in the requirements. However, the required input parameters are primarily an outcome of the implementation and are not orientated on the needs of the end-user. This approach does not appear to be feasible anymore. In the new approach, the input parameters are defined from the point of view of the end-user, *without* taking into account the analysis models and their level of detail.

Usually, the end-user *must* define the input parameters that are required from the tool. But in this approach, the elementary question is what input parameters the end-user is *willing* to define. These input parameters are usually the parameters that the designer wants to change during the design process, in order to optimize the design. Therefore, the number of input parameter is not necessarily as small as possible, as the designer wants to keep control over the most

relevant wing parameters. If the parameterization is determined by the user, the parameterization represents the user's way of thinking, which can differ strongly from the way of thinking of the implementer. Additionally, the parameterization only describes the aircraft itself and the general method that should be used for an optimization or sizing. The parameterization will not include tool specific parameters that are 'only' needed for the generation of the model itself, but do not describe the real aircraft.

Using this approach, a large gap between the parameterization on the one side and the detailed analysis modules on the other side result. This gap must be filled by knowledge rules that are implemented in the central model generator (see Fig. 2.12). Therefore, the central question in the development of the model generator is which knowledge needs to be implemented in order to fill this gap. As this knowledge is usually not available for the implementer, it needs to be captured from e.g. papers, books or the direct contact to disciplinary experts. Next, this knowledge must be understood by the implementer, normalized, formalized and finally implemented.
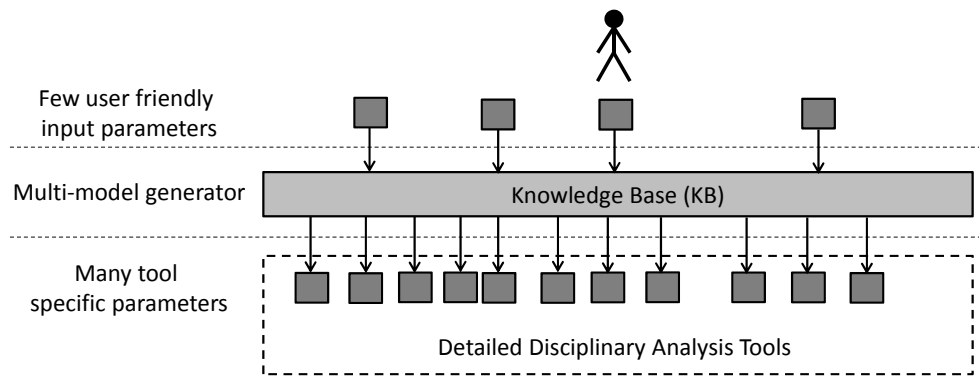
Fig. 2.12: Decoupling of the amount of input parameters from the increasing amount of tool specific input parameters due to the knowledge base.

Software Considerations for the ELWIS Multi-Model Generator

In comparison to 'normal' software languages, the most outstanding characteristic of KBE software languages is the declarative coding style. The declarative coding style is of great advantage if the sequence of the fired rules or functions of the KBS changes, depending on the concrete problem that the program has to solve (see Tab. 2.1). However, the problem which must be solved by a model generator is not of such a nature. During the application of a model generator, the sequence of the functions does not change during different runs. Independent of the number of wings, shape of the wings or structural layout, the sequence of fired function will always be for example:

- Load input file.
- Compute outer shape.
- Place ribs and spars.
- Write tool specific output file.

It occurs that some functions are not always needed or that some additional functions are needed, which can be handled by simple if-then statements. Despite this, the sequence itself will never change, as e.g. the ribs and spars cannot be placed before the outer shape is computed or the input file loaded. Therefore, a declarative coding style does not lead to an advantage for the application of a model generator, wherefore an imperative coding style is used for the implementation of the ELWIS model generator. The main disadvantage of declarative coding is the unclear program structure, which is avoided by the use the imperative programming. For an imperative coding style, no strict functional coding is required, wherefore it is not applied. A nonfunctional programming has the advantage that parameters can be further developed by different functions, without changing the parameters name every time. For example ELWIS, computes the real ribs first, which is followed by various virtual ribs due to different reasons (see chapter 3.3.1). In this example each function adds a rib to the parameter where the resulting mesh is stored, which leads to a clear program structure.

The main advantage of backward chaining is the computational efficiency, as only these computations are performed which are required. An approach which has the same goal is implemented in ELWIS. First, a check is performed, which outputs need to be generated, which wings (of the several defined wings) should be created, which flaps should be included in the wing and so on. Then, only these computations are performed which are required to compute the demanded output.

The way of structuring data is similar to the approach in frame based systems. This means that all parameter are stored in hierarchical data structures, as it is standard in object oriented programming.

2.2.5 Software Languages and Analysis Tools

In the following sections, an overview of the different software languages and analysis tools is given. The structural analysis and sizing is implemented in the FE-program ANSYS, the aerodynamic loads are computed with the vortex-lattice program AVL, while all other tools are implemented in Matlab.

ANSYS

For the structural finite element model, an FE solver is required. As the self-implementation of an FE solver would be a very time-consuming and therefore inefficient task, the commercial solver ANSYS (ANalysis SYStem) is used. ANSYS is one of the major finite element programs, offering a wide range of applications. ANSYS offers different 1-, 2- and 3-dimensinal elements and can be used for linear and non-linear analysis. An important advantage of ANSYS is the possibility to perform multi-body simulations, which is required for the modeling of the flaps and the landing gear. For the connection of the different bodies in such simulations, it is possible to use a wide range of different joint and slider elements [105].

Another advantage of ANSYS is the ANSYS internal script language APDL (ANSYS Parametric Design Language). In this study, APDL is used for the implementation of the structural analysis and sizing module S_BOT+ (Sizing roBOT+).

In other wing mass estimation tool chains (such as in [24]), the structural analysis is performed with an FE solver, whilst the sizing is performed by another tool, implemented in a different language. The use of APDL leads to the advantage that both, the structural analysis and the sizing, can be performed in ANSYS. Therefore, no interfaces are needed between these two parts, which simplifies the implementation and increases the computational speed. Additionally APDL is very efficient in vector operations, which allows the implementation of a fast sizing algorithm.

AVL

For the computation of the aerodynamic pressure distribution, a method based on the vortex-lattice theory is chosen (see chapter 2.2.1). For this computation, the software AVL (Athena Vortex Lattice) [94] is used. AVL is developed by Joungren and Drela from the Massachusetts Institute of Technology (MIT) since 1988.

One advantage of AVL is that it is freeware, which avoids license costs. In addition, the source code of AVL is available, so that modifications can be implemented. As it will be shown in chapter 3.4, it was necessary to slightly modify the AVL source code. AVL is written in FORTRAN, wherefore its computation is very fast.

However, the most important advantage of AVL is its flexibility. With AVL, a wide range of different wing shapes as well as number of wings and fuselages can be computed. This is needed to fulfill the requirement of the research question that it must also be possible to analyze *novel configurations*.

MATLAB

For the WINGmass tool chain, several tools need to be developed. Namely these are the model generator ELWIS, the computation of the engine, landing gear and fuel loads, the framework for the AVL loads computation, the post-processing routine and the WINGmass framework itself. Matlab (Matrix Laboratory) [114] was chosen as the programming language for these tools.

Matlab is a numerical computing environment, which is primary optimized for matrix manipulations. Matlab can also be used for plotting of functions, creation of user interfaces and the implement of algorithms. Matlab allows object oriented programming. Using Matlab, it is possible to start and control external programs, such as e.g. ANSYS or AVL.

In Matlab, it is comfortable to implement and to debug self-written software, as Matlab contains a good editor. Additionally, Matlab contains a wide range of pre-defined functions and toolboxes, which allows quick and efficient programming. By using such toolboxes, it is for example easily possible to read and write xml-files, which is needed for the work with CPACS.

Each program must be able to be improved and updated regularly after its first implementation, even when the original implementer is no longer available. Therefore, it must be ensured, that the successors of the original implementer can familiarize themselves with the software as easily as possible. This is much easier if the successor is already familiar with the programming language. A large number of engineers are familiar with Matlab, as Matlab is often learned during engineering studies. This is different with KBE specific languages like GDL that is used for the MMG of the TU Delft. GDL is a very specific language that can only be handled by a few software specialists. As the syntax of GDL is completely different compared with common languages like Matlab, C++ or Java it is not easy to learn. As shown in the previous chapter, the advantages of such languages are not needed for the implementation of the ELWIS model generator (and also not being necessary for the analysis tools).

Chapter 3

IMPLEMENTATION

Taking the aspects that are described in chapter 2.2 into account, the multidisciplinary WINGmass tool chain is developed. First, an overview over the tool chain is given, followed by the description of the user-oriented parameterization. Next, all analysis models as well as their automated generation process are explained. Finally the structural analysis and sizing as well as the post-processing are described.

3.1 Tool Chain Overview

As described in chapter 2.2.2, the whole tool chain is coupled to the CPACS format. Therefore, a CPACS file is used as input for and output of the chain. The CPACS input file is read by the central multi-model generator ELWIS at the beginning of the chain (see Fig. 3.1). ELWIS generates the tool-specific inputs for all analysis modules, the post-processing routine and the overall WINGmass control routine.

Next, the analysis modules for the loads computation are started: The aerodynamic loads are computed by AVLloads (Athena Vortex Lattice Loads) while the secondary loads are computed by ESEL (Finite Element Secondary Loads). Secondary loads are all non-aerodynamic loads. These are the loads due to the fuel inside the wing, the engine thrust and the ground loads that are transferred from the landing gear in the wing. As the secondary loads depend on the resulting angle of attack of the aerodynamic computation, the aerodynamic loads are computed first.

After the loads computation, the structural analysis and sizing routine S_BOT+ (Sizing roBOT+) is started. S_BOT+ loads the finite element model, applies the loads and analyses all load cases. Based on this analysis, the sizing is performed and the new element properties are computed and applied on the analysis model. This is iterated until the mass of the model converges. Finally, an output file is created, containing all element properties and the wing deflection of all load cases.

By using the computed wing deflection, all loads are recalculated and the structural analysis and sizing is repeated with the new loads. This loop is repeated until the mass of all lifting surfaces of the model converges.

After the mass has converged, the post-processing routine P2 (Post-Processing) is called up. This routine transforms the element results to the masses that are written into the CPACS mass breakdown. Finally P2 generates several plots (e.g. convergence behavior) and writes the CPACS output file.

3.2 Parameterization

As mentioned in chapter 2.2.4, the user-oriented parameterization is crucial for the wing mass estimation tool chain. Flexibility with regard to unconventional configurations and structural concepts and, at the same time, its simplicity and clarity, also for complex wings are the key requirements for the parameterization.

Several authors have proposed parameterizations for finite element wing models that are used for mass estimation in early design stages:

- The parameterization of the NASA Vehicle Sketch Pad (VSP) [57] and the wing mass estimation tool by Hutchins et al. [115] are very simple wherefore new wings can be generated very fast. However, these parameterizations are only applied for simple straight wings with straight spars and simple distributed ribs.
- Dubovikov [116] of TsAGI defines the planform of the wing by a combination of several triangular or square boxes, with each box representing the area between two ribs and two spars. This means, that the inner and outer ends of the box define the rib positions, while the forward and rear ends define the spars. By using this approach, even complex wing structures can be defined, but the definition process is complex and lengthy, as e.g. one spar is defined by many boxes in spanwise direction. If this spar is moved, all boxes in front and behind the spar need to be modified.
- For the definition of the wing structure of the MMG at TU Delft [25], the internal structure is defined within one 'wing trunk'. A wing trunk is the segment of a wing between two airfoils. Within one wing trunk, simple structural layouts can be defined. By combining several wing trunks, complex structures and wings are definable, as well.
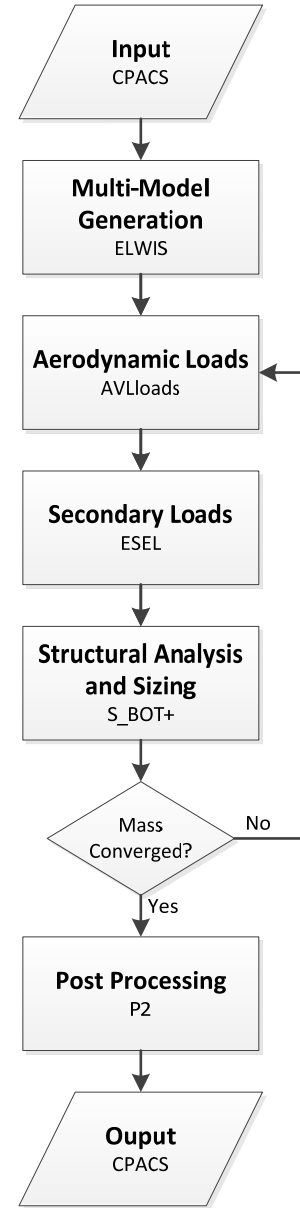
Fig. 3.1: Flow chart of WINGmass tool chain.
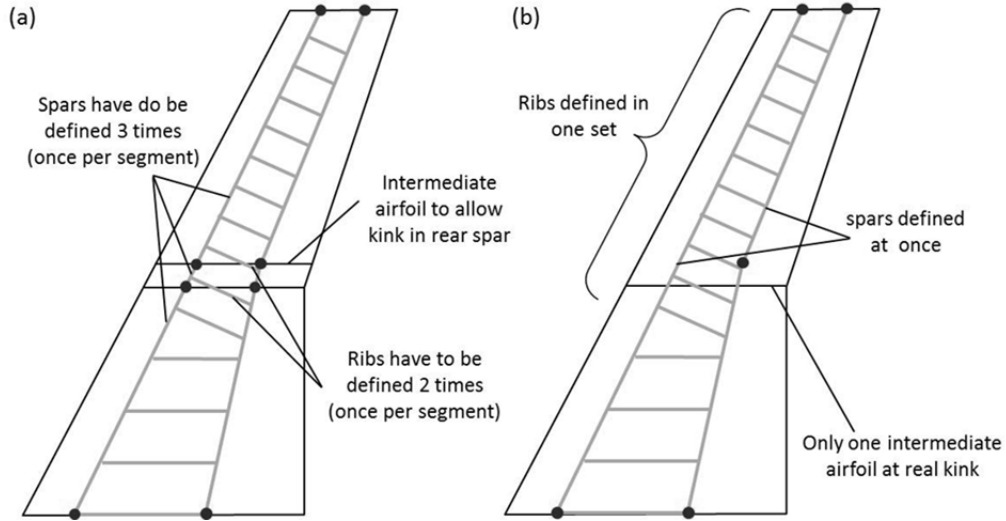
Fig. 3.2: (a) Parameterization of MMG of TU Delft; (b) new CPACS parameterization. The black dots indicate the required spar definition points.

From the described parameterizations, that of the MMG seems to be the most promising, as its ability to define complex structures is shown in several publications. But this parameterizations still has several disadvantages in terms of the simplicity of the definition of complex structures. The main disadvantage of the MMG parameterization is the strict coupling of the definition of the outer shape (airfoils) with the internal structure, which can be shown using the following examples (see Fig. 3.2 (a)):

- One straight spar from root to tip has to be defined separate in each segment of the wing.
- If the spar has a kink at a certain position, a new airfoil has to be defined manually at this position first.
- Should a new airfoil be inserted retroactively e.g. for twist optimization, the structure to the left and right of the new airfoil needs to be redefined manually, although nothing has changed in the structural layout or wing planform.
- Skew ribs, crossing the border of two wing trunks, have to be defined twice, although it is only one rib.

Besides the flexibility of the MMG parameterization, this parameterization has the advantage that the implementation of the model generator is comparatively simple. However, this is to the detriment of the user-friendliness of the parameterization.

As shown above, none of the existing parameterizations meets the requirement of being flexible and simple at the same time. Therefore, a new definition of the wing's internal structure and the high-lift systems is developed in this study and integrated into the CPACS data model. The new development was initiated and led by the author and performed in close cooperation with several partners.

In CPACS, all wing-like structures, such as wings, HTPs, VTPs or canards are defined as wings. The first step in the wing definition in CPACS is the definition of the wing's outer shape.
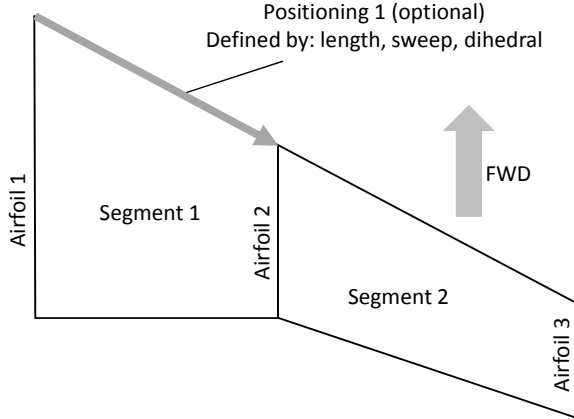
Fig. 3.3: Definition of a simple wing in CPACS.

The outer shape is defined by placing any number of predefined airfoils in the three dimensional space. This placement can either be done by coordinate system transformations or by so called *positionings*. With *positionings* the wing can be constructed with intuitive parameters such as sweep and dihedral. Also a combination of both definition types is possible. After placing of the airfoils, always two neighboring airfoils are combined to one wing *segment* (see Fig. 3.3).

The CPACS parameterization of the wing's outer shape is similar to several other parameterizations, but the newly developed parameterization of internal structures differs. The new parameterization takes the way of thinking of an aircraft designer into account. If an aircraft designer defines the rib and spar layout of a new wing on a traditional drawing board, he would take the planform view of the *whole* wing, would define the spars with a few lines in spanwise direction and would finally draw the ribs between the spars. The new CPACS parameterization follows exactly this approach.

In CPACS, the wing can have almost any shape and can also split up (for example at wing tip fences or H-tails). Therefore, the user has to split the whole wing definition into sub-wings of which he wants to use the planform for further definitions (see example in Fig. 3.4). These sub-wings are called *component segments*. For a conventional wing, the component segment would usually include the whole wing. For a H-tail (half definition), two component segments would usually be created – one for the horizontal and one for the vertical part.

The *component segment* defines the relative spanwise coordinate η and the relative chordwise coordinate ξ. Using these relative coordinates, all further components inside the wing, such as structures, flaps and spoilers can be defined. In a first step, the spars are defined on the wing planform. Therefore, at each position, a spar starts, ends or has a kink, a point is defined in $\eta/$ ξ-coordinates (see black dots in Fig. 3.2 (b)). Next, the spar geometry is defined by a list of these points. Using this parameterization, spars can start, end, have kinks and cross each other at every position on the wing and not only at the positions, airfoils are placed. At the same time, the definition is still simple, short and handy. An example of the definition of a spar is shown in Fig. 3.5.
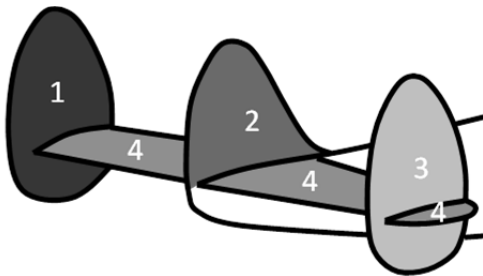
Fig. 3.4: Split of a complex wing in four component segments for further definitions.

e wings		(wing+)
e wing		all(name, description?, par
	@ symmetry	x-z-plane
	@ uID	D150_Wing
	e parentUID	D150_Fuselage
	e transformation	(scaling?, rotation?, transla
	e sections	(section+)
	e positionings	(positioning+)
	e segments	(segment+)
	e componentSegments	(componentSegment+)
	e componentSegment	(name, description?, fromE
	@ uID	D150_Wing_CS
	e fromElementUID	D150_Section1_Element1
	e toElementUID	D150_Section4_Element1
	e structure	(upperShell, lowerShell, int
	e upperShell	(skin, stringer?, cells?)
	e lowerShell	(skin, stringer?, cells?)
	e ribsDefinitions	(ribsDefinition+)
	e spars	(sparPositions, sparSegme
	e sparPositions	(sparPosition+)
	e sparPosition	(eta, xsi)
	@ uID	FrontSpar_P1
	e eta	0
	e xsi	0.10142
	e sparPosition	(eta, xsi)
	@ uID	FrontSpar_P2
	e eta	0.1103
	e xsi	0.10142
	e sparPosition	(eta, xsi)
	@ uID	FrontSpar_P3
	e eta	1
	e xsi	0.33692
	e sparSegments	(sparSegment+)
	e sparSegment	all(name, description, spar
	@ uID	FrontSpar
	e sparPositionUIDs	(sparPositionUID+)
	e sparPositionUID	FrontSpar_P1
	e sparPositionUID	FrontSpar_P2
	e sparPositionUID	FrontSpar_P3
	e sparCrossSection	all(upperCap?, lowerCap?,
	e upperCap	all(area, material)
	e lowerCap	all(area, material)
	e web1	(material, relPos)
	e rotation	90

Fig. 3.5: Example of front spar definition in hierarchical CPACS structure.

Next, the ribs are defined. Ribs are usually placed between two spars or between a spar and the leading or the trailing edge. Therefore, ribs are defined with respect to the spars, the leading or the trailing edge in CPACS. To allow a fast definition of several ribs, it is possible to define rib sets, containing several uniformly distributed ribs. As opposed to the conventional parameterization at the MMG, in CPACS ribs and rib sets can be defined over the entire wing, without regard to the distribution of the outer shape airfoils (see Fig. 3.2).

In CPACS, one default material setting for the upper and the lower shell (skin and stringer) is defined. Different settings on parts of the wing can be defined by *cells*. A cell is a region on the wing that is defined either by relative coordinates or by its bordering ribs and spars. Within these cells, individual material properties for the skin as well as individual stringer properties can be defined. Ordinarily, a user would only utilize cells, to distinguish the material settings of the wing box from the settings of the leading and trailing edge. Structural sizing tools can use these cells to write the detailed skin thickness distribution in the CPACS file.

The definition of the movables (leading edge devices, flaps, ailerons and spoilers) is also inspired by the approach an aircraft designer would chose on the drawing board. As shown in Fig. 3.6, the designer needs to define the corner points of the movable structures on the wing planform in η/ξ-coordinates of the component segments. Next, he can optionally define 3D-properties of the movables such as the airfoils. The definition of the internal structure of the movables is analogous to that of the wing structural definition, but the η/ξ-coordinates refer to the movables instead of the component segment. The deflection path of the movable is defined in a special coordinate system that refers to the hinge line of the movable. This makes the definition comfortable and intuitive for the designer, without the need of thinking on wing sweep or dihedral in the global coordinates.
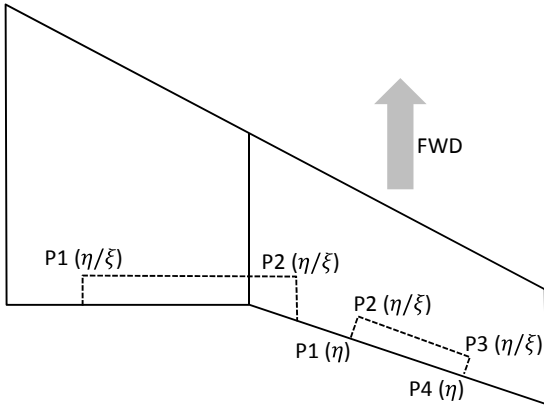
Fig. 3.6: Definition of trailing edge device planforms with 4 (left) respectively 6 (right) parameters.

For the structural analysis in this study, the flap tracks are included. Here, the question which track-related parameter a designer wants to define during preliminary aircraft design arises. The detailed and complex track geometry is not defined by an overall aircraft engineer. Still, the spanwise track position and the kinematic type of the flap track can be defined by such engineers. Therefore, only these two simple parameters and the track materials are requested by the WINGmass tool chain. All further information is computed by the knowledge rules, implemented in the ELWIS model generator. A similar, user-friendly parameterization is chosen for further structures, attached to the wing, such as the landing gear [117] or the engine pylon. Further details of the CPACS parameterization can be found in [118].

In the CPACS wing parameterization, only parameters that describe the real aircraft are included. No parameters that only describe the model can be defined. Therefore, no virtual ribs or spars can be defined in the CPACS wing definition, as would be the case with e.g. the MMG parameterization. This has the advantage that the aircraft designer can focus on the design itself rather than needing to consider the model or the model generation process. A single exception: In the ELWIS tool-specific part of CPACS, the element size of the FE model can be specified optionally. This specification is simple to define, since it is not directly linked to the actual geometry, as virtual ribs or spars would be. If no element size is given, ELWIS uses default values for a medium fine mesh.

The advantages of the new CPACS parameterization become apparent in its growing popularity. Work is ongoing aiming to couple LAGRANGE by CASSIDIAN [119], the MMG of TU Delft [120] and the CEASIOM framework of KTH Stockholm [121] to CPACS and its wing definition.

3.3 Structural Model

The structural model is generated by the ELWIS model generator based on the CPACS parameterization. In ELWIS, the model is created using a strict hierarchical structure as can be seen in Fig. 3.7. On the highest level, all component segments are positioned. Different component segments can be attached to one another or even belong to different wing definitions. However, all component segments are on the same hierarchical level. In CPACS, the movables are defined as cut-outs of the wing. Therefore, the movables are defined as children of the component segments in ELWIS, inheriting several properties from their parent. In case of multiple

slotted flaps or trim tabs on flaps or ailerons, the first movable is the parent of the second movable and so on.

ELWIS treats all lifting surfaces (= wings and movables) in a similar way, as they are all constructed from ribs, spars and skins. For all lifting surfaces, a structured finite element grid is computed from the CPACS data model in an automated process. Therefore, the same program code can be used for all component segments and movables. Small differences occur at the computation of the 3-dimensional key points, which will be explained in chapter 3.3.1.

Besides the lifting surfaces, several additional structures, attached to one or two lifting surfaces, have to be included in the FE model. These structures are for example the flap tracks, the landing gear, the engine pylon or structures for the wing-fuselage connection. In the hierarchical structure in ELWIS each additional structure is the child of one lifting surface. As can be seen in Fig. 3.7, flap tracks, for example, are the children of their flaps and the landing gear is the child of the wing component segment. As these additional structures have a small aerodynamic effect and are not modeled in the aerodynamic load estimation, only the load-carrying parts and no aerodynamic fairings are modeled in the finite element model.

Usually, only one half of the symmetric wing is defined in CPACS. For most analyses, a half-wing model is sufficient, while a full wing model may be required for special analyses. Therefore, the ELWIS user can choose, whether a full- or a half-wing model should be generated. If a full-wing model is demanded, ELWIS automatically copies and mirrors the whole wing definition and a full-wing model is generated. To distinguish between the mirrored and the original wing parts, the uIDs of the mirrored parts are modified with a '_symm' at the end, which is common CPACS standard.
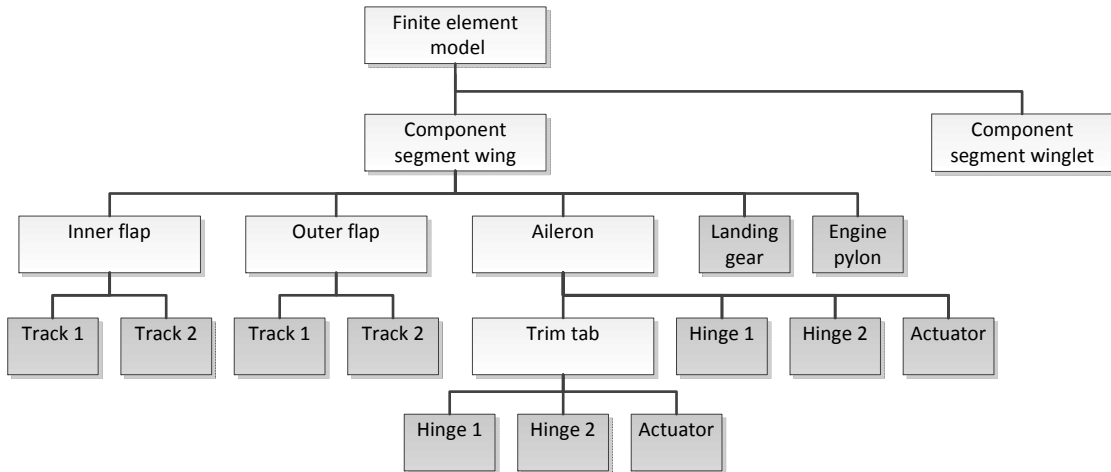
Fig. 3.7: Hierarchical structure of ELWIS FE models of a wing with winglet.

3.3.1 Knowledge-Based Generation of Lifting Surfaces

In a traditional design process, setting up an FE model from a purely geometrical description requires a lot of manual work of FE specialists. All surfaces (ribs, spars and skins) need to be

cut in mainly quadrangular surfaces, in order to ensure a good mesh quality. These cut surfaces must have their borders at the intersections of ribs, spars and skins, at cut-outs or in places where the material changes. In complex wing definitions, this surface segmentation process is well known for being time-consuming. Therefore, the whole process is fully automated in the ELWIS model generation.

To enable the ELWIS model generator performing these tasks, a set of rules that reflect the mental rules, an FE specialist would follow in a manual process is implemented in the model generator. In the following, the approach of the ELWIS model generator is explained, which is directly inspired by an FE specialist's approach: First the wing planform is computed, followed by the segmentation in chordwise direction by placing real and virtual spars. Next the spanwise surface segmentation is performed by placing real and virtual ribs. After the segmentation process is finished, the 3-dimensional keypoints are computed, the element properties defined and the different component segments assembled.

Planform

The outer geometry of the wing and thereby the wing planform is defined by several airfoils, placed in three dimensional space. The airfoils can be placed at any position, can have any orientation and can be scaled to any size. By analyzing of the 3D positions of the leading and trailing edge points of the airfoils, the planforms of the component segments are derived and stored in the hierarchical data structure in ELWIS.

As described in chapter 3.2, the definition of the planforms of the movables in CPACS is carried out with respect to the planform of the parent of the movables. Therefore, these planforms have to be computed after the planforms of the component segments. In case of multi-slotted flaps, the flap that is attached to the component segment must be computed first, followed by the flap, attached to the first flap etc. ELWIS sorts all lifting surfaces in the correct order at the beginning, so that all planform computations can be performed.

Spars

For the chordwise segmentation process, different types of spars need to be considered. The following spars are placed on the wing planform as would be done by an FE specialist (see Fig. 3.8):

- *Virtual spars at the leading and trailing edge:* Usually there is no real spar defined at the leading and trialing edge of the wing. However, the FE model needs a surface border at the leading and trialing edge, wherefore two virtual spars are generated along the leading and the trailing edge.
- *Real spars:* The real spars are defined by the user in the CPACS data model. ELWIS never generates any real spars that are not explicitly defined in CPACS. In CPACS, it is possible to define spars crossing each other without explicitly defining the crossing point or the fact that these spars cross at all. In such cases, ELWIS automatically de-

tects the crossing, computes the crossing coordinates and inserts a new spar definition point.

- *Virtual spars at cut-outs:* At all places, the upper or lower skin has a cut-out in, e.g. due to flaps or spoilers, no elements need to be generated in the FE model. Therefore, a virtual spar is inserted by ELWIS at these positions. If the cut-out is equivalent to a real spar, which can be defined in CPACS, no additional spar is inserted. If the position of the cut-out is explicitly defined in CPACS, this definition is used. If the cut-out is not defined in CPACS, ELWIS automatically computes the cut-out with regard to the outer shape of the movable that is responsible for the cut-out.

  For the cut-out in front of and behind the center wing box, no virtual spars are inserted, as the border of this cut-out is placed on the front and rear spar.

- *Virtual spars due to material definitions:* It is possible to define different material properties in different regions of the skin. To represent the definition in a proper manner, an element border must be placed at the change of material settings. Therefore, a virtual spar is positioned there, if this border is not equivalent to a real spar.

- *Virtual spars due to intermediate structures:* Intermediate structures are structures that are placed between the upper and the lower skin. An example for such structures is a honeycomb structure at the trailing edge of a flap. If such structures are defined in CPACS and the chordwise border is not a real spar, a virtual spar is inserted.
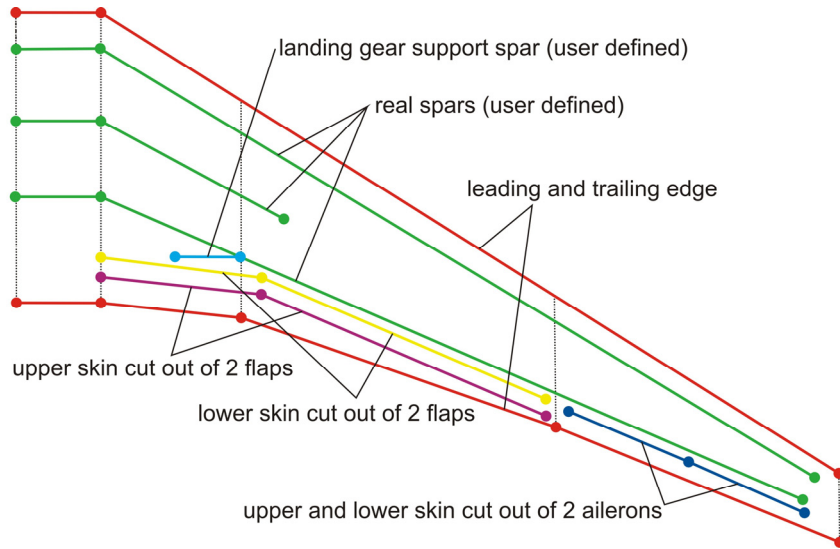
Fig. 3.8: Virtual and real spars, to be placed on the wing planform.

The generation of a structured mesh is the aim of the surface segmentation process. At a structured mesh, the chordwise order of the spars is clearly defined. However, as can be seen in Fig. 3.8, most of the spars are not defined from root to tip. Therefore, a smart function is implemented that defines the order of the spars. This is also performed when short spars are defined at different spanwise location, with no spanwise overlapping.

As already mentioned, spars are not necessarily defined from root to tip. An FE specialist would now extend all spars to the root, respectively the tip. If spars are defined at different

spanwise parts of the wing, it is checked, whether a merging of two spars would result in a better FE mesh, than the individual extension of each spar to the root and tip. The criterion for merging of two or more spars is a combination of the chordwise distance of the spars and the difference in the orientation angle between the already existing spars and the new part that is created between the existing spars. An example is shown in Fig. 3.9, where two spars from the flap cut-out and two spars form the aileron cut-outs are merged to one spar.

If two spars merge beyond a certain point, such as the rear spar and the landing gear support spar in Fig. 3.8, both spars are continued exactly on each other. Before the ANSYS model is created, the double keypoints are detected and deleted. This process is also applied, if more than two spars are have coinciding points. The surfaces at the position at which the spars merge, are triangular instead of quadrangular elements like on the rest of the wing (see Fig. 3.11).

After all spars are extended from root to tip, additional virtual spars are generated to reach the specified element size. The element size can optionally be defined by the user. If no explicit definition is given, ELWIS chooses a medium fidelity element size. An exemplary wing with the segmentation with all real and virtual spars is shown in Fig. 3.9. After the chordwise surface segmentation process, the spanwise segmentation process starts, as it would be done by an FE specialist.

Using the example of the chordwise segmentation process, the advantage of handling the entire component segment at once can be seen nicely. In comparison with the process described by La Rocca et al. in [65], where each aerodynamic segment is considered separately, a process with fewer restrictions, resulting in a better FE mesh, is realized.
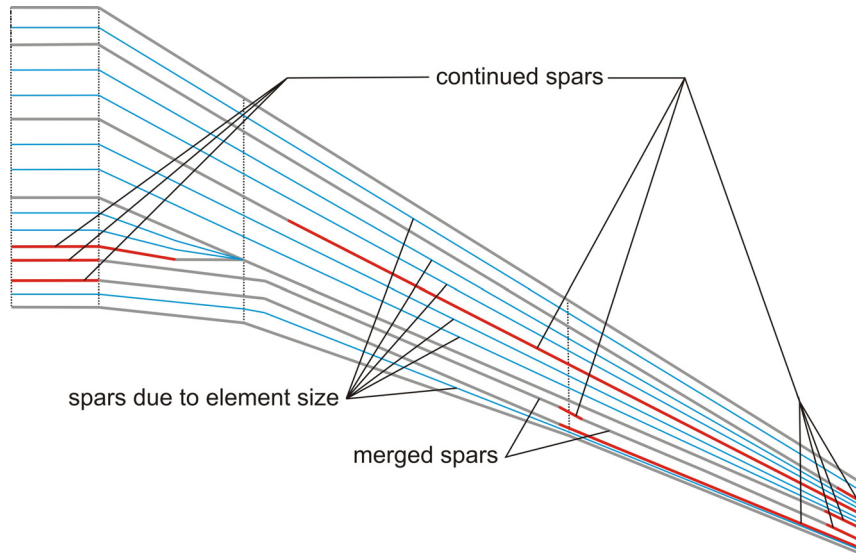
Fig. 3.9: Final spar layout after knowledge-based segmentation process.

Ribs

After the chordwise segmentation process is finished, real and virtual ribs are used for the spanwise segmentation process. As an FE specialist would do, several different requirements have to be considered for the segmentation process. Each requirement is reflected by a virtual or real rib. In detail these ribs are:

- *Virtual rib at the root and the tip.*
- *Real ribs:* ELWIS can handle all kinds of rib definitions that are allowed in CPACS. If ribs are crossing each other, ELWIS automatically detects the crossing point and adds a new rib definition point. If ribs should end after the crossing, ELWIS stops continuing the ribs.
- *Virtual ribs due to kinks:* In case of kinks in the planform, ELWIS automatically inserts virtual ribs at these positions, to ensure that the geometry is represented accurately. This function is optional and can be turned off by the user, as there are several wing configurations where these ribs do not lead to a higher mesh quality. Such a configuration is shown in Fig. 3.10: At the inner kink, a real rib exits while the outer two kinks are very small. Therefore the error in geometry representation is negligible. Additionally, the outer kink rib leads to a worse mesh (see Fig. 3.11).
- *Virtual ribs due to cut-outs.*
- *Virtual ribs due to material definitions of the skin.*
- *Virtual ribs due to intermediate structures.*
- *Virtual ribs due to material definitions of the spars:* If the material properties of a spar should change, a spanwise segmentation is mandatory at this position. If no real rib exists at this position one 'rib point' is inserted. A rib point represents a rib having zero length and no orientation. This rib point is later extended to the leading and trailing edge, similar to all other ribs.
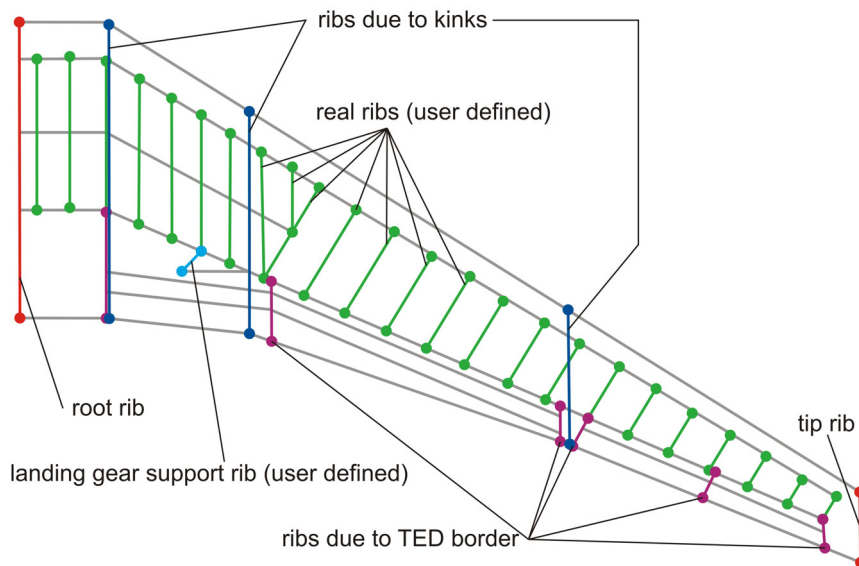
Fig. 3.10: Virtual and real ribs, to be placed on the wing planform.
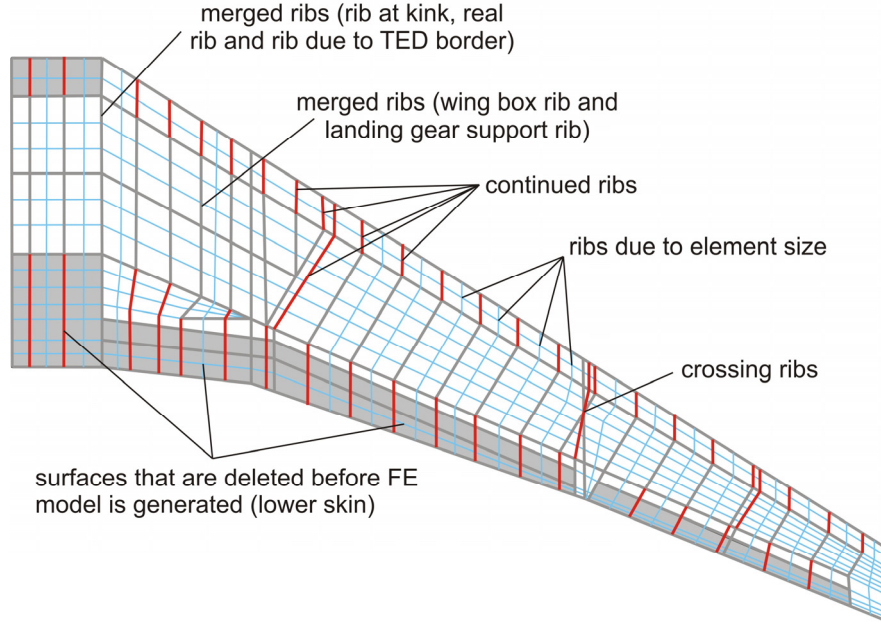
Fig. 3.11: Final rib and spar layout after knowledge-based segmentation process is completed.

- *Virtual ribs at the beginning, ending and kinks of spars:* At every position, where a spar has a definition point, a spanwise mesh border is needed. If this rib does not already exist, a rib point is inserted.

- *Virtual ribs at flap track attachments:* Most flap tracks are attached to the rear spar of the wing. At these positions, keypoints on the rear spar are required. Therefore, rib points are inserted there, if no rib already exists nearby.

Similar to the chordwise segmentation process, the ribs and rib points are extended to the leading and trailing edge (red lines in Fig. 3.11). The orientation of the extension of the ribs is determined with respect to the orientation of the neighboring ribs. Using this approach, a good FE mesh quality is ensured. During the extension process, ELWIS always tries to merge ribs that are defined at different chordwise locations or that lie on top of one another. Ribs are always merged, if this leads to a higher FE mesh quality. Two examples of merged ribs are shown in Fig. 3.11. In case of coinciding rib definitions, double keypoints are detected and deleted automatically.

In case of crossing ribs, a spar has to match the crossing point. This is mandatory in order to get a structured grid, which is the aim of the whole segmentation process. As an FE specialist would do, the three possible options to solve this issue are checked by ELWIS. If the crossing point is very close to a real spar, the crossing point is moved slightly on the spar to ensure a good FE mesh quality. If no spar exists near to the crossing point, ELWIS checks if a neighboring virtual spar can be moved to the crossing point. If this is not possible, a new virtual spar is inserted, matching the rib crossing point.

After all ribs are extended to the leading and trailing edge, the last task of an FE specialist would be to ensure the spanwise mesh size. Therefore, ELWIS automatically inserts virtual ribs to match the demanded element size. Due to namespace reasons, ELWIS generates wing models

with a maximum of 99 ribs and spars. It is easily possible to extend the namespace to 999 ribs and spars. However, as these FE models would require significantly more working memory, the limit is set to 99. If a finer model is demanded by the user, ELWIS modifies the input for the FE meshing in ANSYS. Instead of one element on each segment more elements are generated to match the demanded element size. As can be seen in Fig. 3.12, this higher number of spanwise elements is only applied to the load-carrying structure (wing box) and not to the non-load-carrying elements of the fixed leading and trailing edge. These elements are only used for the load application and do not contribute to the stiffness of the wing. Therefore, more elements would not lead to a better structural representation of the reality but would increase the computational effort.

3-Dimensional Geometry

After the knowledge-based 2-dimensional segmentation process on the wing planform, this mesh is projected on the upper and lower aerodynamic surfaces to obtain the FE mesh of the upper and lower skin. After the keypoints on both skins are computed, an additional layer of keypoints between the two skins is generated. These keypoints are used for the generation of real ribs and spars and as attachment points for additional structures, such as flap tracks or the engine pylon.
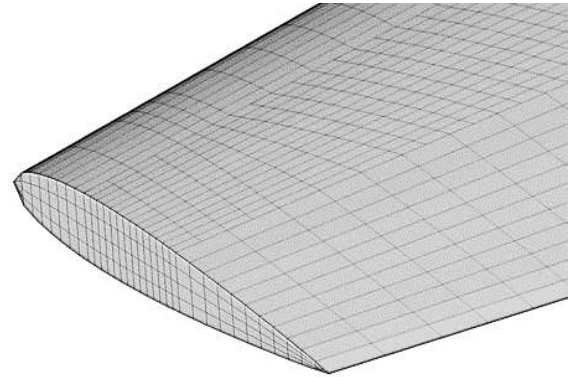
Fig. 3.12: Different element size on wing box and fixed leading respectively trailing edge.

Based on the keypoints, the whole FE model is constructed by an automated process. First, the keypoints are connected with lines, which are used for the generation of surface areas. Next, all areas are meshed, based on the element division that has been computed by the ELWIS model generator. Straight lines are used to connect the keypoints. But for high fidelity analysis, a very fine mesh might be needed. For such meshes, the lines along the ribs can optionally be generated as splines to ensure a smooth surface. For the lines along the spars, splines are not needed, as the surface curvature along spars is much smaller than along the ribs. The dynamic bird strike analysis of flaps generated by ELWIS is an application example of such high fidelity models [123].

The computation of skin keypoints of component segments is performed as follows: First, the normal vector of the planform is computed for each grid point, which is followed by a rotation of these vectors according to the rotation of the corresponding ribs and spars. Next, the intersection point of this vector and the elements of the outer shape definition are computed. To increase the processing speed, a smart function is implemented that estimates which elements of the outer shape definition might be crossed by the vector. Only the crossing points with these elements are computed. This is followed by a check if the estimate was true. If the estimate was wrong, the estimation and the crossing point computation are repeated, based on the new in-

formation. For most of the
points the first attempt is cor-
rect, but especially for strongly
rotated spars and at the areas
close to the leading edge up to
5 iterations may be needed.

Generating the 3D keypoints
of the movables is more compli-
cated, as the airfoils of the
movables are usually not de-
fined in detail during prelimi-
nary aircraft design. However,
for the generation of the FE
model these airfoils are manda-

Fig. 3.13: Knowledge-based generation of TED and spoiler air-
foils, based on parent's geometry. The black dots represent
the control points.

tory. Therefore, an approach is implemented in ELWIS that is derived from the approach an
aircraft designer would choose for the estimation of the movables' airfoils. These estimated air-
foils will not be optimized airfoils, but a good first estimate close to the final airfoil, having simi-
lar structural properties.

The airfoils of spoilers and trailing edge devices are strongly dependent on their parents' air-
foil, as the movable structures and their parents partly share their outer contour. Therefore, the
skin keypoints of the movable structures are computed with the outer shape of their parent first.
In a second step, these keypoints are scaled in height direction to their final coordinates. This
process and the scaling functions are shown in Fig. 3.13. The black dots are used to control the
scaling functions. These control points can optionally be specified by the user. If they are not
specified, ELWIS will use default values for spoilers, ailerons and flaps. These values are derived
from a statistical analysis of existing state-of-the-art aircraft. For flaps and ailerons, the scaling
function is constructed from two ellipses. The scaling function for the spoiler applies only at the
lower skin and is constructed from two straight lines. An exemplary wing including flaps and
spoilers is shown in Fig. 3.14.
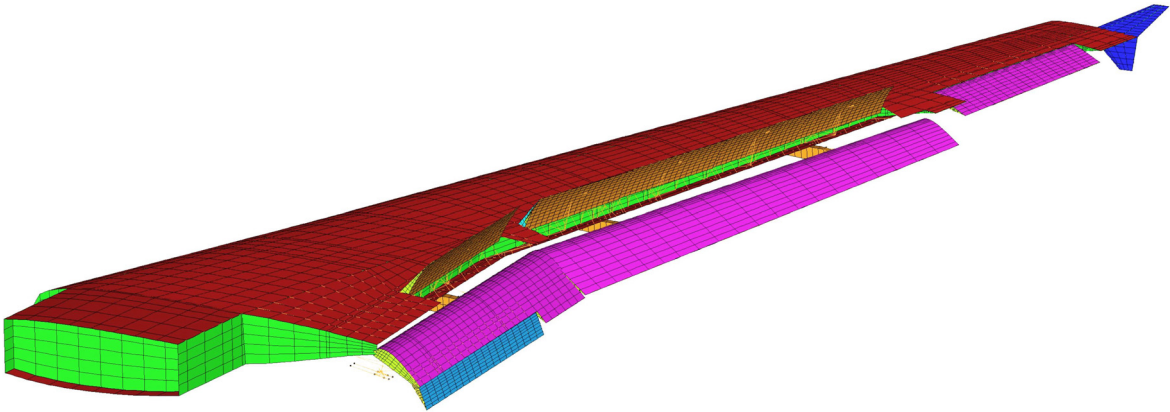
Fig. 3.14: Wing assembly after knowledge-based segmentation process, consisting of 12 lifting surfaces:
the main wing, the upper and lower winglet, the aileron, a single slotted flap, a double slotted
flap and five spoilers.

Element Properties

After the generation of the geometry is performed and the surfaces are meshed, the element properties of the FE model have to be defined. The structural FE model of the lifting surfaces consists of beam and shell elements. The theory behind these element types is described in chapters 2.1.2 and 2.1.4.

All material settings are defined in CPACS and translated by ELWIS into the ANSYS APDL format. The material settings in CPACS are mandatory, as ELWIS never assumes any materials. However, ELWIS does modify material properties, if this is required to ensure correct properties of the FE model. E.g. the stiffness of the skin material in front of the wing box is reduced, as this is a non-load-carrying structure on a real aircraft.

The skins are modeled using FE shell elements. The elements have the thickness and the material properties according to the CPACS definition. If composite materials are defined, multi-layer shell elements are used. Stringers are modeled by an additional shell layer in a smeared representation. This shell layer has the same height as the real stringers and equivalent material properties. The equivalent material properties are computed so that the stiffness of the skin-stringer panel is equivalent to a skin-stringer panel with an explicit stringer model.

Ribs and spars are modeled with shell elements, similar to the skin. But as no stringer can be defined on ribs and spars in CPACS, no additional stringer layer is generated on the shells. The spar caps are modeled by beam elements along the upper and lower spar-skin intersection. The rectangular beam elements have the same width and height as specified in the CPACS input file. In case of composite materials, equivalent material properties are defined for the spar cap beam.

Intermediate structures (filling structures between upper and lower skin) are modeled with volume elements, having the material properties specified in CPACS. For state-of-the-art aircraft, these structures are usually placed in the trailing edge of flaps or within the whole spoiler.

The region of component segments in front of the front spar and behind the rear spar is interpreted as a non-load-carrying structure, as it is the case for all current state-of-the-art passenger aircraft. For flaps, only the part behind the rear spar is assumed not to be load-carrying. Therefore, the elements in these regions must not add stiffness to the load-carrying structures. However, these elements are needed for the application of the aerodynamic pressure forces and this force must be transferred to the wing box. To fulfill these demands, the material properties of these elements are modified as follows: The stiffness of skin elements is reduced by factor of 100, while thickness and density (and therefore their mass) remain as specified in the CPACS file. All real ribs in this region are kept unchanged, while all virtual ribs become real support ribs, having an adequate stiffness, but no mass.

At the areas on the trailing edges, where a movable is applied, real aircraft often have a beam-based support structure to hold the non-load-carrying skin elements. As described in chapter 3.3.2, the ELWIS model generator generates these geometries in an automated process, rather creating the support ribs.

Assembly of Lifting Surfaces

All component segments are generated separately and independently from each other in ELWIS. Therefore, no structural connection between two component segments exists. However, in the example of a wing with winglet (see Fig. 3.14) or an H-tail, different component segments have to be structurally connected. In CPACS, this connection is defined as a wing-wing-attachment. If such an attachment is defined, ELWIS generates rigid links between the neighboring keypoints (respectively nodes) of the component segments. The rigid links are generated between the skins and the spars. Using this approach, even more than two component segments can be structurally connected at one position.

3.3.2 Knowledge-Based Generation of Additional Structures

Most of the structures attached to the lifting surfaces have a complex structural layout. These structures are e.g. flap tracks, engine pylons or the wing mounted main landing gear. They mainly consist of a combination of beam and shell-based components as well as different kinds of hinges. The manual design of these structures is usually performed by a disciplinary specialist in a lengthy and complex process. However, such a process is infeasible for the preliminary wing design phase.

The design of these structures is not an unstructured creative task. Instead, it can be seen as a structured design process, applying a set of engineering rules and taking into account several requirements, restrictions as well as the experience from previous designs. Such a process can be described by mathematical rules and implemented in a computer program, aiming for automation.

To include the additional structures in the WINGmass tool chain, the ELWIS model generator is equipped with the functionality to automatically generate the design of the additional structures. Therefore, a set of knowledge-based engineering rules is implemented for each structure, how this structure is designed. Compared to the surface segmentation process, the knowledge-based generation of the additional structures goes one step further. Here, the whole geometry respectively the design *and* the computational model are generated based on knowledge rules, while 'only' the model is generated automatically during the surface segmentation process.

The user input required by ELWIS for the automatic geometry generation is kept short and simple to understand. The main user input consists of the material settings of the different structural components, as the user should always keep control of the applied materials. For some structures, ELWIS requires an explicit type variable in order to decide which rules should be applied. E.g. the kinematic type of the flap tracks has to be defined. For other structures, such as the engine pylons, the type is derived from the component material settings, as different types have different components. Finally, the position of the additional structure needs to be de-

fined by the user. For the example of flap tracks, this is the spanwise position of the track on the flap in relative flap coordinates.

Tracks and Actuators

All structural connections between a movable and its parent are described in the following section. These connections are different kinematic types of flap tracks for high-lift devices as well as hinges and actuators for ailerons and spoilers. In the current version of ELWIS, 13 different types and subtypes of tracks can be generated automatically. The range of tracks that are implemented represents the most common types of state-of-the-art civil passenger aircraft.

However, some track kinematics of current aircraft cannot be implemented, as there are no ANSYS elements, that can be used to model these kinematics. It is not possible to model tracks with a curved flap track, as the ANSYS slider elements that are used for modeling these tracks, are straight. Such flap tracks are used by e.g. the A310 [78], the B757 [78], the B737 [124] and the B747 [124]. Flap tracks with curved tracks are well-known for being comparatively heavy, which is why they are not considered for newly developed aircraft. As the aim of the tool chain is designing future aircraft, the practical importance of this lack in the chain is negligible.

As shown in Fig. 3.15, most tracks have a massive box-beam structure bearing the carriage, respectively the hinges. This structure connects the primary structure of the wing with the movable parts of the flap track. In real flap tracks, this beam is designed either as an I-beam or more often as a box-beam with internal ribs. The ELWIS model generator models this structure as box-beam with shell elements. All other smaller beam-like structural elements are modeled with beam elements. Hinges, joints and bolts are modeled with joint elements, blocking only these degrees of freedom that are blocked by the real structure. The carriage of the flap tracks is
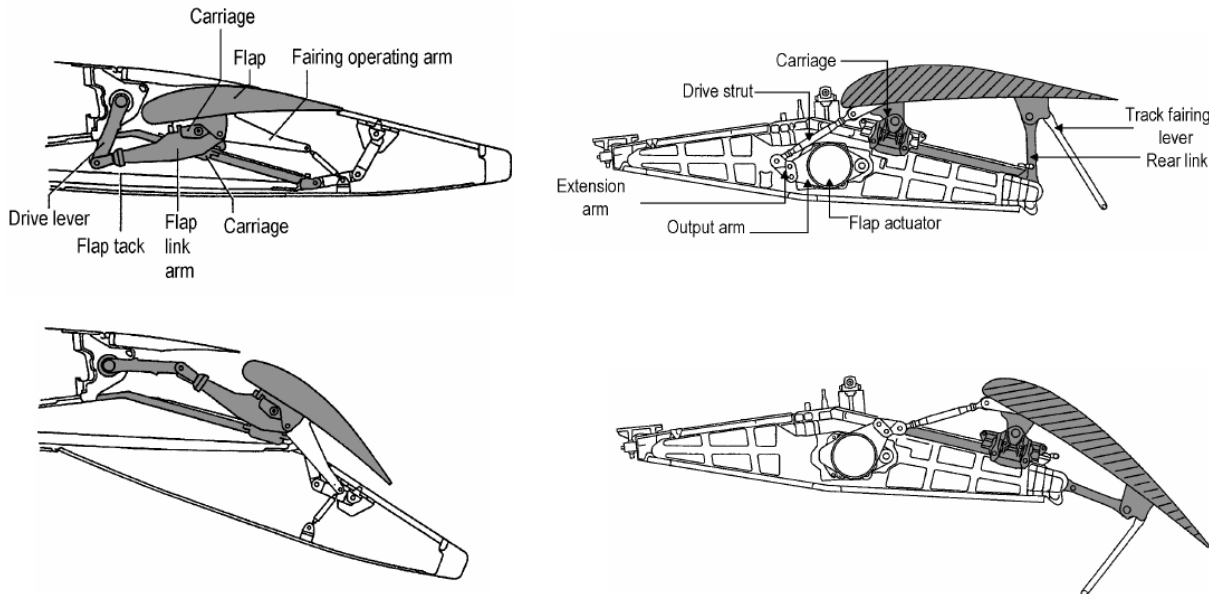
Fig. 3.15: Track kinematics of the Airbus A320 (left) and the Airbus A340 (right) [122].

constructed of several beam elements, ensuring realistic load paths. It is connected with the track by slider elements. A slider element contains one node that can freely translate on a straight track between two other nodes.

The track kinematic is represented realistically. Therefore, the track in the FE model can deflect in a non-linear multi body simulation. The actuation load is the input for this computation. This is used in the structural analysis to generate different solution models, for different load cases. As is described in chapters 3.3.4 and 3.6.1, the deflection process is also a automated process, without any user interaction.

Finally several mass points are included in the track model: mass points are created to represent the mass of the actuators, the hinges and the carriages. Only the load-carrying structure of the tracks is modeled. Therefore, fairings and their kinematics are not taken into account.

In the following, an overview of the different kinematic types that can be created by ELWIS is given (see Fig. 3.16):

- *Dropped hinge 1:* A dropped hinge flap track consists of one simple hinge, similar to the hinge of an aileron. However, this hinge is shifted below the wing to allow a fowler motion. The box beam of the track is attached to the rear spar of the parent as well as to the ribs in front of the rear spar. The rotary actuator is included in the track and attached at the rear spar of the parent in an upside-down position. In [125] it is indicated that such a kinematic will be used for the Airbus A350.

- *Dropped hinge 2:* This type is similar to the *dropped hinge 1*, but the box beam is only attached to the rear spar of the parent, as can be seen in Fig. 3.16. Different non-scientific sources report consistently that this track kinematic is used for the Boeing B787.

- *Link/track mechanism with upside-down forward link:* This type contains a straight track, where the carriage is placed on and an upside-down forward link that is attached to the rear spar of the parent. The track-beam is attached to the rear spar and the ribs in front of the rear spar of the parent. This track type is used for the entire Airbus A320 family [78].
  The specialty of this track type is the integrated functionality of the track
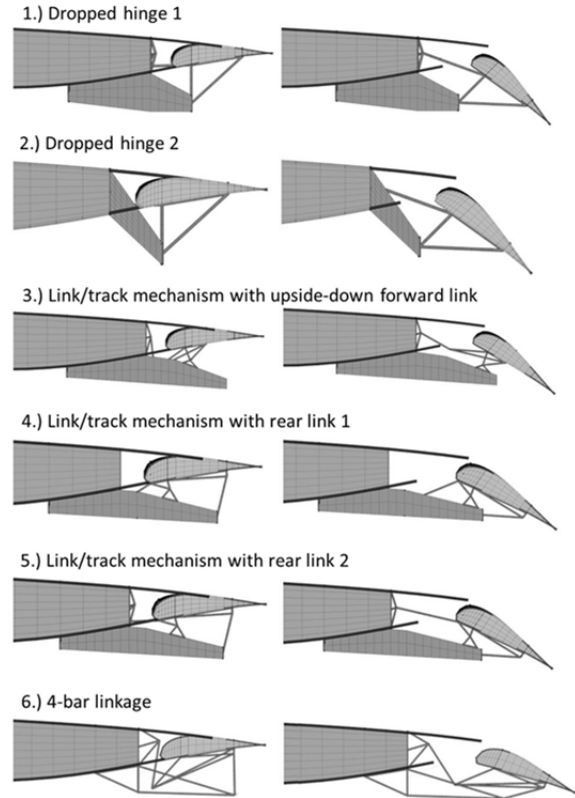
Fig. 3.16: ELWIS flap track models, after automated knowledge-based generation process.

drive. Usually, the actuator only drives the flap while the deflection path is determined by the track. At this kinematic, the drive directly affects the deflection path of the flap (see Fig. 3.15 and Fig. 3.16).

- *Link/track mechanism with rear link 1:* This track contains a straight track and a rear link. The deflection path is defined by these two components, while the drive mechanism is only used as pure drive. The rotary actuator of the drive is placed inside the track beam. This track type is used for the Airbus A330 [78], A340 [78] and A380.

- *Link/track mechanism with rear link 2:* The kinematics of this type are similar to that of the previous one. However, the rotary drive is placed at the rear spar, instead of inside the track beam.

- *4-bar linkage:* This kinematic type contains no carriage. It is constructed with one rear link at the end and a link chain at the front, which is attached to the rear spar of the parent. Instead of a massive track beam, a framework of several beams is used. As actuation, a linear actuator that is attached to the framework is used. The implemented design rules are based on the track of the Boeing 777 [78]. However, 4-bar linkages with slightly different geometries are also used for the Boeing B767 [78] and the Airbus A321 [78].

- *Simple hinge:* This simplest track kinematic contains of one hinge on the hinge line. This hinge is attached to the front spar of the movable and to the rear spar of the parent with several beams. Such hinges are used for ailerons and spoilers.

- *Linear actuator:* This type contains one linear actuator that is attached to the rear spar of the parent and the front spar of the movable. This type is used as drive for ailerons and spoilers.
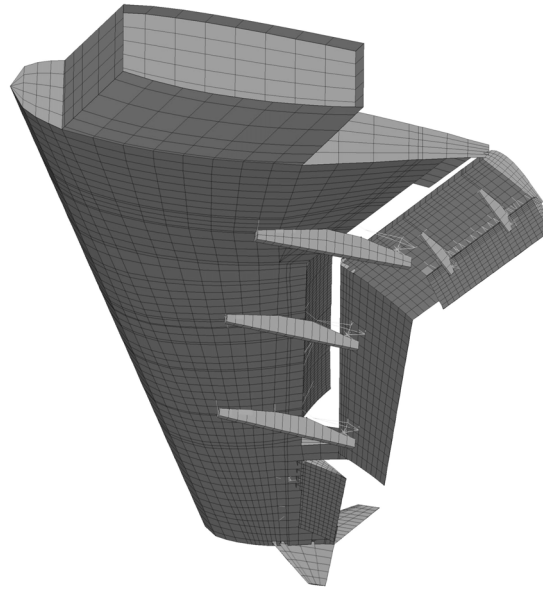
Fig. 3.17: ELWIS wing model including flap tracks.

The inner track of the inner flap is usually placed inside the fuselage, instead of being attached to the wing. These tracks allow the same deflection path, but have a different structural layout due to its different location. As the fuselage is not modeled in ELWIS, no fuselage connection can be realized. In ELWIS, all track types that are used for flaps have a fuselage counterpart. The movable part of the track is equivalently modeled compared to the wing tracks. Instead of modeling the fixed part, the joints on the fixed parts are clamped. On real aircraft, the fuselage track type is not connected by a fixed link to the fuselage. It is attached by several joints, allowing the fuselage track some movement to adapt itself to the bending wing. Therefore a weak clamping is generated by ELWIS, allowing the required movement of the track.

In the following, a description of how the knowledge-based design process is implemented in ELWIS is given. The approach is inspired by the approach, a high-lift expert would choose. For a first design, he would use his experience in combination with mathematical computations, to fulfill the design requirements. The main requirement for flap tracks is the deflection path, respectively the possibility to reach discrete flap positions. The deflection path requirement is usually derived from aerodynamic analysis of the aircraft in takeoff and landing configuration. Such analyses are common already in early design stages. In ELWIS, all tracks are generated with respect to the maximum and minimum deflection position.
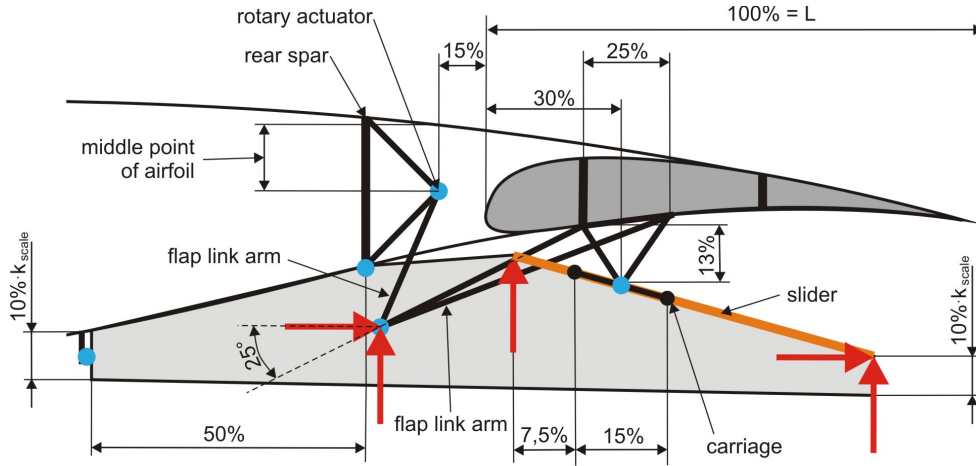
Fig. 3.18: Overview of knowledge-based geometry generation of a flap track (red arrows: dimensions computed from deflection path; blue dots: hinges).

Each track kinematic can be described by the position of the hinges and the connections between the hinges. However, even if the track kinematic and the two flap deflection positions are given, usually several different kinematic solutions exit, which fulfill the requirements. Therefore, in a first step the number of independent variables has to be reduced, until only one possible solution exists. An engineer would use his experience of past designs to do this. In ELWIS, this experience is implemented by mathematical rules, based on existing designs. Therefore, several dimensions of the track are defined with respect to one reference length. Analysis on existing aircraft showed that the track geometry nicely scales with the flap chord. As all tracks of one flap need to have the same reference length, the mean flap chord is chosen. In Fig. 3.18 an example is shown, how the track geometry can be described by using the reference length L and one predefined angle. The red arrows show five parameters that are still missing, but they can be computed from the flap deflection:

- The three slider coordinates are defined by the middle point of the carriage in deflected and retracted position.
- As the angle between the flap link arm and the horizontal line is predefined, the two coordinates in Fig. 3.18 can be reduced to the length of the flap link arm. Only one length of the flap link arm exists, where the required length of the drive lever is the same in the deflected and retracted position.

Dependent on the track positions and the aerodynamic design of the wing, different tracks on the same flap carry different loads. Therefore the geometry of the tracks on one flap differs slightly at real aircraft, although all tracks have the same kinematics and provide the same deflection path. As the loads of the tracks are not known during the geometry generation at the beginning, this cannot be covered by ELWIS. However, if the user expects a track to be high loaded, he can use the optional parameter k_{scale} to scale the height of the track beam on all tracks that apply a box beam design (see Fig. 3.18). This parameter can also be used for a geometry optimization of the track.

As the wings in CPACS can have a general shape including sweep and dihedral, the two dimensional view in Fig. 3.18 is insufficient. To take the dihedral into account, the whole track is generated with respect to a reference plane that is rotated around the aircraft length-axis. The rotation angle is defined by the hinge line that goes from the root to the tip of the flap. This ensures that all flap tracks are generated on parallel planes, which is crucial for their functionality. The sweep has to be taken into account in the orientation of the hinges (blue dots in Fig. 3.18), which is not a trivial task. E.g. in Fig. 3.18, the flap moves back on a line in flight direction on the sliders that are placed within the reference plane. But at the same time, the flap rotates around the hinge on the carriage. The orientation of this hinge is defined by a line between the current position of this hinge and the current position of its counterpart on the neighboring track. Therefore, the rotation is out of the reference plane. This complex movement has to be taken into account in the computation of the exact orientation of the drive mechanism. In general, the orientation of all hinges related to the movable part of the track have to be modified with respect to the 3D position of the other tracks of the flap. In contrast, the hinges that attach the track on the parent are independent from the sweep.

Engine Pylons

The engine pylon connects the engine to the wing. The procedure of designing a pylon is performed step by step and each step can be described by a set of design rules. These rules are implemented in ELWIS and are derived from the approach an engine pylon specialist would choose in a manual design process.

As can be seen in Fig. 3.19, the pylons consist of one massive shell-based box structure, attached to the engine and the wing. By an analysis of state-of-the-art aircraft, two construction principles for engine-to-pylon connections and two for the pylon-to-wing connections can be identified. From the two times two design principles, four different possible pylon designs result. These four designs can be generated by the ELWIS model generator. The two different pylon-to-wing attachments are:

- *Fig. 3.19 (a) and (b):* The pylon is attached to the front spar of the wing with two shackles and one spigot fitting. Between the forward and the rear wing attachment, the pylon has a box beam design, attached to the two load-carrying wing ribs with a triangular shackle at the rear. This principle is e.g. used for Airbus aircraft [126].

- *Fig. 3.19 (c) and (d):* The forward pylon attachment is at the front spar of the wing with two joints and two upper links. The rear attachment to the load introduction ribs is implemented by a drag strut. This principle is e.g. used for Boeing aircraft [126].

The two different engine-to-pylon attachments are:

- *Fig. 3.19 (a) and (c):* The pylon is attached to the engine by bolts. The forward bolts are located at the rear end of the inner side of the fan casing and the rear bolts are located close to the turbine stages. This principle is e.g. used for Airbus aircraft [126].
- *Fig. 3.19 (b) and (d):* The pylon is attached to the engine by bolts at the outer side of the fan casing at the front and bolts close to the turbine stages. These bolts are oriented in flight direction and are not carrying the engine thrust force. The thrust force is carried by two tangent links at the side of the engine. This principle is e.g. used for Boeing aircraft [126].
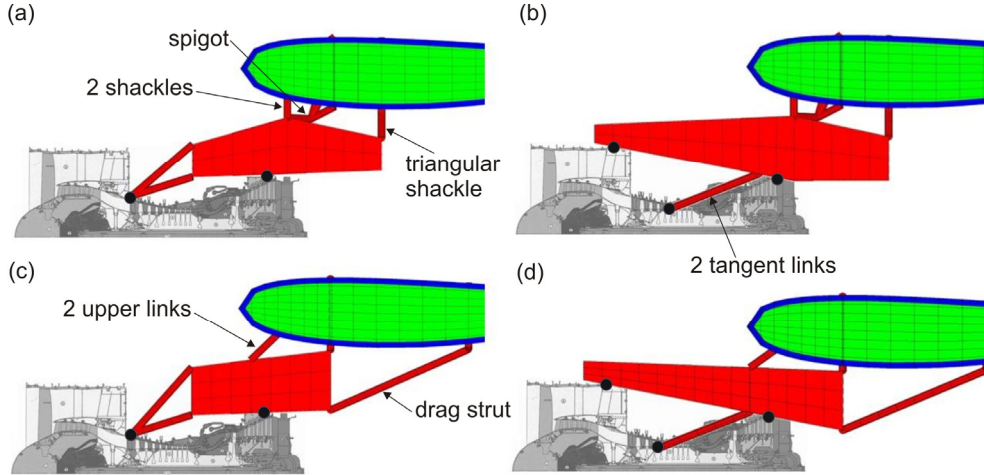
Fig. 3.19: Engine pylon types that can be generated by ELWIS. Black dots indicate connection hinges to the engine (CFM56 cutaway from [127]).

ELWIS determines the pylon type from the user-given material properties. In CPACS, one set of material properties can be defined for each component of the pylon. For example if the material settings for the drag strut and the tangent links are given, a pylon of the type (d) in Fig. 3.19 is generated. After the type is determined, the corresponding engineering design rules are applied and the pylon model is generated. Beside the material settings, ELWIS is using the wing and engine geometry as well as the position of the engine to generate the pylon model.

The pylon box is modeled with shell elements, while all other components are modeled with beam elements. All bolts and the spigot fitting are modeled with joint elements, blocking the corresponding degrees of freedom. The aerodynamic fairings are not modeled, as they are not load-carrying. In addition, no aerodynamic loads should be applied on the pylon in the WING-mass tool chain, wherefore there is no need to model the fairings. The engine itself is modeled as point mass, connected via rigid links to the bolts of the engine pylon. This point mass is used to apply the engine thrust force in the structural analysis.

Landing Gears

The main landing gear (MLG) of state-of-the-art passenger aircraft is attached to the wing. Therefore, additional loads are transferred to the wing that have to be considered for the sizing of the wing structure. Similar to the already mentioned additional structures, the generation of the MLG is performed automatically by the ELWIS model generator. The MLG module was developed by Klatt [128] under the supervision of the author. The details of the module are explained in [128]. Therefore only a short overview of the different kinematic types is given. There are three different options, how the landing gear can be attached to the wing:

- *Attachment using a rear support beam (Fig. 3.20 (a) and (d)):* If a rear support beam should be used, it is automatically created as a double-T beam. The MLG is attached to the rear support beam and the rear spar. As no fuselage is modeled, the inner end of the rear support beam is clamped.

- *MLG is attached to one spar (Fig. 3.20 (b) and (e)):* If the MLG is placed in front of or behind a real spar, a shell-based structure, similar to the landing gear support spar and rib, is created automatically. The pintle-strut is connected with beam elements to the spar and the created shell structure.

- *MLG is attached to two spars (Fig. 3.20 (c) and (f)):* In this case the pintle-strut of the landing gear is connected with beam elements to both spars.
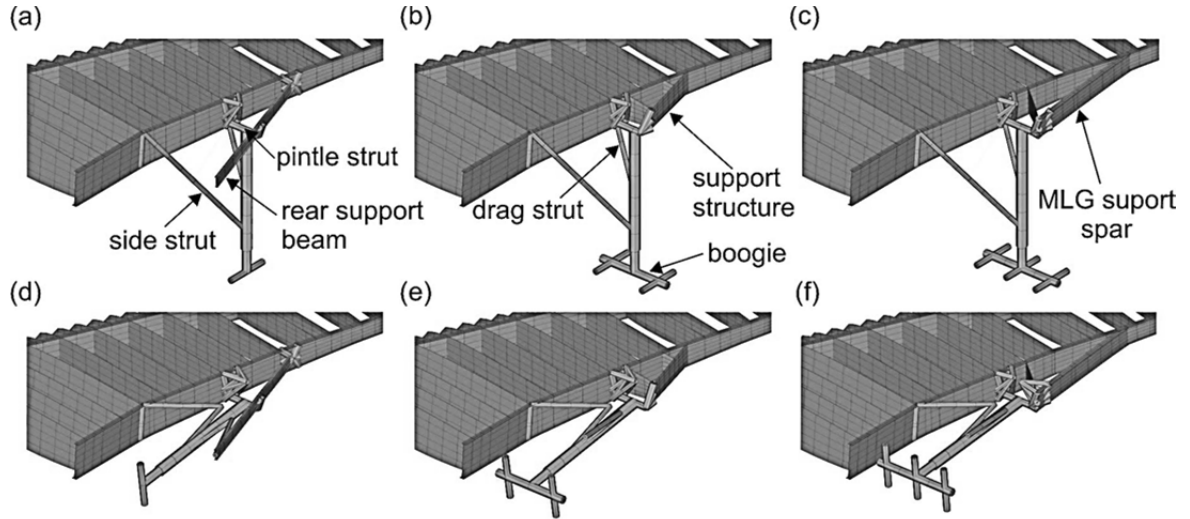
Fig. 3.20: Examples of MLGs that can be generated by ELWIS.

Independent from the wing attachment type, the MLG can be created either with one side strut and a drag strut (Fig. 3.20 (a) - (c)) or with two side struts and no drag struts (Fig. 3.20 (d) – (f)). The first possibility is traditionally preferred by Airbus, while the second one is used at several Boeing aircraft as well as the A350. The boogie and the axles are created automatically with respect to the user-defined number of wheels. The number of wheels is independent from the other components of the MLG.

The MLG is generated in extended position. But as ELWIS creates ANSYS multi-body models, including joints and actuators, the landing gear can retract, dependent on the load case. On real aircraft, landing gears in retracted position are not held by the landing gear actuator. Instead, the lower end of the main strut snaps in a hook, which holds the landing gear during flight. The hook is attached to the fuselage. This is handled in the WINGmass chain by clamping the corresponding node of the main strut, if the landing gear is retracted.

Fixed Trailing Edge Support Structure

As mentioned in chapter 3.3.1, the stiffness of the skin elements between the rear spar and a movable is reduced by a factor of 100. To avoid unrealistic deformations and to transfer the aerodynamic load on these elements to the rear spar, a so called fixed trailing edge support structure is generated by ELWIS. This structure is only generated at positions where a flap or a spoiler is placed. Otherwise additional ribs are used to transfer the loads to the rear spar. As it can be

Fig. 3.21: Automatic generated fixed trailing edge support structure.

seen in Fig. 3.21, this structure is constructed from beam elements and is created at each virtual and real rib station. Similar designs are used at current state-of-the-art aircraft. The generation of the support structure is implemented by engineering rules, wherefore the material settings are the only required user inputs.

Wing-Fuselage Attachment

Although the fuselage is not part of the presented tool chain, the structural connection has to be considered to ensure realistic load paths. For conventional low-wing configurations, no additional structural components are needed. The wing can be clamped along the symmetry plane and at the root rib. However for high-wing configurations and tails, the wing-fuselage connection is usually realized by several bolts, respectively the trim actuator of the HTP. ELWIS connects the bolts respectively the trim actuator to the wing box by a beam-based structure. If the user specifies the trim actuator in CPACS, ELWIS models the actuator similar to the linear actuator of an aileron. This means, that the HTP can be deflected according to the load case description like a flap or an aileron.

In CPACS, the positions and orientations of these bolts can be defined. The geometry of the attachment of the bolts on the wing is computed by applying mathematical rules. ELWIS checks the position of the bolts relative to the skins, ribs and spars of the wing. Dependent on this relative position, the beam-based attachment structure between the bolts and the next spar, rib or skin is generated. The bolt itself is modeled as a hinge, connecting the attachment structure on the one side and a clamped node on the other side. In case of a trim actuator, the actuator is clamped on the fuselage side and connected with a joint to the attachment structure.
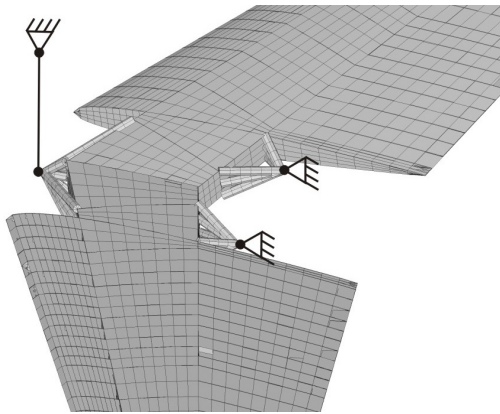
Fig. 3.22: HTP including wing-fuselage attachment (trim actuator is displaced as line).

In Fig. 3.22, an example of a HTP including the wing-fuselage attachment structure is shown. Behind the rear spar, two hinges are attached to the rear spar – one on each side. On a real aircraft, these hinges are connected with the fuselage structure. In front of the front spar, one attachment is generated in the middle of the HTP, on which the trim actuator is placed.

The described modeling approach is very user-friendly and flexible. For a continuous wing-fuselage attachment at low-wing configurations, the user has to define only the root rib. For all other attachments, the attachment positions and the material properties of the beam structure have to be defined in addition. The whole geometry of the attachment structure is computed automatically by ELWIS. Using this modeling approach, the attachment structure of VTPs, HTPs or high wing configurations can be generated by the ELWIS model generator.

Interconnection Struts

As shown in Fig. 3.23, the interconnection strut is a structural connection between two neighboring flaps. Under normal condition, no load is carried by the strut. But in case of a broken actuator, the strut acts as second load path. In place of the actuator, the load is taken over by the neighbor flap. To allow the normal relative deflection between the two flaps during the flap extension, the interconnection strut is designed as hydraulic cylinder, allowing a certain free movement. If the actuator breaks, the allowed deflection is exceeded and the interconnection strut blocks.

The mass of the strut is not relevant for the purpose of wing mass estimation. However, the described load cases are critical load cases for the flap bodies and the flap tracks, wherefore they have to be considered in the WINGmass tool chain. Therefore, the interconnection strut is included in the finite element model.

The analysis type of the structural analysis in the sizing routine is linear static. Therefore, a model representation of the strut, allowing a certain free movement between two borders is not expedient, although it would be possible in ANSYS. It is decided to model the strut in the blocked position as rigid beam. To avoid, that the strut takes over loads in non-failor load cases, the strut is automat-
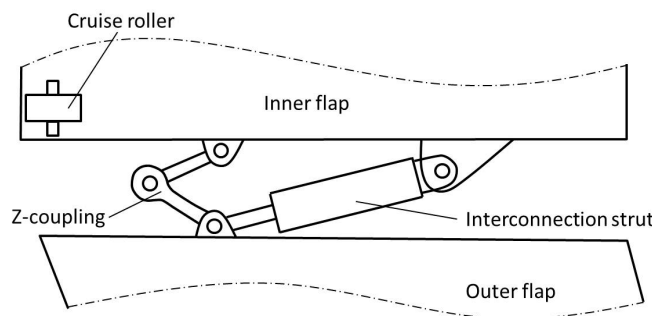
Fig. 3.23: Sketch of two coupled flaps including cruise roller, z-coupling and interconnection strut.

ically deleted by the sizing algorithm for these load cases (see chapter 3.6).

For the generation of the strut, the user has to define the positions of the two hinges and the material settings of the attachments. The geometry of the attachments is generated automatically by ELWIS with beam elements. Therefore, engineering design rules are implemented, how the attachments on the flap ribs and spars have to be designed.

Z-couplings

Some aircraft are fitted with so called Z-couplings (see Fig. 3.23). Z-couplings couple two neighboring flaps in height direction, but not chordwise or spanwise. As the middle joint of the Z-coupling is a spherical joint, the rotational degrees of freedom are not blocked. These couplings are installed for static reasons and to prevent structural damage through counter wise vibrations of the flap ends. Their weight is unimportant for the purpose of wing mass estimation, but as they influence the deflection of the flaps under aerodynamic loads, they have to be modeled for a realistic representation.

Similar to the interconnection strut, the user has to define the attachment positions as well as the materials. Based on this data and the flap geometries, the Z-coupling is generated by ELWIS based on implemented engineering rules. The coupling is modeled by a combination of beam and joint elements.

Cruise Roller/Midspan-Stops

During flight phases with retracted flaps, the bending lines of the wing and the flaps are only linked at the flap tracks. Due to different loads and stiffness, the spanwise bending curve can differ between the tracks or at the end of the flap. For a good aerodynamic performance, the bending curves have to be very similar during cruise flight. Therefore, so called cruise roller respectively midspan-stops are installed at some aircraft.

These components consist of a small roll, which is installed at the leading edge of the flap (see Fig. 3.23) and a small track, attached to the rear spar of the wing. In retracted position, the roll drives on the track, which blocks the deflection of the flap in height direction. This modifies the bending line of the flap and makes it very similar to the wing bending line.

ELWIS models the cruise roller with several beam elements that are attached to the front spar of the flap and the rear spar of the wing. The roller/track construction is modeled by a special kind of hinge that only blocks the height degree of freedom. In CPACS, the user has to define the position of the cruise roller and the materials of the attachments.

3.3.3 Model Optimization Settings

The sizing of the finite element model is performed separately for each element in a first step. In a second step, several elements are combined to sizing/optimization regions, where the com-

puted values (e.g. thickness) are made equal for all elements. This approach takes weight increases due to manufacturing reasons into account. In addition, it leads to a better convergence behavior of the sizing algorithm. The optimization regions are also used to specify different sizing parameters for different regions. E.g. the minimum thickness, the safety factor or the sizing criteria might be different for different parts of the wing.

These regions have to be specified before the sizing starts. In a manual process, the FE specialist would select the elements, combine them and specify the sizing parameters for each region. Depending on the sizing algorithm, often more than 20 sizing parameter have to be specified for each region. This manual process is time consuming and tedious and therefore error-prone, as the rules that are applied are usually very simple. Such a rule for the segmentation process can e.g. be "one new optimization region after each rib/spar/skin intersection" (see Fig. 3.24). The set of sizing parameters is often the same for all optimization regions on e.g. the upper skin. Therefore, this process is well suited to be automated by a knowledge-based process, which is implemented in a computer program.
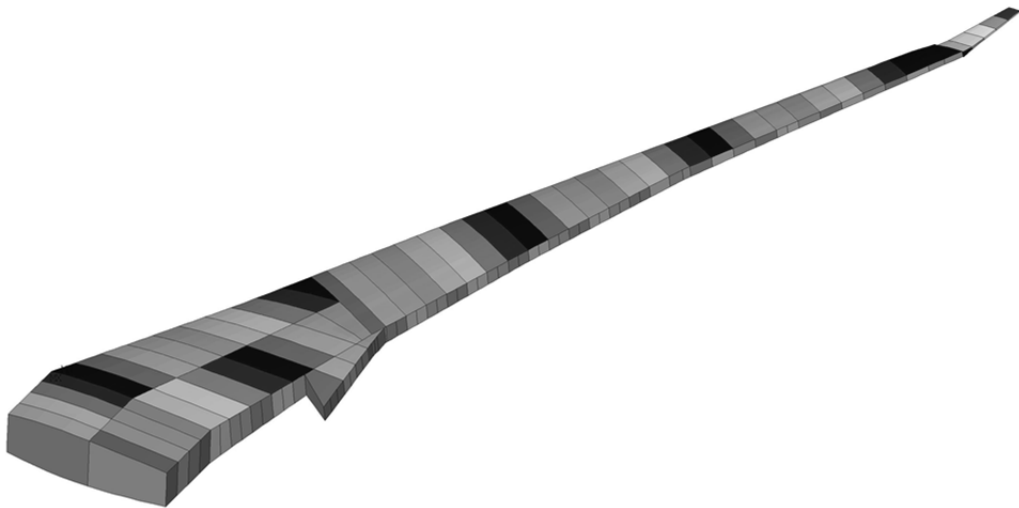
Fig. 3.24: Automatic generated optimization regions on a finite element wing model.

In the WINGmass tool chain, this process is implemented in the ELWIS model generator. The optimization parameters can be specified in the tool specific part of the CPACS definition on a global point of view for the whole wing. But it is also possible, to go deeper in detail and specify part specific optimization parameters on different levels of detail. Parameters that are not given are set by ELWIS with proper values. For the segmentation for the stress sizing on lifting surfaces, currently four different options are implemented in ELWIS:

- No optimization and therefore no sizing areas.
- One sizing area between each rib and each spar.
- One sizing area between each rib and the front and rear spar.
- One sizing area for the whole upper and lower skin, each spar and each rib is one sizing region.

Usually, each rib is a separate sizing region in all cases. However, the root rib is used to clamp the wing. Therefore the loads on the root rib are unrealistic which would result in unrealistic sizing results. Therefore, the root rib and its inner neighboring rib are combined to one sizing group, which results in more realistic thickness results for the root rib. This coupling of the two ribs is only performed, if the wing should not be used together with a fuselage, as there is no clamping on the wing in this case.

In the case of flaps, the fixed leading edge is load-carrying, wherefore also optimization regions are generated there. An example for the second segmentation option is shown in Fig. 3.24. This wing includes one mid spar in the inner part and merging ribs at the end of the mid spar.

For the additional structures, three options for the sizing groups are implemented:

- No optimization and therefore no sizing areas.
- One sizing area for each area (shells) or line (beams).
- One sizing area for similar areas or lines, e.g. the sidewalls of the box beam structure of the track in one optimization region.

Beside the stress optimization regions, the sizing algorithm S_BOT+ needs regions for the buckling/stability as well as for the stringer sizing. The buckling regions are defined by the physics of the wing. Therefore, they are generated automatically, without any user-defined options. For the stringer sizing regions, currently one option is implemented. Each region, where a set of stringers is defined, is one stringer optimization region. For example if only one stringer set is defined for the whole upper skin, all stringers will be sized together, but if different sets are defined in spanwise or chordwise direction, each set will be sized separately.

3.3.4 Rigid Body and Deflection Templates

As it will be described in chapter 3.6, one separate solution model is generated in S_BOT+ for each deflection case. A deflection case represents one set of movable and landing gear settings. For example one deflection case might be the cruise case with all flaps and the landing gear retracted. Another case would be the approach case with all flaps in landing configuration and extended landing gear. To enable S_BOT+ to move the movable structures and the landing gear, two additional ANSYS APDL files are generated.

The deflection is performed by a non-linear multi-body simulation in ANSYS, which is numerically expensive. To reduce the numerical effort, the elements from each movable lifting surface are replaced by one rigid body element. In addition, all component segments and unrelated additional structures are deselected during the solution process. Therefore, only the elements of interest (such as the flap tracks) are remaining, which leads to a more efficient computation. The first additional input file contains all commands that are needed to generate these rigid bodies.

The second additional input file contains all commands that are required for the deflection process itself. The commands in this file deflect the movable structures with respect to a predefined relative deflection parameter for each movable respectively the landing gear. This relative

deflection is derived from the load case description by S_BOT+ and has a value between zero and plus one for flaps, spoilers and landing gears, respectively a value between minus one and plus one for ailerons.

3.4 Aerodynamic Loads

The aerodynamic pressure loads are computed using the freeware code AVL (Athena Vortex Lattice) [94]. AVL was developed by Joungren and Drela from the Massachusetts Institute of Technology (MIT) since 1988 and is used in many preliminary aircraft design projects. AVL is based on the vortex-lattice theory, which is derived in chapter 2.1.1.

The model generator ELWIS generates one AVL geometry input file for each load case, as the Mach number or the flap deflection. Therefore the AVL geometry can differ for each load case. The computational time for loading a geometry file is negligible, wherefore no disadvantage appears, if several load cases have the same geometry file.

The AVL computations are controlled by the module AVLloads. AVLloads runs all AVL computations, interpolates the resulting pressure distribution on the structural grid and writes the pressure loads output file. If the wing deflection from a prior structural analysis exits, AVLloads modifies the geometry input file accordingly.

As it is shown in chapter 4.1, a very dense mesh of vortexes is needed for the application of load estimation on high-lift configurations. However, the freeware version of AVL has a low number of maximum vortex elements, wherefore a modified version of AVL is used. The modifications where performed by Moerland [129]. In detail, he increased the maximum number of elements, wings and strips until the maximum possible number according to FORTRAN limitations was reached.

3.4.1 Model Generation

The vortex elements of a vortex-lattice mesh are arranged in a structured mesh, which is generated by the ELWIS model generator for each load case. The AVL model can contain all wings and fuselages, which are defined in CPACS. The full CPACS flexibility in terms of wing geometry can be handled by the ELWIS model generator. Therefore, also complex wing structures, such as splitting wings, can be generated. The wings include an explicit representation of the flaps and slats. Their chordwise deflection (fowler motion) as well as their change in angle of attack is represented in the model. Therefore, the vortex elements that represent the flaps are moved in x-direction according to the fowler motion. The deflected angle of attack of the flaps and slats is modeled by a rotation of the normal vector of the vortex element. According to Werner-Spatz [130] and Werner-Spatz et al. [131], this modeling approach leads to the best results.

The program functions in ELWIS that are used for the vortex-lattice mesh generation are the same as used for the structural models, which is described in chapter 3.3.1. Only the input of the functions differs, as different kinds of ribs and spars are used to generate the vortex-lattice mesh.

In the structural model, all ribs and spars are generated between the leading edge ($\xi = 0$) and the trailing edge ($\xi = 1$) of the wing. But due to the chordwise deflection of the flaps and slats, vortex elements (and therefore ribs and spars) in front of the leading and behind the trailing edge are needed. Therefore, the planform is extended in chordwise direction by the introduction of additional spars at $\xi = $ -1 and $\xi = 2$ (see Fig. 3.25 (a)). This approach virtually extents the planform of the wing wherefore the mesh generating function believes that there is a larger planform. In the next step, all needed ribs and spars are inserted in the model. For the vortex-lattice model, ribs are inserted at the root, the tip, the kinks and the spanwise borders of leading and trailing edge devices. In addition to the spars at the leading and trailing edge of the component segments, spars are introduced along the leading and trailing edge of the movable structures in deflected position, according the load case description. Such a rib and spar layout is shown in Fig. 3.25 (a).

Modeling the translation of the leading edge devices (LEDs) in the aerodynamic computation, while not modeling them in the structural model, leads to issues in the interpolation of the load on the structural grid, as both wing planforms do not fit together. Therefore, the translation in x-direction of the LEDs is currently not used, unless the LEDs are also included in the structural model. Tests showed that this has a negligible effect on the load distribution on the wing.

The sequence of model generation of the vortex-lattice model is the same as for the structural model: first all ribs and spars are introduced. Next ribs and spars are extended to the root/tip respectively leading and trailing edge and merged if possible. No ribs and spars are inserted due
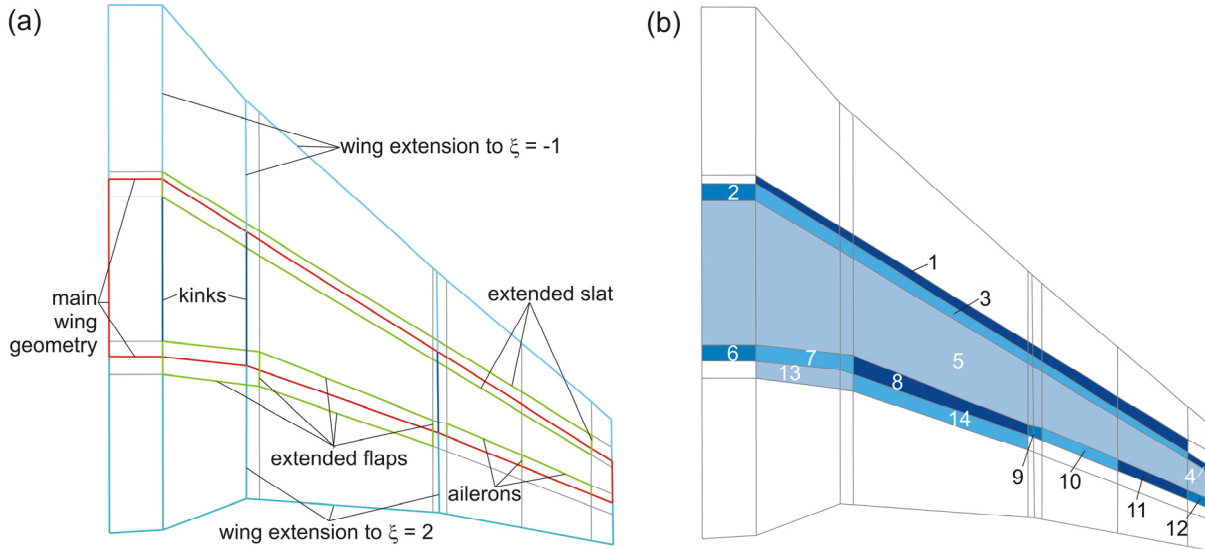
Fig. 3.25: (a) Ribs and spars for the generation of a vortex-lattice structured mesh; (b) different wings of the AVL geometry definition.

to the element size, as the element size in chord and spanwise direction can be defined in AVL for each segment. The element size can either be specified by the user or is set by ELWIS.

In AVL, all spanwise element borders (= ribs) have to be aligned exactly in flight direction. However, skew airfoils or movable borders can be defined in CPACS. Therefore, ELWIS needs to translate this CPACS definition as good as possible in the AVL geometry. ELWIS does this in three different ways: In case of skew profiles at the root or tip, a straight root/tip rib having the original leading edge position is used. In case of skew profiles within the wing, two ribs in flight direction are inserted – one at the leading and one at the trailing edge point of the skew rib. This approach ensures an exact planform representation. In case of skew movable structures definition, the spanwise position of the movable structures' leading edge is chosen.

On some configurations, two ribs might be placed extremely close to each other, e.g. if the spanwise border of the flap is very close to a kink in the wing. At this position, very small elements would appear which would lead to poor results due to numerical effects. Therefore, these 'double' ribs are detected and merged to one rib. To avoid too small elements in chordwise direction, a check is performed prior to the spar placement.

Unfortunately, it is not possible to directly define such complex wings in AVL. In AVL, no steps in the leading or trailing edge of a wing can be defined and only one profile can be defined at each station. However, ELWIS wings have steps along the leading and trailing edge. Additionally, different airfoils have to be placed at one spanwise position at the inner and outer borders of flaps and slats. Therefore, ELWIS splits the wing in several sub-wings that are defined as independent wings in AVL (see Fig. 3.25 (b)). ELWIS always tries to define as few sub-wings as possible, because the number of wings is still limited in AVL. Therefore, ELWIS tries to combine as most spanwise segments as possible to one wing (see Fig. 3.25 (b)).

The wing generation process, described above, is performed separately for each component segment including its movable structures. However, in CPACS a wing can be constructed from several component segments that are attached to each other. Therefore, these different component segments have to be combined and it has to be ensured that the vortex elements of all component segments are matching each other at their borders. ELWIS combines the component segments by adding additional spars where it is necessary and equalizes the chordwise element distribution of neighboring component segments. As an example, a wing including winglet is shown in Fig. 3.26. Here, a new spar is inserted on the main wing at the position of the leading edge of the winglet, in order to ensure an exact element matching. As different component segments can be defined independently in CPACS, the matching position of two neighboring component segments is often not exact. ELWIS checks these positions and places the border ribs of the component segments on exactly the same coordinates.
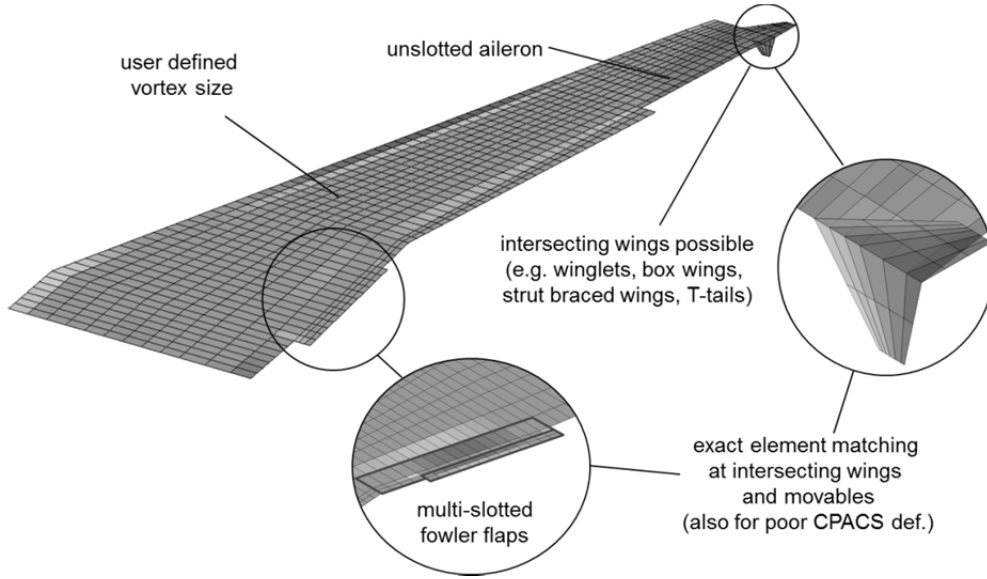
Fig. 3.26: Vortex-lattice mesh of a wing including multi-slotted flap and winglet.

Finally, it has to be mentioned, that the ELWIS model generator can also generate fuselages in AVL. In AVL the fuselage is modeled by sources and sinks. AVL only needs the side view of the fuselage as input, which is computed by ELWIS from the CPACS definition. However, tests showed, that the modeling of fuselages in AVL usually has a negligible influence on the load distribution of the wing. Therefore, this functionality is not used and not further mentioned in this study.

3.4.2 Static Aeroelastic Loop

The loads computation in the WINGmass tool chain is used in a static aeroelastic loop. Therefore, the AVL geometry has to be modified according to the results of the structural analysis.

Prior to the aerodynamic loads computation of each load case, the routine AVLloads checks, if a structural displacement field is available. If yes, this displacement field is loaded. From the absolute displacement of all nodes of the finite element model, the spanwise displacement distribution of the front spar and the rear spar from all lifting surfaces is extracted. From these distributions, the displacement on the leading edge as well as the spanwise twist distribution is computed.

Next, the AVL geometry model is modified accordingly. In AVL, a wing is defined by the three dimensional leading edge positions and the twist of the airfoils. Therefore, only these two values are modified for each defined airfoil.

3.4.3 Loads Interpolation

After the aerodynamic analysis of AVL, the pressure distribution is interpolated on the structural ANSYS grid by the AVLloads module. The most detailed output from AVL is the delta pressure of each vortex element. However, for the structural model, the absolute pressure values on the upper and the lower skin are needed. Therefore, the delta pressure from AVL is split in two pressure values – one for the upper and one for the lower skin. The split for deflected trailing edge devices is 50% upper and 50% lower skin, while all other surfaces have 80% of the pressure load on the upper and 20% on the lower skin. However, the exact numbers of this split have no influence on the sizing, as the local pressure force is irrelevant. For the wing load, only the chordwise and spanwise pressure distribution is important, which is not affected by the split between the upper and lower skin.

Compared to the chordwise slope of the pressure distribution, the AVL mesh is relatively coarse. This is due to the pressure peak at the leading edge of each wing, which leads to high gradients between two neighboring elements (see Fig. 3.27). Additionally, the structural mesh might also be coarse at the leading edge, as these elements are unimportant for the structural computation of the wing, wherefore no fine mesh is needed. These coarse meshes and the high gradient of the pressure distribution can lead to an increasing interpolation error. To avoid this error, the interpolation is performed in several steps, as is described in the following. The interpolation is performed separately for each lifting surface:

- Initially one delta pressure value is given at the center of each vortex, which is in the middle of the 25% line of each element.
- For each strip, the delta pressure is interpolated on a higher resolution grid (ten times higher than original mesh).
- The delta pressure value at the leading and the trailing edge of the strip is set to zero, as it is at real aircraft.
- A correction is applied, to make the total lift of each strip equivalent prior and after the interpolation.
- A correction is applied, to make the chordwise center of lift of each strip equivalent prior and after the interpolation.
- The delta pressure is interpolated on the spanwise element borders of the vortex-lattice mesh.

(a)   (b)
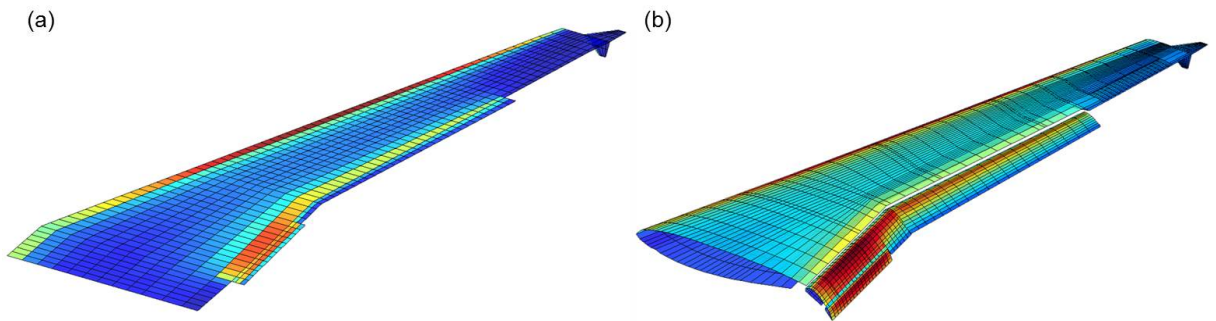
Fig. 3.27: (a) Delta pressure distribution on aerodynamic mesh; (b) pressure distribution on structural mesh. Red equals high pressure/delta pressure values, blue low values.

- The pressure is interpolated on a structural mesh, with ten times higher chordwise resolution.
- The pressure is summed up on each structural element.
- A correction is applied to make the total lift equivalent to the original lift of the vortex-lattice model.

The magnitude of the last correction is usually smaller than 0.5%, which shows the high accuracy of the total interpolation procedure. After the load is interpolated on the structural grid, one APDL file for each load case, containing the pressure load, is generated by AVLloads. In this file, one constant pressure value is defined on each skin surface.

3.5 Fuel, Landing Gear and Engine Loads

Besides the aerodynamic loads, the loads of the fuel inside the wing, the landing gears that are attached to the wing and the engine thrust loads are considered in the WINGmass tool chain. Compared to the aerodynamic loads, these loads are smaller, but still relevant for the total wing load and therefore for the sizing of the wing. As they are smaller, they are named secondary loads in this study.

No tools have been available for the computation of these loads. Therefore, the new tool ESEL (finite Element SEcondary Loads) is developed. The input for ESEL is also generated by the ELWIS multi-model generator. In the following three subchapters, an overview over the computation of the three loads, their needed inputs form CPACS and the model generation in ELWIS is given.

3.5.1 Fuel Loads

ESEL computes the detailed distribution of the fuel in the wing. Therefore, the pressure force of the fuel on each skin, rib or spar element that is part of the fuel tank border is computed. Finally this fuel pressure load is transformed in an ANSYS APDL file, which can be read by the structural analysis and sizing algorithm.

The definition of wing fuel tanks in CPACS is a list of the bordering ribs and spars. The fuel tank is located between the upper and lower skin as well as the ribs and spars of this list. This is a very user-friendly approach, as only the links to the ribs and spars have to be defined and not parameters, like the spanwise or chordwise coordinates. This approach ensures, that the fuel tank definition is still valid, if e.g. the wing's outer shape or the internal structural layout is modified in a parameter study. The fuel tank adopts itself automatically on the new design. By using this definition, also tanks having more than four borders can be defined in a simple way. Such fuel tanks are e.g. shown in Fig. 3.29, where the tank layout of the Airbus A330/340 is depicted.
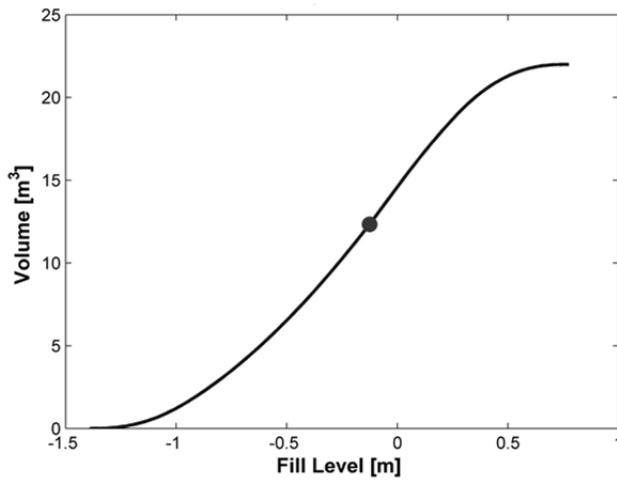
Fig. 3.28: Filling curve of a fuel tank. The dot indicates the fill level the of current load case.

The loading conditions of the fuel tanks are defined in the CPACS load case description. Here, the relative fill level, the aircraft acceleration, the aircraft rotation and the fuel properties are described.

The model for the fuel loads computation is generated by the ELWIS model generator. ELWIS directly uses the structural ANSYS mesh and derives the bordering rib and spar elements for each fuel tank. The ELWIS output for the ESEL computation includes the load case description, the structural mesh and a list of all border areas, where the fuel pressure has to be computed.

This is a good example of the advantage of one multi model generator as opposed to several discipline specific model generators. ELWIS forwards the structural ANSYS mesh to the ESEL computation, which has two major advantages:

- Less implementation and computation time in ELWIS for the computation of a mesh for ESEL.
- No interpolation between the ESEL result and the ANSYS structural mesh is needed, which saves implementation and computation time and increases the accuracy.

The computation of the fuel load is performed separately for each fuel tank and each load case. If two fuel pressures are computed on one element, as e.g. on the rib between two fuel tanks, the two values are added and only the resulting value is written in the output file. The computation is performed in several steps, which is described in the following:

- Rotation of the wing mesh in a way that the resulting acceleration vector is heading along the negative z-axis.
- Computation of the maximal and minimal z-position of the fuel tank.
- Division of the z-range in 100 equal distributed steps.
- Generation of one z = const. plane for each step.
- Computation of the surface area of the cut surface of this planes and the fuel tank.
- Multiplication of each surface area with the distance between two planes to get a set of finite volumes.
- Summation of these volumes, which results in the fill curve shown in Fig. 3.28.
- Computation of the z-coordinate of the fuel surface from filling curve and the relative fill level from load case description (point in Fig. 3.28).
- Computation of the z-distance between each fuel tank border area and the free surface of the fuel.

- Computation of static pressure on each border area, based on the z-distance, the fuel density and the acceleration.

As the fuel loads are changing due to a bending wing in the static aeroelastic loop, the wing deformation has to be considered during the fuel loads computation. Therefore, it is checked at the beginning of the computation, if the displacement field for the current load case is available. If yes, it is loaded and the displacement of each keypoint is derived from the displacement field of the nodes. For each keypoint, one coincident node exists. Therefore, no complex interpolation is needed. Finally, the coordinates of the ESEL input mesh and the displacements are added which results in the modified mesh for the fuel loads computation.
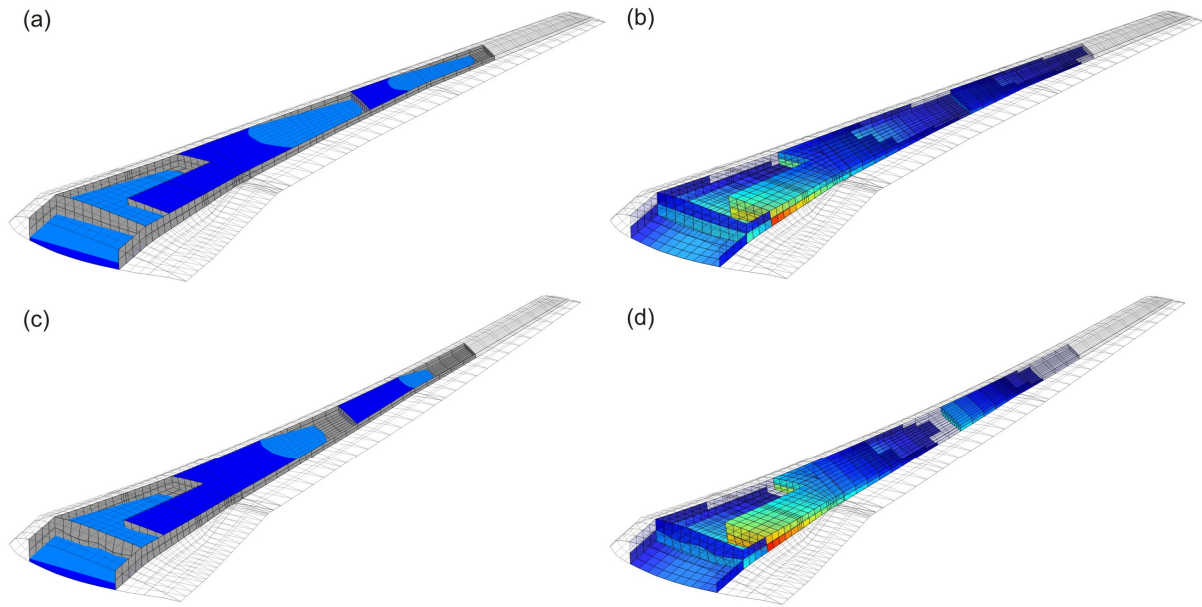
Fig. 3.29: Exemplary fuel distribution (left column) and resulting pressure load (right column) without (upper row) and with (lower row) static aeroelastic wing deformation. Red equals high pressure values, blue equals low pressure values.

3.5.2 Engine Loads

The engine thrust is modeled as a force vector, acting on the engine mass point that represents the engine (see chapter 3.3.2). The engine force is defined in the CPACS load case description by the relative thrust setting. This thrust setting, the flight conditions (height, speed) and the engine performance map is used to compute the force vector in ELWIS. The needed CPACS input is read by ELWIS and written in the ESEL input file.

In case of a bending wing in the static aeroelastic loop, the orientation of the thrust vector changes due to the twist of the wing. If a displacement field of the current load case can be found by ESEL, the engine thrust vector is rotated correspondingly.

3.5.3 Landing Gear Loads

The loads on the landing gear can be computed in a straight forward process from the CPACS load case description. The acceleration and the rotation of the aircraft is given. For touch down load cases, it is assumed, that the aircraft produces lift which is equivalent to its weight (= 1g flight) and that the total acceleration is caused by the landing gear. For pure ground load cases, such as taxiing, it is assumed that no lift is produced and the total acceleration force plus the aircraft weight is carried by the landing gear. From these assumptions, the total force per landing gear can be computed. The total force per landing gear is distributed equivalently over all wheels of the landing gear.

The landing gear force is always aligned along the acceleration vector, wherefore the static aeroelastic deformation of the wing has no influence on the loads computation.

3.6 Structural Analysis and Sizing

The structural analysis and sizing is performed by the program S_BOT+ (Sizing roBOT+). The structural analysis and sizing in S_BOT+ is implemented in the ANSYS internal programing language APDL. This has the advantage, that no interfaces between the analysis and the sizing have to be established (such as in [24]). The tool specific input for S_BOT+ is defined in CPACS and compiled by the ELWIS multi model generator.

S_BOT was originally developed by Nagel [62, 91] in order to size simple wing models based on different fully stressed design criteria. The further development to S_BOT+ that was needed for the integration in the WINGmass tool chain includes a complete rework of the code, coupling to CPACS, introduction of several new functionalities and new sizing criteria, such as stability/buckling criteria or gap/angle sizing (see chapter 3.6.3). Currently, S_BOT+ is further developed to be able to size global-FEM (GFEM) models, constructed from ELWIS wing models and fuselage models from research partners. However, these further developments are beyond the scope of this study.

3.6.1 Program Workflow Overview

The workflow of S_BOT+ can be split in five main components: The model preparation at the beginning, the structural analysis of all load cases, the sizing of the elements, the update of the model with the new thicknesses and the output routine. The structural analysis, the sizing and the model update are looped, until the mass converges or the maximal allowed number of iterations is reached.

The model preparation part loads the S_BOT+ input file first. Next, it is checked, if the structural FE model already exists in the database folder (from a previous analysis) or if a new model has to be generated. If new models have to be generated, S_BOT+ reads in the geometry

file, which is created by ELWIS and which contains all APDL commands to create the model. Next, the model is analyzed and several parameters are initialized.

If an already existing model was loaded, all analysis parameters are cleared and the model preparation part is finished. For new loaded models, various different solution models are generated. For each so called deflection case (DC) one separate model is generated, which is later used for the structural analysis. A DC represents one setting of the wing as e.g. the landing configuration with all flaps extended and extended landing gear. The DCs are derived by ELWIS from the CPACS load case description.
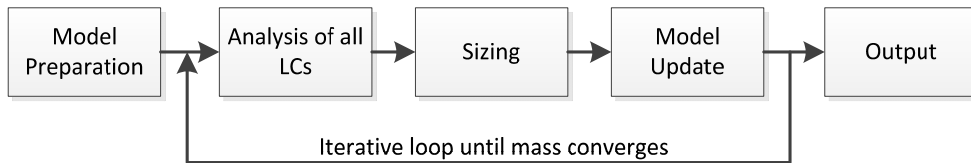
Fig. 3.30: Workflow overview of S_BOT+ structural analysis and sizing routine.

To generate the DC models, all movable structures are fully extended in positive and negative direction first to track their deflection path. In a next step, the actuation load for each movable component and each DC is computed from the deflection paths and deflection settings for each DC. Next, all movable structures are deflected according to the actuation load off each DC. Finally, unneeded elements are deleted (see chapter 3.6.2) and one separate ANSYS data base file is saved for each DC.

The last step of the model preparation module is the definition of several parameters and matrixes that are used for the sizing process. Examples for these parameters are matrixes that contain the thickness or material limits of the elements.

In the structural analysis module, all load cases are analyzed. Therefore, the corresponding DC model is loaded, the loads of the load case applied and the structural analysis performed. Finally, the stress and strain values on all elements are read and stored in matrixes for the sizing.

Based on the structural results of the different load cases, new element thicknesses are computed in the sizing part of S_BOT+. The sizing is explained in detail in chapter 3.6.3.

In the model update part, the new computed element properties (such as thickness or material orientation) are fed back in all deflection case models. Therefore, each model is loaded and updated with the new element properties. Additionally, several element tables are generated, which can be used for the visualization of the new computed properties of the current iteration.

The last module of S_BOT+ is the output module, which generates various different outputs. All outputs are stored in separate text files. The different outputs are:

- The deflection of the wing model of all load cases, which is needed for the aeroelastic coupling.

- The element properties of all elements. This file is used by the post-processing routine P2 of the WINGmass tool chain, to compute the different masses of the CPACS mass breakdown.
- The convergence history.
- A log-file.

3.6.2 Types of Load Cases

Within S_BOT+, different types of load cases can be handled. The core of S_BOT+ is the fully stressed design, which is usually performed with ultimate loads. Fatigue load cases are considered by reduced material limits. This means, that S_BOT+ makes no difference between ultimate and fatigue load cases, as the difference is represented by the material limits, which is an input that is compiled by the ELWIS model generator.

For the sizing of several components, (static) failure load cases are considered. In the WINGmass tool chain, broken actuators can be simulated. In case of a broken actuator, the interconnection strut acts as alternative load path, which changes the load distribution on the flap bodies and tracks. The broken actuator is represented by deleting the actuator element in the solution model of the corresponding deflection case. For non-failure cases, it has to be ensured, that no load is taken by the interconnection strut, which is modeled as rigid link. Therefore, the interconnection strut is deleted in all non-failure deflection cases. A similar approach is chosen for the cruise rollers respectively mid-span stops. They are only acting in case of retracted flaps, wherefore the connection joint is deleted in case of extended flaps.

In order to ensure a good aerodynamic performance of bending wings, the bending of the flap and the main wing must be very similar. Therefore, two additional design requirements are defined: The first requirement is the spanwise gap distribution on extended flaps. Due to different bending lines of the flap and the wing, the gap differs along the span. This difference is kept within the margin by stiffening of the flap body (see chapter 3.6.3). The second requirement is the deflection angle of the flap which must stay within a small margin for loaded flaps. This can be reached by adequate stiffening of the flap tracks (see chapter 3.6.3).

3.6.3 Sizing

The sizing part is the core element of S_BOT+. In the following, the different sizing criteria that are currently implemented are explained.

Fully Stressed Design of Beams and Shells

The fully stressed design (FSD) is the most common structural sizing method in preliminary aircraft design. The basic idea behind this principle is, that the material thickness of each ele-

ment is chosen in a way, that the maximum stress level of all load cases equals the maximal allowed stress.

$$\frac{\sigma_{\text{acutal}}}{\sigma_{\text{crit}}} = 1 \qquad\qquad\qquad (\ 3.1\ )$$

For statically determined structures, where all components can be sized independently form each other, this approach leads to a design having minimal mass. For other structures, like an aircraft wing, this design approach is not necessarily leading to the mass optimal design. However, the FSD solution is usually very close to the mass optimal design, wherefore it leads to good estimations of the wing mass during preliminary design [58].

As the load inside a structure changes depending of the thickness values of the structure, the FSD is implemented in an iterative loop. The thicknesses of the next iteration is computed with the formula

$$t_{i+1} = t_i \cdot \left(\left(\frac{\sigma_{\text{acutal}}}{\sigma_{\text{crit}}} - 1 \right) \cdot k_{red} + 1 \right) \qquad\qquad (\ 3.2 \ )$$

with k_{red} being a reduction factor, which is used to control the convergence behavior. If k_{red} equals one, the standard FSD is applied. For k_{red} smaller than one, the thickness change between the two iterations is slower, but more robust. For k_{red} larger than one, the thickness change is faster, but the process might not converge. Usual values for k_{red} are one or slightly smaller than one.

The ratio between the actual and the critical stress is computed for all load cases and all layers. Finally, each element is sized with respect to the largest value of all load cases and element layers. All elements are sized separately and independent from each other.

In S_BOT+, various different possibilities are implemented, which stress has to be chosen as σ_{acutal}, respectively how it is computed. For shell elements with isotropic materials, such as metals, the equivalent stress criterion of von Mises [132] is used. For shell elements with anisotropic materials, such as CFRP, the user can chose between the maximum stress criterion [133], the Puck criterion [134] and the Tsai-Wu criterion [133]. These three criterions consider several stresses in different directions, which is why the FSD is performed with several values for σ_{acutal} and the most critical ratio $\sigma_{\text{actual}}/\sigma_{\text{crit}}$ is chosen for the sizing of the whole laminate. This means, that the whole laminate is scaled with the same factor and the relative thickness of the laminate layers is not changed. For beam elements, the user can decide between the maximum stress criterion and the von Mises criterion. As the von Puck criterion and the Tsai-Wu criterion are developed specifically for multi-layered structures, they cannot be used for beam elements.

The sizing criteria can optionally be specified by the user. If the user is not specifying it, ELWIS chooses the von Mises criterion for isotropic shells, the maximum stress criterion for anisotropic shells and the maximum stress criterion for beam elements.

Material Orientation of Shell Structures

In case of anisotropic materials for shell elements, S_BOT+ can modify the material orientation, in order to reach an optimal material usage and therefore a lightweight wing. The approach is simple, but leads to good results for preliminary aircraft design.

If this option is used, S_BOT+ aligns the representative layer of the laminate along the principal stress direction. This means that the orientation of the best material properties is in the same direction than the principal stresses. S_BOT+ rotates the whole laminate as it is and is not changing the relative orientation of the different layers. As different load cases lead to different direction of the principal stress, the average principal stress direction is used.

Stability of Shell Structures

In S_BOT+, all shell structures are sized against buckling/stability criteria. Due to the processing time, the structural analysis in S_BOT+ is linear static, wherefore no non-linear FE buckling analysis can be performed. Therefore, the stability sizing is performed by employing hand book methods, which are taken from Bruhn [135]. The methods of Bruhn are based on the assumption of flat shells with no curvature. As the curvatures of the shell elements in the structural model are small and the neglect leads to conservative results, the neglect is acceptable for preliminary aircraft design.

The principal approach for the stability sizing is similar to the FSD sizing, as the actual stress values are compared with the critical stress values, which results in new element thicknesses. However, the value for the critical stress σ_{crit} is not based on material allowables. For the stability analysis the following formula is used.

$$\sigma_{crit} = \frac{\pi^2 k E}{12(1 - v^2)} \left(\frac{t}{b}\right)^2 \qquad (3.3)$$

with σ_{crit} being the critical stress value, k the buckling coefficient, E the Young's module, v the poisons ration, t the sheet thickness and b the shorter dimension or the loaded edge of the buckling plate. The buckling coefficient k is a coefficient, which depends on the edge boundary conditions and the sheet aspect ratio a/b. The parameter k is derived from graphs in [135] that have been digitized and implemented in the ELWIS model generator. ELWIS sets the k values in advance for each buckling field. Equation 3.3 can be used for the computation of buckling due to compression and due to shear loads. The difference between the computations is only a different value for k. In S_BOT+, the ratio $\sigma_{actual}/\sigma_{crit}$ is computed for both, compression and shear loads. As both buckling modes are not independent from each other, both ratios are combined to a final ratio, which is used for the computation of the new skin thickness.

The size of the buckling field, which is represented by the parameters a and b is computed by ELWIS in advance. E.g. for spars, b equals the height of the spar and a the distance between two ribs. For stringer stiffened skins, b equals the stringer pitch. This means, that the value of b varies during the sizing process (see stringer sizing below).

The material limits for the FSD sizing against ultimate loads may be in the non-linear plastic region of the material. To take this into account, the Young's modulus E in equation 3.3 is replaced by the tangent modulus E_T, which is a reduced Young's modulus in the plastic region. An exemplary slope of E and E_T is shown in Fig. 3.31. This approach is based on the work of Ramberg and Osgood [136]. They developed a stress-strain relation, which is also valid in the non-linear material regime:

$$\epsilon = \frac{\sigma}{E} + K \left(\frac{\sigma}{E}\right)^m \qquad\qquad (\ 3.4\ )$$

With K and m being coefficients, which are material properties and describe the characteristics of the stress-strain curve. The parameter m is called Ramberg-Osgood coefficient and available in material data bases such as [137]. Based on this work, Hill [138] developed the following equation for the tangent modulus, which is used for the stability analysis:

$$E_T = E \left(1 + 0.002 \cdot E \cdot \frac{\sigma^{m-1}}{\sigma_2^m} \cdot m\right)^{-1} \qquad\qquad (\ 3.5\ )$$

With σ_2 being the proportional limit stress. As E_T depends on the actual stress level, and the value of σ_{crit} depends on E_T, an iterative approach is chosen:

- E_T is computed with an initial guess for σ (here σ_2).
- σ_{crit} is computed with this E_T.
- E_T is recomputed with the value of σ_{crit}.

This is repeated until a convergent result is reached. As the function of $E_T(\sigma)$ has the slope of a smooth step function (see Fig. 3.31 (a)), a strong damping is applied to the iteration, to reach a convergence.

The buckling computation of composite laminates is still subject of current research. However, the critical buckling stress of symmetric and balanced composite laminates can be computed
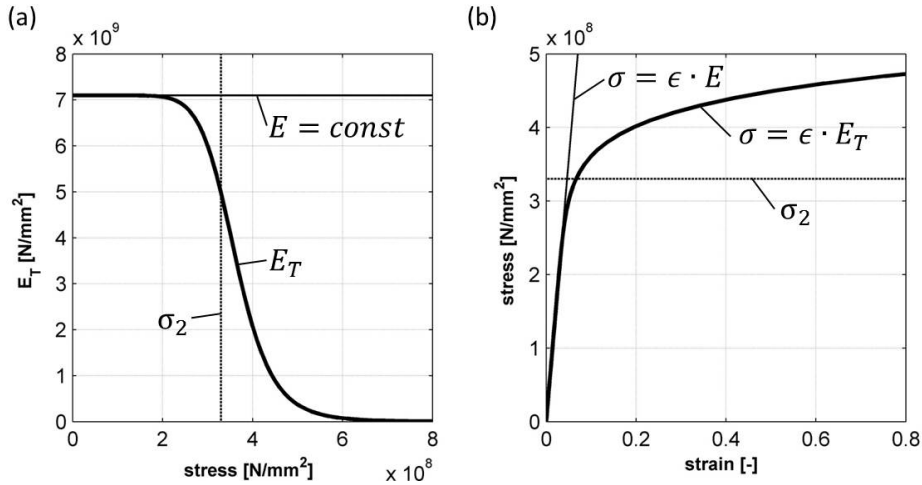
Fig. 3.31: (a) Tangent modulus as function from stress according to Ramberg-Osgood equation; (b) stress-strain relation computed with tangent modulus.

by hand book methods. The buckling equations for shear and compressive buckling are taken form the HSB [139]. These equations can be transformed in equation 3.3. Therefore the Young's module E has to be replaced by $E = E_x$ for shear buckling respectively $E = \sqrt[4]{E_x E_y^3}$ for compressive buckling. Additional, the Poisson ratio ν has to be replaced by $\nu = \sqrt[2]{\nu_{12} \nu_{21}}$. These replacements are already done by ELWIS during the model generation, which means that no additional implementation effort in S_BOT+ is necessary. The buckling coefficients k for composite buckling are also taken from [139].

Stringer Sizing

The sizing of the stringer-stiffened panels is performed in four steps. First, the new stringer pitch is computed. Therefore, the shell buckling criteria described above is used. Instead of adopting the skin thickness, the stringer pitch (parameter b in equation 3.3) is adopted. The idea behind this is, that the stringer pitch has to be chosen in a way that the skin does not buckle.

In the next step, local buckling of the stringer is analyzed. The equation for the local stringer buckling has the same shape as equation 3.1. However, the buckling coefficient k depends only on the stringer geometry and the ratio t/b refers to the thickness of the stringer web and the web height. The parameter k is computed by the ELWIS model generator. Dependent on the ratio between the critical local buckling stress and the actual stress, the thickness of all stringer sheets is scaled. As the coefficient k depends on the ratio of different thicknesses of the stringer and geometrical parameters of the stringer cross section, k is not changing during the sizing process. As there is no general hand book method for local buckling on composite stringers available, the sheet thickness of composite stringers is not sized due to local buckling criteria in the current S_BOT+ version.

The next criterion is the check against buckling of the whole skin-stringer panel. According to Shanley [39], it can be assumed that the skin-stringer panel behaves like an Euler column, wherefore the Euler/Engesser equations for beams can be used. This criterion is used to scale the whole stringer (height, width and material thicknesses). This approach is applied for composite as well as metal stringer.

The chosen approach for the stringer sizing ensures that all three analyzed buckling modes occur simultaneous, which is known as the optimal design, having the lowest weight.

As the stringer sizing regions are usually very large (e.g. the whole upper skin, see chapter 3.3.3) the stringer properties are the same within these large regions. This means, that the one most critical element of the sizing region would determine the properties of all elements in this region. This would lead to an extremely sensitive behavior of the stringer sizing and therefore stringer mass, as one element can change the mass of a large region. In order to make the sizing more robust and to improve the convergence behavior the average sizing properties of each buckling region are used to determine the sizing properties of the whole stringer sizing area.

Finally the orientation of the stringer is adopted. Therefore, the same approach as for the orientation of composite materials is chosen: the stringers are aligned in the direction of the mean principal stress.

As described in chapter 3.3.1, stringers are modeled in a smeared representation by an additional shell layer. Therefore, all stringer sizing parameters, like pitch, height, width and so on, are not represented explicitly in the FE model. These parameters are defined by ELWIS as properties of the buckling optimization areas and are used to compute the equivalent properties of the smeared stringer layer. This approach is not exact and cannot be used for a detailed design. However, for the purpose of mass estimation in preliminary aircraft design, it delivers good results within adequate complexity and computational costs. The smeared stringer representation has the additional advantage, that the stringer pitch is a sizing criterion that can be changed during the sizing like e.g. the skin thickness. In an explicit modeling approach, the whole model generation process must be repeated if the stringers pitch should change, which is rather expensive computationally.

Stability of Beam Structures

For the sizing of beam elements against stability criteria, the stability criteria according to Euler [39] are used. The selection, which of the four Euler cases needs to be used is undertaken by the ELWIS model generator and stored as property of the sizing region. S_BOT+ modifies the cross section of the beam element, so that the FSD criteria and the Euler criteria is fulfilled.

Optionally, the stability criteria of Engesser [39] can be used instead of the Euler criteria. Engesser uses the same equations than Euler, but he uses the tangent Young's module E_T instead of E. This means, that the approach from Engesser can also be used beyond the proportional limit stress. As already described for the shell buckling, an iteration between E_T and the critical stress is needed in this case.

Flap Gap Sizing

To guaranty the good aerodynamic behavior of extended high-lift devices, the deflection of the flap, relative to the wing, must stay within a small margin. This relative deflection can be measured by the spanwise distribution of the gap between the extended flap and the wing. Special load cases are defined where the gap distribution has to be within the margin.

The gap close to the flap tracks is only changing a bit under load, as the flap body is clamped by the track. But at the tips of the flap and in between two tracks, the gap can change significantly. For specified load cases, S_BOT+ checks the difference of the gap at the flap tracks, on the tips and in the middle between two tracks. If the difference exceeds the margin, the flap body is stiffed by the application of an additional safety factor. This approach is inspired from the work of Anhalt [89].

The size of the margin has to be specified by the user and is expressed as percentage of flap chord. Usual values for this margin are around $\pm 1\%$.

Flap Angle Sizing

Due to the applied loads, the flap track bends, which reduces the deflection angle of the flaps. In S_BOT+ special load cases can be defined, where the difference of the flap deflection angle under loads and unloaded must stay below a specified user-defined value. For these load cases S_BOT+ derives the delta angle at all flap track positions. If the delta angle is too high, S_BOT+ stiffens parts of the tracks structure by the application of an additional safety factor.

Mass Points

In the ELWIS FE wing models, some structural masses are modeled as mass points. These masses are the joints and the carriage of the flap tracks. For these complex structural components that are modeled in a very simple way, no classical sizing, such as FSD, can be applied. Therefore, the mass equations developed by Holert [124, 140] are implemented in S_BOT+. Both equations are statistical quadratic equations based on the mass values of real aircraft. The input of the equations is the maximal force that is transferred by the joint respectively the carriage. In S_BOT+, these forces are derived from the neighboring elements of the mass points.

Sizing with Respect to Other Optimization Regions

The user might wish that the element thickness of one region is equivalent to the element thickness of a neighboring region. If this option is chosen, ELWIS determines from which other optimization region the thickness values should be taken for the current one. For this option, S_BOT+ copies the thickness values directly from one region to the other one.

Currently, two different cases are implemented in ELWIS. The first one is the sizing of the spar caps. At many aircraft, the spar web and the spar cap is one C-shaped part. However, in the FE model, the spar web is modeled by shell elements, while the spar caps are modeled by independent beam elements in different optimization regions. Therefore, the user can specify, that the caps should get the same thickness as the web.

The second application field is the leading edge of the flap body. The leading edge of the flap is usually also load-carrying and might be the same part as the skin behind. Therefore, the user can specify that these elements should get the same thickness values than the skin behind the front spar of the flap.

Thickness Limits

After the computation of new thicknesses, S_BOT+ checks, if the new element thickness is below a minimum or above a maximum value. If this is the case, the element thickness is set to the minimum, respectively the maximum value. These values can either be specified by the user or are defined by the ELWIS model generator, if the user is not defining them.

Usually, only the minimum value is of practical importance. The minimum value represents e.g. manufacturing constraints, as shells can only be manufactured if they are thicker than a certain value. The maximum value is usually only reached, if an error in the simulation occurs.

Filter for Optimization Regions

The whole sizing, described above, is performed separate for each element. Thus, the last step of the whole sizing process is, to make the element properties of each optimization area equivalent. This approach takes restrictions into account, like manufacturing constraints, and also leads to better convergence behavior of the whole sizing. This function can be turned off by the user.

For shell and beam elements, the sizing regions that are used for the FSD are used. For the equivalent stringer shell layer, the stringer optimization area is used. Usually, one stringer optimization area is the whole wing, which means that the stringers properties are the same over the whole wing.

For the determination of element thicknesses, the highest thickness value of one element of the region is chosen for the whole region. Also for the stringer shell layer, the elements, representing the largest stringer and the smallest pitch are chosen as reference for the whole region. For the orientation angle of composites and stringers, a weighted average value of the optimization area is chosen.

3.7 Post-Processing

The last tool of the WINGmass tool chain is the output module P2 (Post-Processing). The task of this module is to generate the CPACS output file and several plots, if this is specified by the user.

The masses in the CPCAS mass breakdown are divided into several sub masses, such as skins, ribs, spars, flaps, flap tracks, etc. P2 loads the output file from S_BOT+ where the new properties from all elements of the FE model are stored. Next, P2 computes the mass, the center of gravity and the moment of inertia of each component of the CPACS mass breakdown. This mass from the FE model is then multiplied with the non-optimum mass factors that are derived in chapter 4.2.3. Currently, the mass properties and the material thickness distribution after sizing are written back to CPACS. If requested for further applications, this can be extended to e.g. the track geometries that are an outcome of the knowledge-based model generation process in ELWIS.

Beside the CPACS output file, different plots can be generated by P2. An example is shown in Fig. 3.32, where the convergence of different components of the wing box of the research configuration D150 is shown. In this plot the mass of different components is plotted over the iteration number. The vertical lines indicate a new loads computation of the static aeroelastic loop while between two vertical lines the convergence of each S_BOT+ run is shown. It can be seen that the aeroelastic deformation of the wing relieves the wing which leads to lighter skins, while the ribs, spars and stringer are nearly not affected by the static aeroelastic loop.
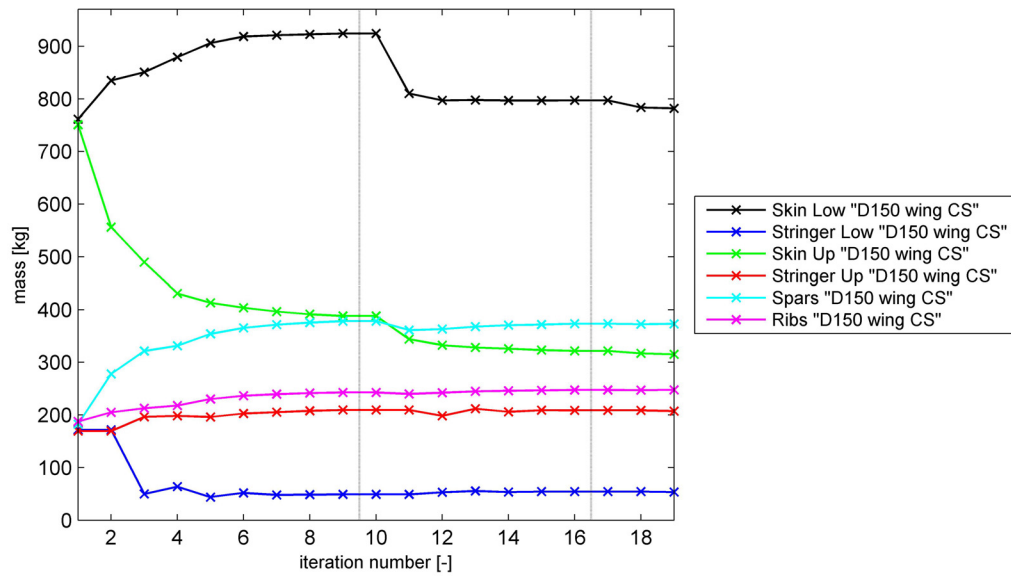
Fig. 3.32: P2 exemplary convergence plot of different wing components (vertical lines indicate a new static aeroelastic iteration).

Chapter 4

VALIDATION AND APPLICATION

The calibration and application of the developed wing mass estimation system that is described in chapter 3 is presented in the following. First, the validation of the aerodynamic load estimation process is depict, which is followed by the derivation of the non-optimum mass factors that are used to compute the final mass from the mass of the FE model. Next, the applicability of the WINGmass tool chain on five unconventional configurations and structural layouts is demonstrated. Finally, the developed tool chain is applied in a multidisciplinary aircraft design process.

4.1 Validation of the Aerodynamic Load Estimation

Accurate load estimation is crucial for an accurate wing mass estimation. The tool AVL, respectively vortex-lattice methods in general, are widely used for the aerodynamic load estimation in preliminary aircraft design. However, the use of these methods for load estimation of wings, including its high-lift devices, is not jet published. It is indicated in Werner-Spatz [130], Werner-Spatz et al. [131], Rajeswari et al. [141] and Heilmann [142] that vortex-lattices methods can deliver reliable results for wings in high-lift configuration. However, none of the previous mentioned authors focused on the application as load estimation. Therefore, the validation of the implement AVL method for high-lift wings is presented in the following.
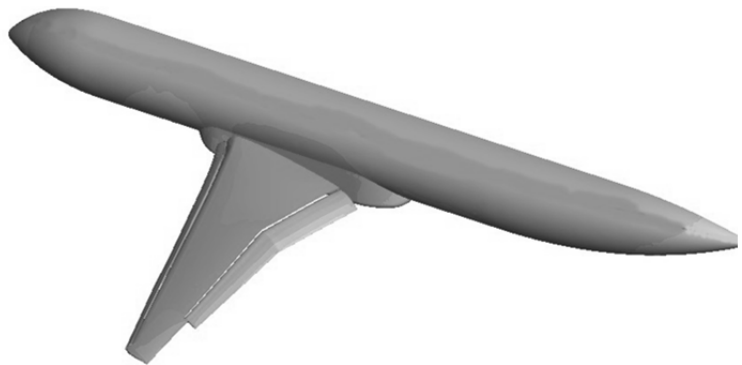
Fig. 4.1: Geometry of FNG reference configuration.

For the purpose of wing mass estimation, the lift distribution and the split of the lift between the wing and the movable structures are the most important aspects. Additionally, the chord-

wise center of lift on the flaps is of high importance, as it considerably influences the loads on the flap tracks. The last important aspect is the estimation of the angle of attack for a given lift, as a wrong angle of attack would lead to an inaccurate lift distribution on a twisted wing.

For validation, the AVLloads computation is compared with CFD RANS results. The reference aircraft is the so called FNG configuration [143]. The CFD results are taken from an earlier study [144]. The FNG is a wing-fuselage research configuration of an aircraft having a fuselage of the size of the A321, a 174m^2 wing area, single slotted fowler flaps and slats along the whole leading edge. The geometry of the FNG aircraft in landing configuration can be seen in Fig. 4.1. The validation case is the FNG wing-fuselage model at zero angle of attack, a Mach number of Ma $= 0.2$ and a Reynolds number of Re $= 1.8 \cdot 10^7$. The high-lift system is in landing configuration with flaps extended 32° and slats extended 23°.

The lower curve in Fig. 4.2 shows the error in total lift of the AVL computation for dif-
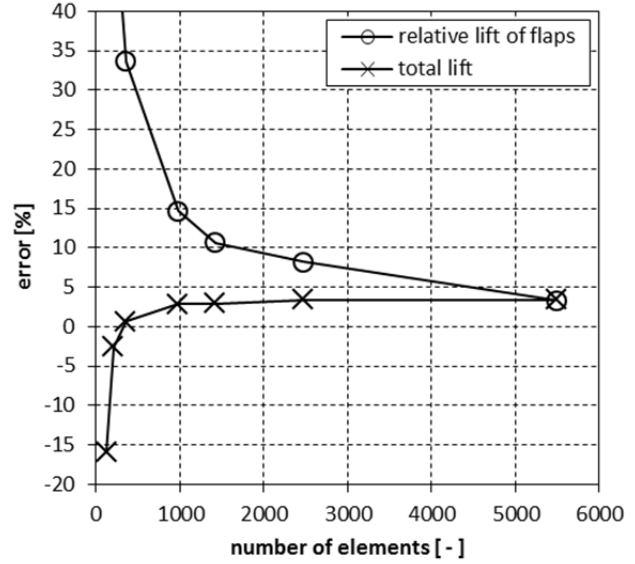
Fig. 4.2: Comparison of vortex-lattice and RANS computation for different number of vortex-elements.
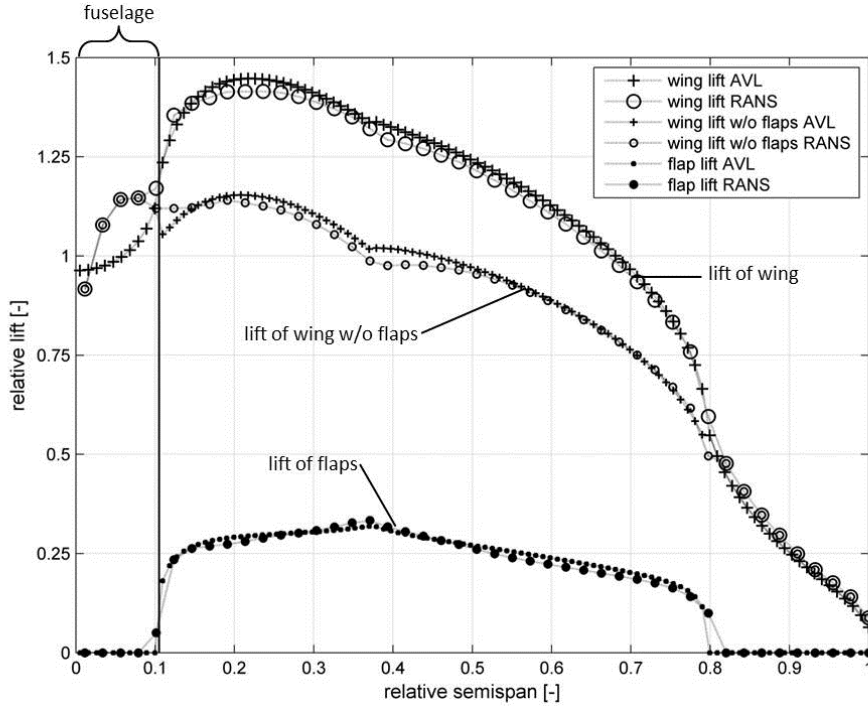
Fig. 4.3: Comparison of vortex-lattice and RANS spanwise lift distribution.

ferent numbers of vortex elements. It can be seen, that the total lift in the AVL computation is not changing significantly, if more than 1000 vortex elements are used. For the maximum number of elements, a difference of 3.4% in total lift results. As the total lift is a load case input in the WINGmass tool chain, the difference in lift computation would be transformed to a different angle of attack in the tool chain. The 3.4% difference in lift equal 0.6° difference in angle of attack, which is a good result, if one considers the simplicity of the vortex-lattice method, compared to the RANS computations.

In Fig. 4.3, the spanwise lift distribution of the RANS and the AVL computation with the highest number of vortex elements is plotted. It can be seen, that the main difference occurs at the wing root where the fuselage is placed. As the fuselage is not modeled in AVL, a high difference in this region is expected. Trials to model the fuselage by a source-sink model in AVL did not improve the accuracy. The differences in the lift distribution close to the wing root have a minor effect on the spanwise wing bending moment, which is the most important parameter for the wing sizing. Therefore, the differences in lift in the root area can be neglected.

The upper curve in Fig. 4.2 shows the error of the relative lift of the deflected flaps. The relative lift is the share of lift that is produced by the flaps, compared to the total lift of the configuration. It can be seen, that the error in relative flap lift strongly depends on the number of vortex elements. For the computation with the highest number of elements, the flaps produce 18.0% of the total lift in AVL, while the flaps produce 17.4% of the total lift in the RANS computation. This results in an error of only 3.4%. As can be seen in Fig. 4.3, also the spanwise lift distribution of the flaps matches well with the RANS result.

As mentioned above, the number of vortex elements needs to be very high to obtain accurate results for high-lift configurations. However, the maximum number of vortex elements in the original AVL version is limited. Therefore, a new version from Moerland [129] is used for the WINGmass tool chain. This AVL version can handle up to 6500 vortex elements. A further increase of the number of vortexes is not possible due to FORTRAN limitations.

Beside the total lift, the chordwise position of lift on the flaps is very important. As the flap bodies are usually connected at two discrete points with each flap track, the chordwise center of lift is crucial for the forces, acting at these two points. By changing the chordwise center of lift, the lift force can be shifted between the two connection points. This greatly influences the sizing of the flap track. The validation computations show that the chordwise center of lift on the flaps is
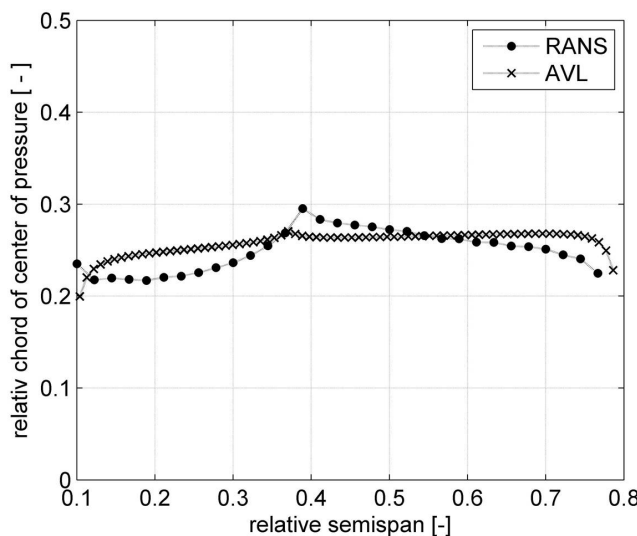
Fig. 4.4: Comparison of spanwise center of pressure on the flaps of RANS and corrected AVL computation.

too far back. Therefore a correction is implemented in the AVLloads module. This correction shifts the center of lift more to the front, without changing the spanwise lift distribution or the total lift. After the correction, the maximal difference of center of lift of AVLloads and the center of lift of the RANS computation is reduced to only 4% flap chord. A comparison spanwise distribution of the corrected center of lift and the center of lift of the RANS computation is shown in Fig. 4.4.

4.2 Derivation of Non-Optimum Mass Factors

All finite element models that are used during preliminary aircraft design represent a simplification of the real aircraft geometry. For example, spar webs are modeled with flat shells and the spar caps with rectangular beam elements. In contrast, a real spar might have reinforcements, stiffeners, holes, rivets or cut-outs. Due to these simplifications, the resulting mass of the sized finite element model represents only a theoretical optimum mass, which is less than the real mass. Since the early beginnings of wing mass estimation, the most popular approach to calibrate the optimum mass by using a power function of the shape $m_{real} = a \cdot m_{optimum}^{b}$. The coefficients a and b are derived by regression analysis. In this regression analysis, the mass of several real aircraft is compared with the modeled mass. As b is usually close to one, it is often set to one, which simplifies the equation to the non-optimum mass factor a, multiplied with the physics-based optimum mass. For the purpose of wing mass estimation, usually one non-optimum mass factor is derived to compute the total wing mass from the total modeled structural mass. However, if more detailed data is available, the regression analysis can also be performed on component level.

According to Pincha [145], 30-80 % of the real structural aircraft mass can be modeled by finite element based analyses. In the Airbus FEMMAS project, it is stated that typical values for wing primary structures are around 60-70 % [67]. The same values as those published by Pincha are also given by Österheld [58]. However, she corrected the allowed stress values instead of the modeled mass. As long as no aeroelastic coupling is considered, these two approaches should result in similar masses. In case of an aeroelastic coupling, differences will occur as the stiffness of the wing and therefore the loads will change.

The exact value of the non-optimum mass factors cannot be stated in a general manner as it depends on various aspects. The factors depend on the structural component on which they are applied, the degree of simplification of the model, the applied sizing criteria, the considered load cases as well as several maintenance and production aspects that influenced the real design, but are not taken into account in the mass estimation process. This incomplete list shows that the non-optimum mass factors have to be derived for each new wing mass estimation method respectively tool chain. Additionally, after each change at one of the analysis modules, the non-optimum mass factors must be recalculated.

In the following, the derivation of the non-optimum mass factors for the WINGmass tool chain is presented. First, the reference aircraft are described, followed by a list of the considered

load cases. Finally, the non-optimum mass factors are derived and the difference between the final WINGmass results and the real aircraft mass is shown.

4.2.1 Reference Aircraft

For the derivation of the non-optimum mass factors, it is favorable to use as many aircraft as possible. However, for the WINGmass tool chain, very detailed information on the aircraft, such as the airfoil shape, material properties and spanwise thickness and twist distributions, are necessary. This detailed information is usually confidential, wherefore it is only available for few aircraft. Therefore, the non-optimum mass factors are derived based on two reference aircraft, for which the necessary information are available to the author: the Airbus A320-200 and the Airbus A340-200.

The A320 is a typical twin-engine short and medium range aircraft, manufactured by the European aircraft manufacturer Airbus [146]. The A320 is the basic aircraft of the A320 family that also consist of the shrunk A318, A319 and the stretched A321. Although its first flight was 1987, the A320 still represents the state-of-the-art in its class. The A320 can carry 180 passengers in a standard single-class layout for more than 3000 nm. During its 25 years of production, several different weight variants of the A320 have been developed. For the analysis in this study, a weight variant with 77t MTOM is chosen, which is the most common and at the same time almost heaviest current weight variant. Therefore, this weight variant is well-suited as a reference for the derivation of the non-optimum mass factors.

The A330/340 aircraft family is a typical long range aircraft family. The family consists of the A330-200 and -300 and the A340-200, -300, -500 and -600. The -200 and -300 versions of both aircraft share the same wing, although the A330 is equipped with two engines, while the A340 is equipped with four engines. The MTOM of the A340 is considerable higher than the MTOM of the A330 aircraft. Therefore the A340 is better suited to be used as reference aircraft, as the common wing is designed to withstand the higher loads on the A340. The A340-200 [147] with its highest weight variant and a MTOM of 275t is chosen as reference configuration. The A340-200 has a standard seating capacity of 303 passengers that can be carried over more than 6500 nm.

4.2.2 Load Cases

The two reference aircraft are analyzed with respect to the most critical load cases for the wing box, the flaps and the ailerons. The chosen load cases are assumed to be the most critical load cases, according to different publications and expert opinion. In detail, the load cases in Tab. 4.1 are included in the analysis. In addition to the load cases mentioned in Tab. 4.1, more load cases were tested in preliminary analysis. However, it was found, that these load cases are not critical for the sizing of the wing. Therefore, they are neglected for the derivation of the non-optimum mass factors.

Tab. 4.1: Overview of considered load cases.

Nr	Acceleration	Mass	Velocity	Flaps	Ailerons	Remarks
1	2.5g	MTOM	V_D	Cruise	0°	
2	2.5g	MTOM	V_A	Cruise	0°	Only used for A320 as A340 cannot reach 2.5g at V_A.
3	computed	MZFM	V_C	Cruise	0°	Gust load case; acceleration to be computed for each aircraft.
4	-1g	MTOM	V_C	Cruise	0°	
5	1g	(MTOM - MZFM)/2	V_C	Cruise	0°	Fatigue load case with reduced material limits.
6	2g	MTOM	V_F	Take-off	0°	
7	2g	MLM	V_F	Landing	0°	
8	1g	MLM	V_F	Landing	0°	For gap and track bending angle sizing.
9	computed	MLM	V_F	Landing	0°	Touchdown according to CS 25.473 (2); acceleration to be computed for each aircraft.
10	computed	MTOM	V_F	Landing	0°	Touchdown according to CS 25.473 (3); acceleration to be computed for each aircraft.
11	2g	MRM	0 m/s	Cruise	0°	Bump on rough taxi way.
12	1.667g	MTOM	V_D	Cruise	0°	Reference load case for aileron load cases 14 and 15.
13	1.667g	MTOM	V_D	Cruise	max	Angle of attack from load case 13.
14	1.667g	MTOM	V_D	Cruise	min	Angle of attack from load case 13.

4.2.3 Non-Optimum Mass Factors

The WINGmass tool chain is applicable for the analysis of the wing and its trailing edge devices. However, the user can choose, which trailing edge devices should be analyzed. Therefore, the non-optimum mass factors are derived for three different analysis cases:

- Analysis of the wing box.
- Analysis of the wing box and the flaps.
- Analysis of the wing box, the flaps and the ailerons.

For the analysis of the pure wing box, only load cases 1 - 5 and 9 - 11 (see chapter 4.2.2) are used, as these load cases are responsible for the majority of the loads on the wing primary structure. For the analysis of the wing box and the flaps, also load cases 6 - 8 are considered, as these load cases represent the main loads of the flaps. For the analysis of the wing with flaps and ailerons, all load cases are considered, including the aileron specific load cases 12 - 14.

The non-optimum mass factors differ slightly for the three analysis cases, due to two main reasons: as mentioned above, different sets of load cases are used for the three analysis cases. Although e.g. the flap load cases mainly size the flaps, they slightly influence the sizing of the main wing. The second reason is that the flaps and the ailerons interact with the primary structure of the wing, wherefore the loads and therefore the sizing of the whole wing differs.

Tab. 4.2: Non-optimum mass factors for analysis of wing primary structure.

	A320 mod. mass [%]	A340 mod. mass [%]	Non-optimum mass factor [-]	A320 error [%]	A340 error [%]
Skin and stringer	61.5	60.4	1.640	1.0	-1.0
Spars	75.4	80.0	1.287	-2.9	2.9
Ribs	67.5	79.7	1.359	-8.3	8.3
Sum	**64.6**	**66.5**	**-**	**-0.9**	**1.1**

Tab. 4.3: Non-optimum mass factors for analysis of wing primary structure and flaps.

	A320 mod. mass [%]	A340 mod. mass [%]	Non-optimum mass factor [-]	A320 error [%]	A340 error [%]
Skin and stringer	59.9	61.8	1.643	-1.6	1.6
Spars	77.2	80.2	1.271	-1.9	1.9
Ribs	65.7	80.7	1.366	-10.2	10.2
Sum prim. struct.	**63.5**	**67.7**	**-**	**-2.8**	**2.9**
Flap bodies	40.5	42.5	2.409	-2.5	2.5
Flap tracks	47.2	44.3	2.185	3.2	-3.2
Carriages	103.0	86.1	1.058	9.0	-9.0
Sum flaps	**49.0**	**48.1**	**-**	**0.7**	**-0.9**
Sum	**61.6**	**65.9**	**-**	**-2.3**	**2.6**

Tab. 4.4: Non-optimum mass factors for analysis of wing primary structure, flaps and ailerons.

	A320 mod. mass [%]	A340 mod. mass [%]	Non-optimum mass factor [-]	A320 error [%]	A340 error [%]
Skin and stringer	59.9	60.3	1.664	-0.3	0.3
Spars	77.9	80.5	1.263	-1.7	1.7
Ribs	65.4	81.0	1.366	-10.7	10.7
Sum prim. struct.	**63.6**	**66.8**	**-**	**-1.9**	**2.1**
Flap bodies	40.0	42.7	2.418	-3.4	3.4
Flap tracks	47.5	43.1	2.208	4.9	-4.9
Carriages	102.8	88.1	1.048	7.7	-7.7
Sum flaps	**48.8**	**48.0**	**-**	**0.8**	**-1.0**
Aileron	60.0	59.1	1.680	0.7	-0.7
Sum	**61.6**	**65.0**	**-**	**-1.5**	**1.8**

In Tab. 4.2 to Tab. 4.4, the deviation of the non-optimum mass factors and the resulting accuracy is depicted. Column two and three show the ratio of the modeled mass of the FE model compared to the real mass of the component. Due to the confidentiality of the absolute mass values, only the ratios can be published here. The non-optimum mass factor is the reciprocal value of the average of these ratios. The last two columns show the resulting error between the corrected FE mass and the real mass. Due to the way of computing the non-optimum mass factor, the absolute percentage of the error for the A320 and A340 is the same for each component, but with different signs. As the relative mass of the different components, compared to the total mass of the wing, differs for the A320 and A340, the error values of the sums have different values.

4.3   Demonstration of Possible Fields of Applications

According to the research question in chapter 1.3, the developed wing mass estimation process should be able to handle *novel configurations or structural concepts.* Therefore, the flexibility of the tool chain is presented on five example studies in this chapter. These studies are performed to demonstrate the *geometrical flexibility* of the developed process. They do not represent complete aircraft or wing design studies.

4.3.1   Strut Braced Wing

Strut braced wing configurations are characterized by a tensile loaded strut that supports the wing. The strut reduces the wing's bending moment and therefore the wing mass. Strut braced wings are usually used at small turboprop aircraft. However, due to the potential in wing mass reduction, they are considered for large future passenger aircraft.

The analyzed wing consists of one unswept main wing in high wing configuration and one strut that supports the wing. The wing is mounted with four joints on the fuselage, while the strut is attached to the fuselage on the lower side. The wing has a reference area of 72m^2, a high aspect ratio of 18 and two fowler flaps on each side. Each flap is connected with two dropped hinge flap tracks to the rear spar of the main wing (see flap track type 2, chapter 3.3.2). This
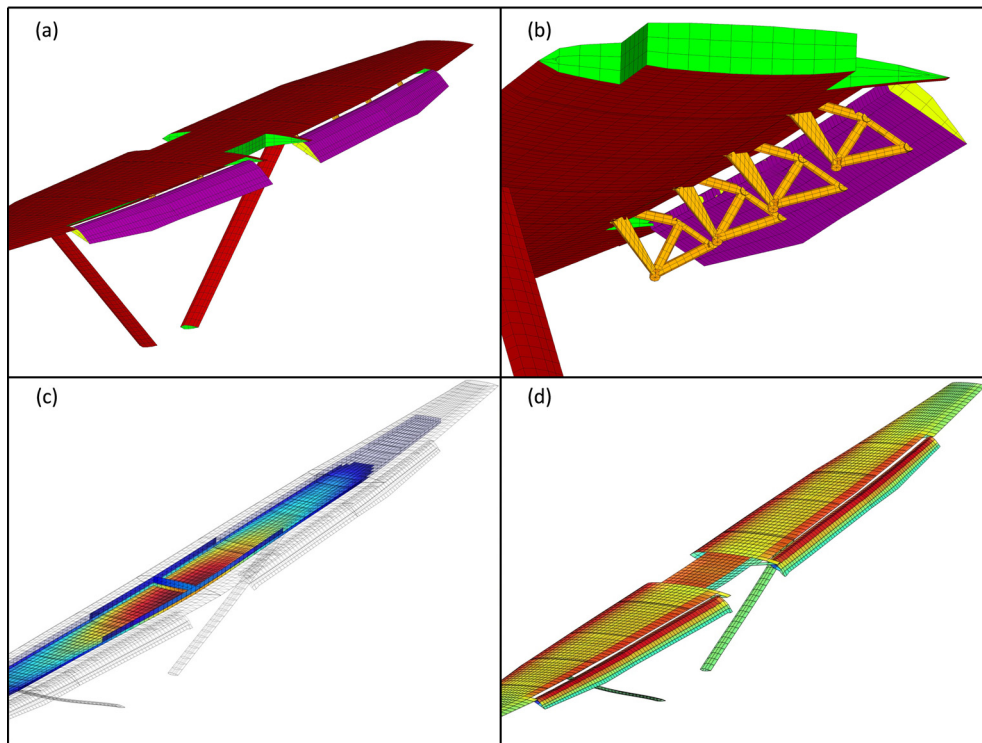
Fig. 4.5: (a) Finite element model, (b) high-lift systems details, (c) fuel loads and (d) aerodynamic pressure loads of the strut braced wing (for analysis results: red equals high values, blue equals low values).

track type is very common at large turboprop aircraft. The finite element model, the aerody-
namic pressure loads and the fuel loads for a 2.0g pull up maneuver of the strut braced wing are
shown in Fig. 4.5.

The mass of the primary structures, the flaps and the strut of the computed wing results in
5.2 t. The same wing without strut has a mass of 10.7 t. This means, that the introduction of
the strut results the wing weight by around 50%. This shows the high potential of a strut on the
wing.

4.3.2 Blended Wing Body

The blended wing body (BWB) configuration consists of an airfoil shaped body and smoothly
blended wings that are attached to the body. Both, the body and the wings produce lift. As the
configuration has no tube-like fuselage and no tails, good aerodynamic properties are expected
from this configuration. The passenger cabin is located inside the body, which allows new very
wide cabin concepts. One of the largest challenges of the design of BWBs is the structural lay-
out of the body, as the pressurized cabin has no round cross section.

The analyzed BWB configuration is based on a research configuration developed by Ciampa
et al. [10]. This very large BWB is designed to carry more than 750 passengers over a range of
10000nm. The reference area of the BWB is 2680m^2 which is much larger than today's largest
aircraft. The finite element model, the deformed model, the fuel load distribution and the aero-
dynamic pressure load for a 2.5g pull up maneuver are shown in Fig. 4.6.

Fig. 4.6: (a) Finite element model, (b) node displacement, (c) fuel loads and (d) aerodynamic pressure
loads of the blended wing body (for analysis results: red equals high values, blue equals low val-
ues).

As the current version of the WINGmass tool chain can only generate a structural layout that is constructed from ribs, spars and skins, a mass estimation of BWBs with their complex structural cabin layout cannot be performed. Therefore this demonstration only shows that the WINGmass system is applicable on BWB-like wing shapes, but not the reliable application on BWBs.

4.3.3 Box Wing

The box wing aircraft configuration is a non-planar wing concept. The box wing consists of one forward and one rear wing that are connected at their tips via a third horizontal wing. Usually, the forward wing is attached to the lower side of the fuselage, while the rear wing is attached to the upper side of the fuselage or on top of the vertical tail. The fuselage of the box wing configuration is similar to conventional tube-like fuselages. The closed wings of a box wing aircraft is expected to lead to a considerable reduction of the wingtip vortex, which leads to lower drag and therefore fuel consumption.

The analyzed box wing aircraft is similar to a configuration that is developed by Frediani et al. [11]. At this configuration, the rear wing is mounted on top of the two vertical stabilizers that are placed on the wide tail of the fuselage. This box wing has the same reference area than the A340-200, the same fuselage, the same design masses and design mission. The finite element model of the box wing, the deformed FE model, the fuel and the aerodynamic load distribution for a 2.5g pull up maneuver is shown in Fig. 4.7.
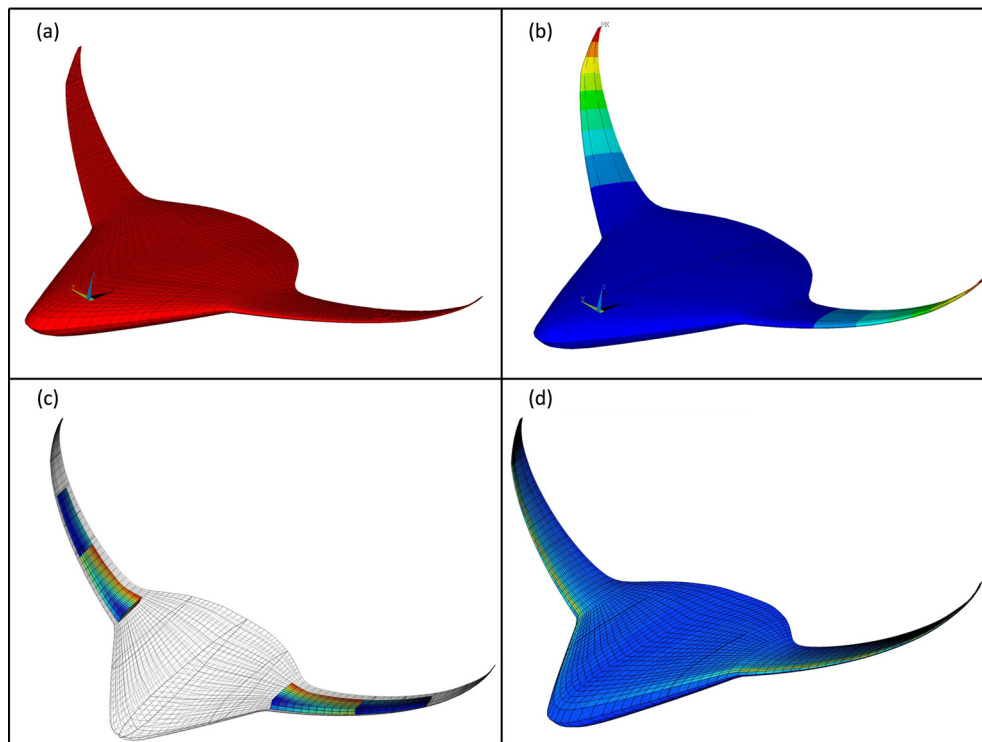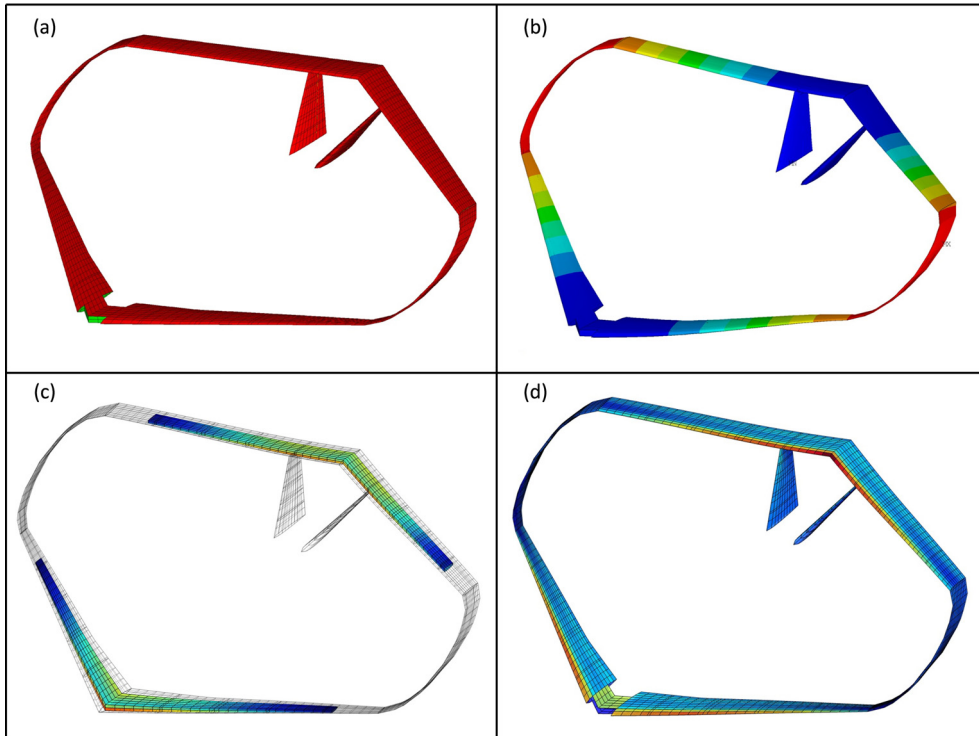

Fig. 4.7: (a) Finite element model, (b) node displacement, (c) fuel loads and (d) aerodynamic pressure loads of the box wing (for analysis results: red equals high values, blue equals low values).

The results of the analysis show a total mass of the wing primary structure of 51.7t, which is almost 1.9 times heavier than the primary structure mass of the A340 wing and tails. However, one has to consider, that the upper and the lower wing of the box wing configuration have an aspect ratio of 15.4, which compares to 9.3 on the A340. According to the statistical equation in [36] such an aspect ratio increase would lead to a 2.1 times higher mass. This means that the box wing configuration seems to be slightly lighter, than a conventional configuration with an aspect ratio of 15.4 would be.

4.3.4 Multi-Spar Flap

The multi-spar flap concept is a novel structural concept for high-lift flaps. The concept is mainly driven by manufacturing considerations. At multi-spar flaps the ribs and stringers are replaced by a set of spars that ensure good buckling characteristics of the skin. Ribs are only used as load introduction ribs at the flap tracks and at the tips of the flap.

In this analysis, the outer flap of an A320 is replaced by a multi-spar flap, having the same outer geometry, but a different structural layout. The multi-spar flap FE model, the skin thicknesses of the flap after sizing and the stress distribution on the multi-spar flap for a 2g pull up maneuver are shown in Fig. 4.8.

The sizing results show an increase in mass of the flap body of +40%, which equals 41.1kg additional mass per flap. The mass reduction due to less ribs and the absence of stringer is over-
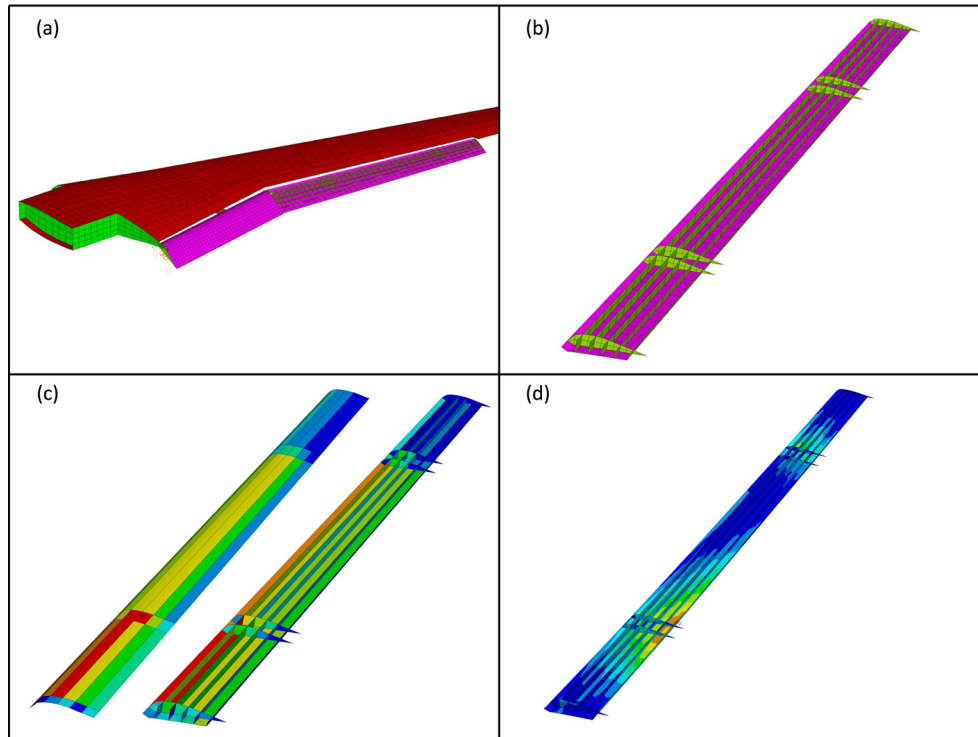
Fig. 4.8: (a) Multi-spar flap on the A320 wing, (b) detailed FE model, (c) thickness and (d) stress distribution of the multi spar flap (for analysis results: red equals high values, blue equals low values).

compensated by the higher number of spars and higher skin weight due to buckling constraints of the skin. However, further optimization of the number of spars, spar location and the split in sizing regions might lead to better results.

4.3.5 Double Slotted Flap

A doubled slotted fowler flap is a flap configuration where a second small flap is attached to the first flap that is attached to the wing. Double slotted flaps are used for several decades to increase the maximal lift coefficient of the aircraft. However, due to their high mass and drag values, double slotted flaps are usually not used for new state-of–the-art developments.

At the development of the Airbus A321, it turned out that the original A320 wing cannot provide sufficient lift. Therefore, the trailing edge of the A320 was enlarged and a second flap attached to the flaps. The second flaps are attached to the main flaps by a 4-bar-linkage flap track mechanism [78]. A similar approach is taken in this analysis. Here, a second flap is attached to the inner flap of the A320 wing. The flaps are linked by a 4-bar-linage (flap track type 6 in chapter 3.3.2). In Fig. 4.9 the finite element model and the stress and pressure distribution on the wing's shell structure for a 2g pull up maneuver is shown. The results show, that the additional flap including its tracks contribute with 77.6kg to the overall wing mass.
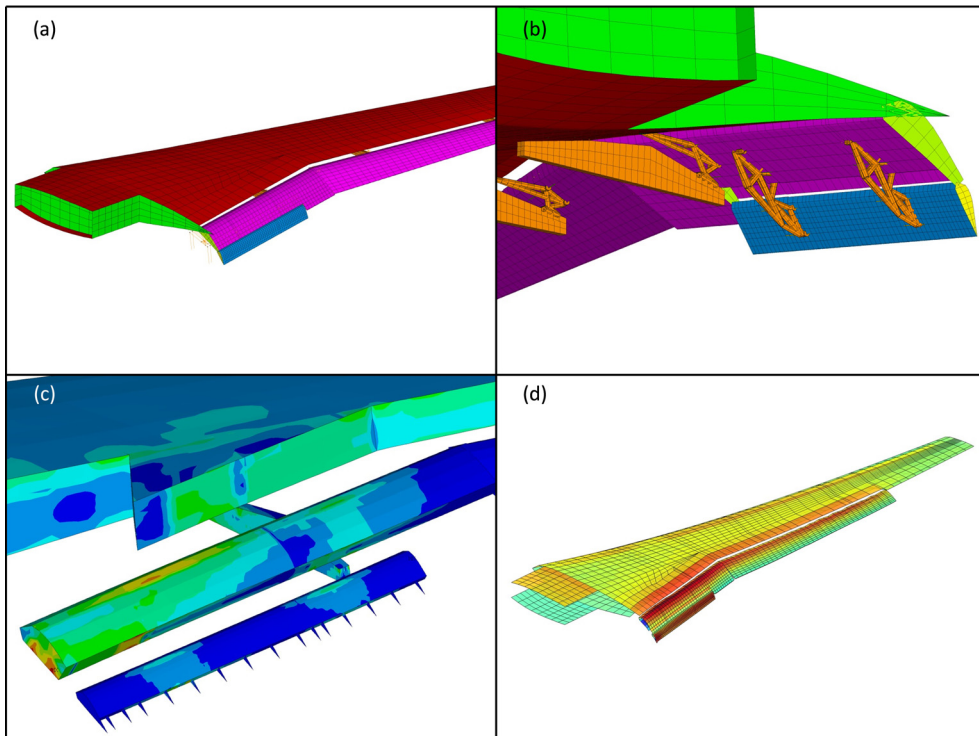
Fig. 4.9: (a) Double slotted flap on the A320 wing, (b) detailed FE model, (c) stress and (d) pressure distribution of the double-slotted flap (for analysis results: red equals high values, blue equals low values).

4.4 Aircraft Design Study

The WINGmass tool chain is applied in an aircraft design study, to demonstrate the capabilities of the chain. Therefore the WINGmass system is used together with several disciplinary aircraft design and analysis tools. The aim of the so called 'WingOpt' study is to compute the optimal wing shape for a medium range aircraft.

4.4.1 Objective of the WingOpt Study

The objective of this study is to compute the optimal wing shape in terms of mission fuel consumption as a function of the take-off field length. Therefore, a parameter variation on the wing geometry is performed. The baseline aircraft is a medium range aircraft, similar to an A320. On the one hand, the wing's dimensions are scaled from 90% to 110%, which results on a scaling of the reference area from 81% to 121%. On the other hand, the chordwise size of the flaps is varied. At the baseline aircraft, the chord of the flaps at the wing kink equals 27% of the wing chord. This value is varied from 17% to 37%. The rear spar position of the wing is adapted to the size of the flap, which changes the dimension of the wing box. An overview of the resulting wing geometries is given in Fig. 4.10.

The resulting mass and the aerodynamic performance of the new wing are used to scale the engine to meet the CS-25 climb requirements and the cruise thrust requirement. The design masses of the aircraft are recomputed with respect to a mission where a 15t payload is carried over 3000nm. Next, the take-off field length and the mission fuel for the design mission is computed. Based on these results, the optimal wing can be chosen for each take-off field length.

It would be possible to compute the engine thrust with respect to a given take-off field length. However, this would lead to oversized engines for all other flight phases and therefore to suboptimal designs. Therefore, the engine is only sized with respect to climb and cruise requirements.

Within this study, it is assumed, that the analyzed changes in wing geometry are small enough that no redesign of the whole
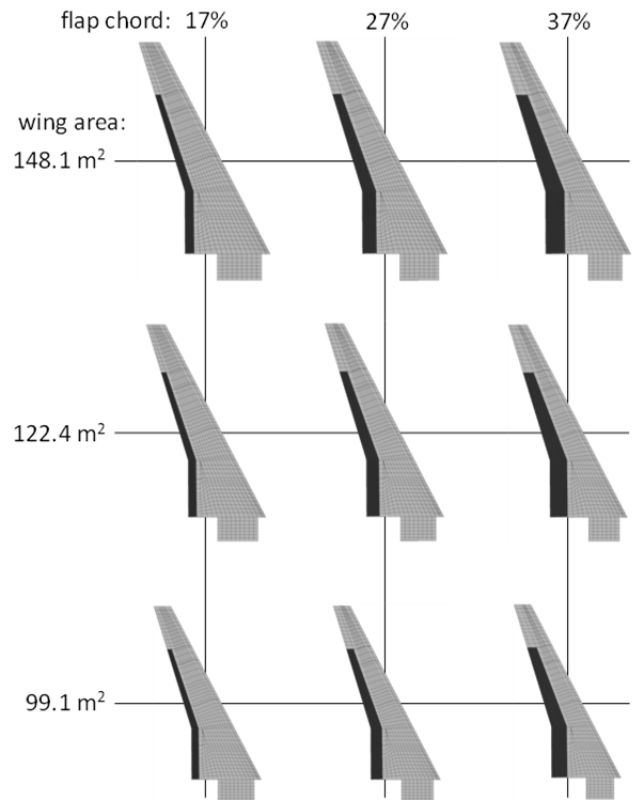
Fig. 4.10: Overview of wing geometry variation.

aircraft is necessary. Therefore the geometries and masses of all other components of the aircraft are kept unchanged.

4.4.2 WingOpt Tool Chain

For this study a tool chain is developed that includes several aircraft design tools of different disciplines. The tool chain is implemented within RCE (Remote Control Environment), which is developed in order to support interdisciplinary and distributed design in several projects [148]. An overview of the tool chain is given in Fig. 4.11.
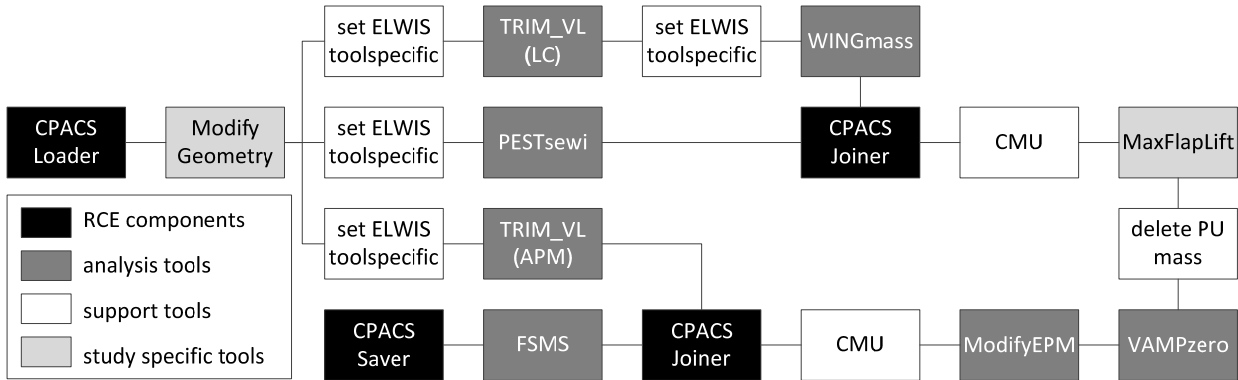
Fig. 4.11: WingOpt tool chain overview.

All black boxes in Fig. 4.11 represent RCE components that are used to load a CPACS file at the beginning, to store it at the end or to join two CPACS files, if two parallel tracks are merging. The dark grey components are the analysis tools that are used for different disciplinary analysis. The white components are very small tools that are modifying the CPACS file in order to prepare the file for the next analysis tool. As four of the analysis tools are based on the ELWIS model generator, the ELWIS tool specific has to be adopted for each tool. For example, the TRIM_VL (TRIMming with Vortex-Lattice) calculations are analyzing the whole aircraft including tails, while the WINGmass system is only analyzing the main wing. This difference has to be defined in the tool specific part of the CPACS parameterization. The light grey components are small tools that are specifically developed for this study.

The tool chain starts with loading the CPACS input file, which is followed by the ModifyGeometry tool. This tool scales the wing and changes the flap size. Next, the chain splits up in three parallel tracks. The first track (upper track in Fig. 4.11) starts with the tool TRIM_VL, which is based on the Vortex-Lattice tool AVL [94] and performs trim calculation for all load cases that should be used for the structural analysis of the wing. TRIM_VL is followed by the WINGmass system. WINGmass uses the lift coefficients of each lifting surface that are computed by TRIM_VL as load case input. In this study, the WINGmass tool chain is used to compute the mass of the wing primary structure and the flaps including flap tracks. All other secondary masses are computed by the tool PESTsewi (Preliminary mass ESTimation – SEcondary WIng structures) in the second track of the chain (middle track in Fig. 4.11). PESTsewi is based on the latest mass equations for secondary wing structure of the LTH [85]. The first and

the second track are merged by the CPACS Joiner so that all sub-masses of the wing are stored in one CPACS file. Next, CMU (CPACS Mass Updater) sums up all component and sub-component masses up to the OME, which finishes the wing mass estimation process.

The next analysis tool is the preliminary aircraft design tool VAMPzero [149]. VAMPzero is used to compute the landing and take-off field length, the new design masses, the engine scaling factor and the new power units mass. To enable VAMPzero to do these computations, two small additional tools are called in advance. On the one hand, the power-units and the design masses have to be deleted from the CPACS file, which forces VAMPzero to compute them. On the other hand, VAMPzero is currently not able to compute the additional lift and drag coefficients of the high-lift system accurately. As these coefficients are required for the computation of the take-off field length and the engine thrust, the small tool MaxFlapLift is developed. In this tool the handbook methods of Roskam [150] are implemented.

Next, the new engine performance map (EPM) is computed by ModifyEPM with respect to the scaling factor from VAMPzero. ModifyEPM is based on TWdat (TriebWerks DATenbasis) that can scale several existing engines based on precalculated high-fidelity data that is stored within TWdat. Next, CMU is called again to update the mass breakdown with the new power units mass.

The third track (lower track in Fig. 4.11) of the tool chain computes the aerodynamic performance map (APM) with the tool TRIM_VL. The APM is merged in the CPACS file of the main track and forwarded to FSMS (Fast and Simple Mission Simulator), which is the last analysis tool of the tool chain. FSMS performs a mission simulation for the 3000nm design mission and computes the required fuel mass of the mission. Finally, the CPACS file is saved.

4.4.3 Results of the WingOpt Study

In total 25 different wing configurations are analyzed within this study. The main results are plotted in Fig. 4.13 and Fig. 4.15, where each black dot indicates the computed parameter combination. The reference configuration is represented by a black triangle in the middle of the plot.

Fig. 4.12: Finite element models of wings with (a) 37% flap chord and (b) 17% flap chord.

In Fig. 4.13 (a), the mass of the flaps including the flap tracks is shown. It can be seen that the mass of the flaps is very sensitive on the relative flap chord. The increase of the relative flap chord form 27% to 37% (+37% flap area) results in an increased flap mass of +62%. This high sensitivity results from the increased flap size, but also from the higher loads on the flaps and the grown flap tracks (see Fig. 4.12). In contrast, the sensitivity of the flap mass with an increased wing area is much lower. Increasing the wing ref-

erence area from 122.4m² to 148.1m² (+21% flap area) leads to a mass increase of only 26%. A comparison between the flap masses computed by the WINGmass system and the statistically determined flap masses by PESTsewi is shown in Fig. 4.14. As both methods are calibrated for the reference configuration, the difference is zero for this wing. For a pure variation of the wing area, PESTsewi results differ up to 7% from the WINGmass results, which is acceptable for preliminary aircraft design. But for a pure variation of the relative flap chord the results differ up to 20%. The highest difference occurs for the smallest wing with the smallest flap, where the results differ almost 33%. This clearly shows the advantage of the physics-based approach in the WINGmass system. A statistics-based tool that computes the flap mass as function of the flap area is able to capture the effect of a larger or smaller wing accurately, but not to capture the
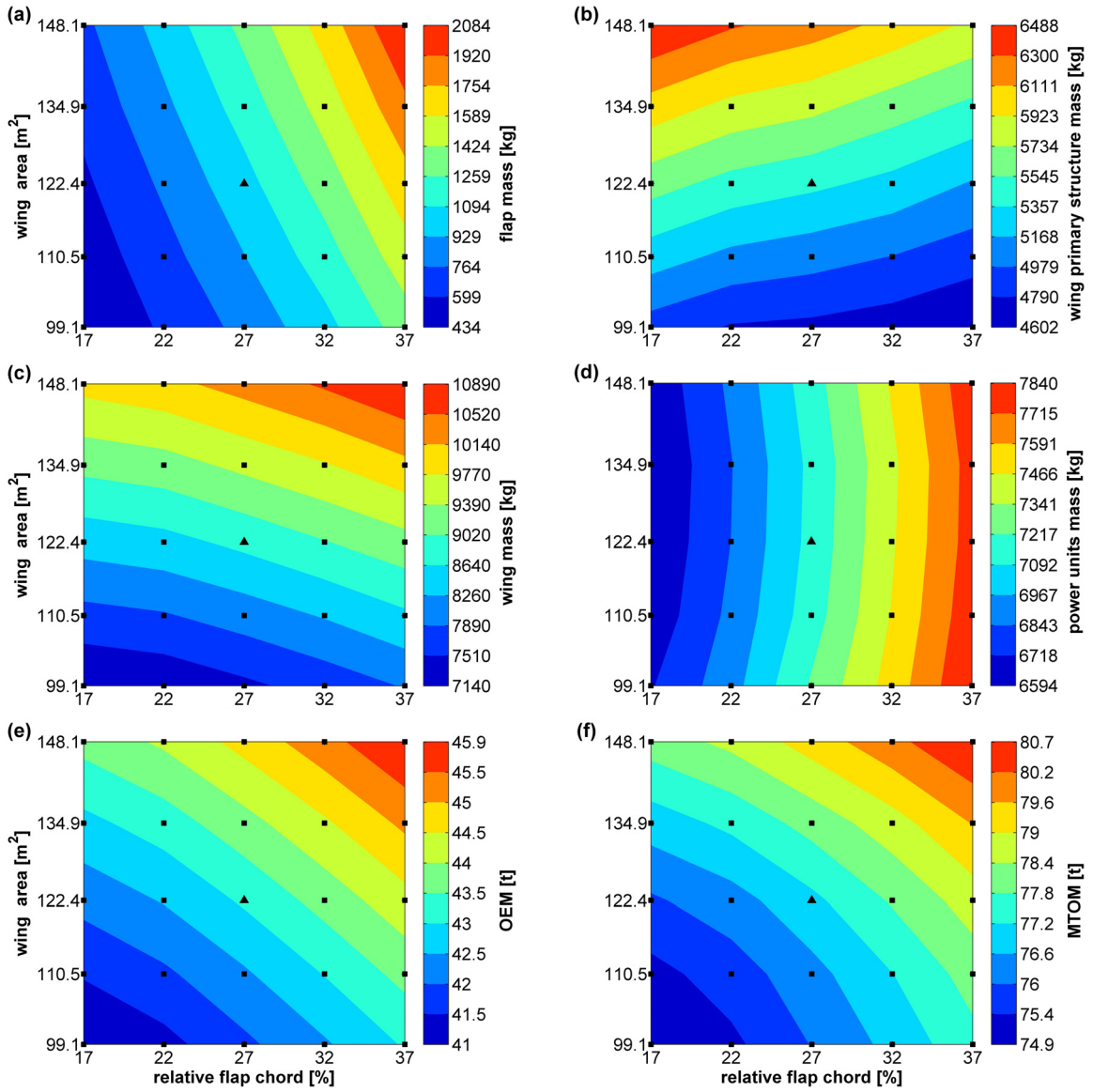
Fig. 4.13: Color maps of the (a) flap mass (incl. flap tracks), (b) wing primary structure mass, (c) wing mass, (d) power units mass, (e) operating mass empty (OEM) and (f) maximum take-off mass (MTOM) as function of wing area and relative flap chord. The black dots indicate the computed points. The black triangle in the middle of each plot marks the reference configuration.

effect of different flap geometries.

In Fig. 4.13 (b), the mass of the wing box is shown. An increase of the wing area of $+21\%$ (from 122.4m^2 to 148.1m^2) leads to an increased wing box mass of $+14\%$. This low sensitivity is caused by the decreasing area loading if the wing area increases. The increasing flap size (respectively decreasing wing box size) leads to a slight decrease in wing box mass. The total bending loads on the wing box are not affected by the different flap sizes. Therefore one might expect that the material to resist these loads is the same. But due to the airfoil shape, the average height of the smaller wing box is a bit larger, which makes it more efficient. Therefore slightly less mate-

Fig. 4.14: Difference between physics-based and statistical flap mass estimation as function of wing area and relative flap chord. The black dots indicate the computed points. The black triangle in the middle of the plot marks the reference configuration.

rial is required, which leads to a lower wing box mass. The sum of the masses of the flap, the primary structure and some additionally secondary masses leads to the wing mass, which is shown in Fig. 4.13 (c).

The new wing design is evaluated in VAMPzero in the next step, which computes the new engine and the new design masses in an iterative process. In Fig. 4.13 (d) the mass of the new power units is shown. As the power units' mass is a function of the thrust, the thrust distribution is almost equivalent to the power units' mass distribution. It can be seen in Fig. 4.13 (d), that the required thrust for the second segment climb requirement increases with increasing flap sizes, but is rarely influenced by the wing size. The higher drag of the wings with larger flaps is responsible for the higher required thrust. The small influence of the wing area on the engine thrust can be explained by the area loading of the wing. Although an increasing wing area leads to higher wing masses, the lower area loading leads to a lower induced drag during the climb phase, which counterbalances the higher weight.

The combination of the wing mass distribution in Fig. 4.13 (c) and the power units mass distribution in Fig. 4.13 (d) leads to the OME distribution in Fig. 4.13 (e). The OME mass, the constant mass of passengers and cargo and the fuel mass for the 3000nm mission results in the MTOM in Fig. 4.13 (f). The mission fuel mass distribution is shown in Fig. 4.15. The block fuel is represented by the color map that is overlaid by lines of constant take-off field length. The black area indicates infeasible designs as the maximum landing speed requirement of 70m/s is not fulfilled. By following the lines of constant take-off field length, the optimal wing design can be found for each take-off field length. The dashed line in Fig. 4.15 indicates the optimal design as a function of the required take-off field length.
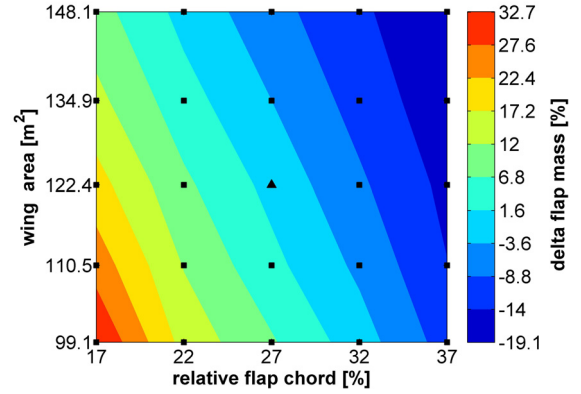
It can be seen, that for take-off field lengths that are shorter than 2000m, the optimal wing area is nearly constant while the flap size increases. A reduction of the take-off field length from 2000m to 1700m would lead to an increased fuel consumption of around 1.2%. In contrast, a reduced wing area and a reduced flap size leads to the optimal wing for take-off field lengths exceeding 2000m.

Additionally it can be seen, that the reference configuration is not on the line of the optimal wing shapes. However, the difference in block fuel for the 3000nm between the reference configuration and the optimal configuration with the same take-off field length is only around 0.2%. Therefore, other additional consideration might have led to the wing of the reference configuration.
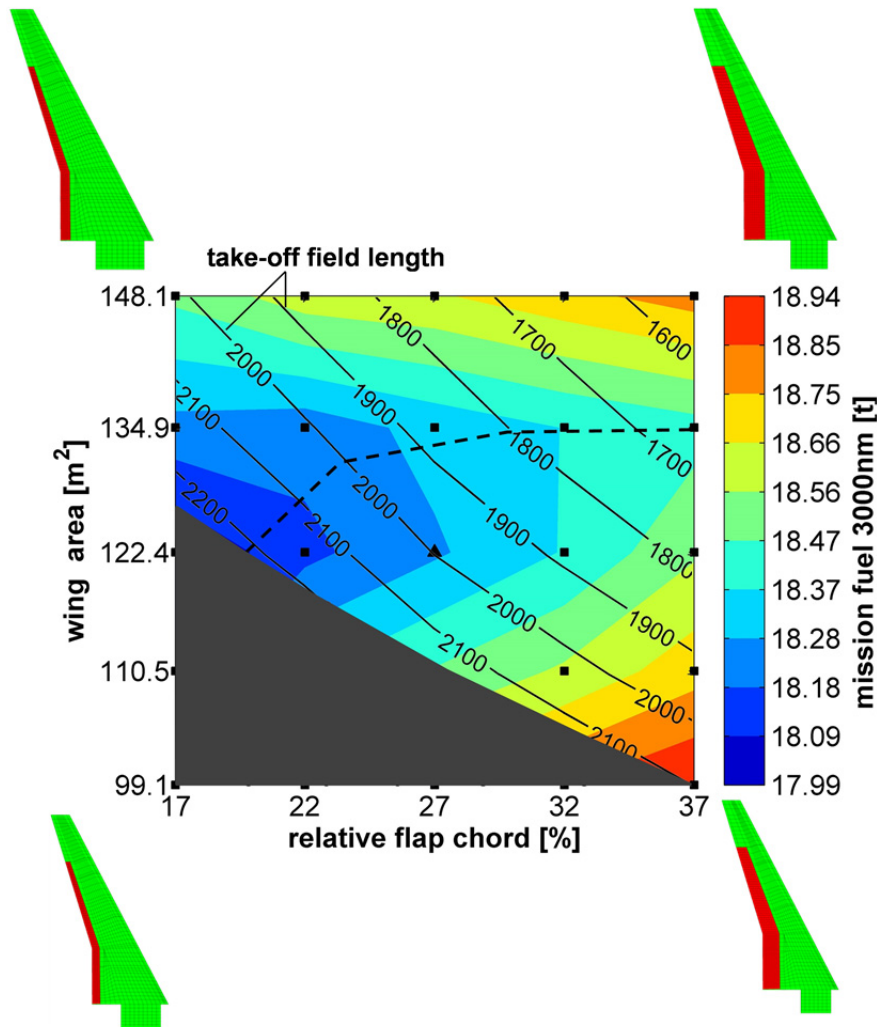
Fig. 4.15: Color map of the block fuel for the 3000nm design mission as function of wing area and relative flap chord. The lines indicate the take-off field length under ISA conditions on sea level. The black area indicates infeasible designs as the requirement of a maximal landing speed of 70m/s is not fulfilled. The dashed line indicates the optimal designs for each take-off field length.

Chapter 5

DISCUSSION AND RECOMMENDATIONS

This study focuses on the development of a flexible wing modeling and physical mass estimation system for early aircraft design stages. In the last chapter of the study the research work is summarized first. Next, the model generation process, which is a key element of the study, is discussed. This is followed by a discussion of the wing mass estimation system as a whole, its results, accuracy and applicability. The performed aircraft design study is discussed briefly. The study concludes with recommendations for further research in the field of wing mass estimation.

5.1 Summary of Research

A new developed extended physics-based wing mass estimation system is presented in this study. The tool chain is highly flexible in terms of geometries and therefore applicable for conventional and unconventional wings and novel structural layouts. Compared to state-off-the-art wing mass estimation tools, the physical modeling and therefore the physics-based mass estimation is extended beyond the wing primary structure. The developed mass estimation system includes the mass of the heaviest secondary structures, which are the flaps including flap tracks and carriages as well as the ailerons including their wing attachment. Additionally, the load-carrying structure of the engine pylon and the landing gear is included in the structural model, to take their influence on the wing structure into account.

The interdisciplinary WINGmass tool chain includes all disciplines that are required for a mass estimation system. Besides the structural analysis and sizing capability, the tool chain consist of the loads calculation modules for the aerodynamic loads, the distributed fuel pressure load, the landing gear loads and the engine thrust loads.

The structural wing model is based on finite element shell models, which is state-off-the-art in wing mass estimations processes. The flap and aileron bodies are also model with shells, while the load-carrying structures of the flap tracks are model by a combination of shell, beam, mass and hinge elements. This enables the deflection of the flaps in the FE model and ensures realistic load paths in the tracks, which is mandatory for a realistic sizing.

The aerodynamic load estimation is based on the vortex-lattice theory. The vortex-lattice model includes a representation of the slats and flaps that takes the fowler motion of the flaps into account. The flap flower motion is usually neglected in Vortex-Lattice models, but the consideration of it increases the accuracy of the load estimation. The validation of the vortex-lattice results is performed by comparing the vortex-lattice results with RANS results and shows a high accuracy.

The estimation of the fuel loads on the wing is performed by a detailed modeling of the fuel in the wing, which allows the accurate computation of the distributed fuel pressure on the wing skins, ribs and spars. The ground forces on the landing gear and the engine thrust are considered as force vectors in the finite element model, while the engine itself is modeled as a mass point that is attached to the engine pylon.

The mass estimation process includes a static aeroelastic loop that feeds the wing deformation back to the load estimation tools. For the aerodynamic loads, this represents the state-off-the-art method. However, in the developed wing mass estimation system, this loop also includes the computation of the fuel and the engine loads, which further increases the accuracy of the process.

Beside the analysis tools, the developed multi-model generator ELWIS is the core element of the mass estimation system. The generation of complex analysis models, as in the WINGmass tool chain, usually requires a huge amount of user-defined input parameters. This makes such models infeasible for preliminary aircraft design. Therefore, a knowledge-based approach is chosen for the ELWIS model generator. This means, that a large amount of engineering rules are implemented in ELWIS, wherefore the model generation process is performed automatically based on few user-friendly input parameters. The data model CPACS is chosen as input format. Therefore, the WINGmass tool chain is easy to integrate in a wider aircraft design environment, which is favorable for analysis tools of the preliminary design phase.

The mass output of the WINGmass tool chain is calibrated with respect to two reference aircraft: the Airbus A320 and the Airbus A340-200. During the calibration, the non-optimum mass factors (respectively the calibration factors) are determined and the difference between the real aircraft mass and the calibrated WINGmass output is shown. The calibration factors are determined for three different cases: the analysis of the wing's primary structure, the analysis of the wing's primary structure and the flaps and the analysis of the wing's primary structure, the flaps and the ailerons. Due to the interaction of the movables with the primary structure, slightly different calibration factors result for each case. The calibration shows very small differences between the calibrated results and the reference aircraft, which shows the high accuracy of the tool chain.

To demonstrate the required flexibility of the wing mass estimation system, exemplary studies on five different configurations are performed. The configurations include a strut braced wing, a box wing, a blended wing body, a conventional wing with a double slotted flap and a conventional wing with a multi-spar flap.

To demonstrate the benefit of the extended physics-based modeling and the application of the WINGmass system in an interdisciplinary aircraft design environment, an aircraft design study is performed. The objective of this study is to compute the optimal wing shape in terms of mission fuel as a function of the take-off field length. Therefore, a parameter variation on the wing and flap geometry is performed, the engine scaled correspondingly and the mission fuel evaluated.

5.2 Discussion of the Model Generation Process

One core element of the WINGmass system is the ELWIS multi model generator. The multi model generator is developed to fulfill the requirement of the research question that the wing mass estimation system needs to be applicable *already in early design stages*. This needs to be achieved, although very detailed and complex analysis models are required as the research questions demands a reliable analysis of the *total wing mass, including the major secondary structures*. These models are more complex than the tools in state-off-the-art wing mass estimation processes. ELWIS is the first published model generator that is able to generate structural FE wing models of the wing primary structure and a realistic representation of all trailing edge devices including their attachments to the wing box. The kinematics of the load-carrying structure of the flap tracks are modeled three dimensionally in the wing model, which is an approach that was never published before for a wing mass estimation process in early design stages.

The research question demands for a process that can handle *novel configurations or structural concepts.* The geometrical flexibility in terms of wing configurations is demonstrated in chapter 4.3, where example studies on a box wing aircraft, a blended wing body and a strut braced wing are presented. Additionally, conventional wings with winglets and wing tip fences (which is modeled as wing that splits up in two wings) are used as examples throughout the study. These wing shapes and configurations include all wing configurations that are in focus of today's international research activities. However, due to the flexible implementation of ELWIS and the equal flexible parameterization in CPACS, additional new and innovative wing shapes can be analyzed. On the structural configuration side, almost all configurations that are constructed with ribs and spars are definable in CPACS and can be processed by ELWIS. Spars can merge or cross each other and can start and end at every wing position. A similar flexibility is realized for the ribs. Summarizing, the combination of the CPACS parameterization and the ELWIS model generation allows a flexible analysis of all wing-like structures that are in focus of today's international research activities.

The geometry of all non-wing body structures, such as the flap tracks, the engine pylon and the landing gear, are generated automatically by ELWIS, based on implemented engineering rules. This ensures the usability during early design stages, where the designer is not caring about the detailed geometry of e.g. the flap track. The flap track geometry is computed based on the user-defined kinematic type, the position of the track on the wing, the wing and flap geometry and the minimal and maximal deflection position of the trailing edge device. For a nor-

mal flap, this is the cruise and the landing position. For some kinematic track types this is absolutely sufficient. For example for dropped hinge flap tracks, the whole deflection path is exactly defined based on these two positions. However, for other kinematic types the deflection path between the maximal and minimal position can be changed in a limited range by the detailed design of the flap track geometry. Therefore, the ELWIS model generator cannot ensure that e.g. the take-off position of the flap can be reached exactly with the generated flap track geometry. However, as only small variations of the path are possible within one kinematics type, this simplification in the model generation process is acceptable for early design stages. Especially, as this simplification also reduces the amount of user-defined input parameters.

The flaps and slats are included in the vortex-lattice model by modeling their flap fowler motion and the rotation. The generation of the vortex-lattice model allows the same flexibility in wing configurations as the generation of the structural model. The vortex-lattice model can contain crossing or splitting wings, so that wings with winglets, wings with wing tip fences, H-tails, strut braced wings or box wings can be modeled. A special module is implemented, that ensures that the interconnection of different parts of the wing (e.g. wing and winglet or wing and flaps) is exact and that the element split is the same on all neighboring parts. This avoids unrealistic numerical effects at the intersections. It would be possible to model the spoiler in the same way in the vortex-lattice model. However, the vortex-lattice theory is already at its limits with the flaps and slats and the modeling of the spoiler would not lead to useful results.

The model generation process of the fuel tank model is highly efficient, as the already generated structural model is directly used. Therefore hardly any additional numerical effort is required to generate the fuel tank model. Additionally, this approach avoids the need for an interpolation between the fuel mesh and the structural mesh as it is needed for the aerodynamic loads.

Dependent on the complexity of the wing, a CPACS model, including the definition of the internal structures and the movables, can be created in a few hours. If the new wing is based on an already existing CPACS file, which is mostly the case, this time can be reduced further. Therefore, the use of the CPACS format for the analysis is well feasible during early design stages. Also the low model generation time in ELWIS is well feasible for early design stages. Dependent on the analysis, ELWIS usually runs between 1 and 5 minutes, which is negligible compared to the runtime of the whole WINGmass system (see next subchapter).

Referring to the research question in chapter 1.3, the generation of the required complex analysis models out of the user-oriented and discipline neutral data format CPACS is feasible during early design stages, by applying a knowledge-based model generation approach as it is demonstrated in ELWIS. The computation time for the model generation as well as the time for setting up an analysis in CPACS is well feasible for the use in preliminary aircraft design.

5.3 Discussion of the Wing Mass Estimation

The developed wing mass estimation system is the first published system that is able to estimate the mass of the wing primary structure, the flaps, including flap tracks and the ailerons physics-based. Within the system, all six characteristics of a state-off-the-art physics-based mass estimation system are included (according to [24]; see chapter 1.1.3): the multi-model generation capability, the load generation capability, the load application capability, the structural analysis capability, the structural sizing capability and the aeroelastic feedback capability.

The validation of the aerodynamic load estimation in chapter 4.1 shows that the vortex-lattice method is well suited for the wing mass estimation process. Although the absolute lift of a wing can be computed accurately with a low number of vortex elements, the accurate computation of the flaps requires a high amount of vortex elements. However, at the computations with the most vortex elements, only four elements are placed in chordwise direction on the flap body. Therefore the term 'high' means high compared to usual vortex meshes on flapless wings. But by considering the flap as a wing, the number of elements is rather low. These four elements are sufficient for an accurate prediction of the lift of the flap (3.4% error compared to RANS results). However, the chordwise center of lift cannot be represented accurately with only four elements. Therefore a correction is applied that shifts the chordwise center of lift on deflected flaps more to the front. At every spanwise position of the flap, the corrected center of lift is less than 4% flap chord away from the RANS results.

The fuel loads are applied as pressure load on the structural model, similar to the aerodynamic loads. This approach leads to a high accuracy, as the pressure load takes the fuel distribution into account. Usually, only the aerodynamic loads are updated with respect to the wing deformation in state-off-the-art wing mass estimation systems. Besides the aerodynamic loads, also the fuel and engine loads are included in the static aeroelastic loop in the WINGmass system. This leads to a further increase in accuracy, as the spanwise fuel distribution has a considerable influence on bending moment distribution.

The structural analysis and sizing methodology in the WINGmass tool chain is similar to the sizing of comparable tool chains. However, as the WINGmass tool chain considers the wing primary structure and the trailing edge devices, special sizing criteria are used in addition. It would be possible to introduce higher level sizing criteria in S_BOT+, such as e.g. FEM buckling instead of the handbook buckling criteria or non-linear analysis instead of linear analysis. However, these methods would require significant more computation time. As the WINGmass system is already computational demanding (see Tab. 5.1), a further increase in computation time should be avoided. Additionally, the mentioned higher level capabilities are not required for the majority of analysis.

The calibration of the tool chain and the resulting errors for the two reference aircraft is presented in chapter 4.2.3. The accuracy of the WINGmass system with other FEM-based wing mass estimation tools can only be compared with the tool of Österheld [58], as she is the only author who published her validation/calibration results. Österheld developed an FEM-based aircraft mass estimation tool for the structure of wings, tails and fuselages that is included in the

aircraft design program PrADO (see chapter 1.2.3). The validation by Österheld shows an error of -0.7% for the A320 wing, -0.1% for the A340-300 and -9.8% for the A340-600. This compares with -0.9% for the A320 and 1.1% for the A340-200 for simulations of the wing primary structure in the WINGmass tool chains (see Tab. 4.2). This shows that both tools deliver very accurate results and a very small database of reference aircraft. Therefore no statement can be given whether the WINGmass system is more accurate or the tool of Österheld.

The very small total errors of the WINGmass tool chain result from counterbalancing errors of its subcomponents (see Tab. 4.2). The error of the skin and stringers computation is ±1.0%, while the error for the spars is ±2.9%. As both components have a comparable simple structural layout and clear structural load paths, small errors can be expected. The spars have a modeled mass is around 80%, which is a very high value. This can be explained by the conservative buckling sizing criterion that is used. The spars are sized to prevent buckling, while post buckling criteria are applied at real aircraft. The error at the rib computation has an absolute value of ±8.3%, which is comparatively high. A detailed analysis of the masses of the ribs showed, that the mass of the ribs, close to the wing root, is too high. This effect is higher for the larger A340 wing than for the smaller A320 wing. The reason for that can be found in the modeling of the ribs with shell elements and the fact that each rib has a constant shell thickness. Therefore only one small high loaded element of the rib significantly increases the mass of the whole rib. At real aircraft, the ribs in the center wing box are often constructed from several struts or have large cut-outs to reduce the rib mass. Therefore, a more detailed modeling of the ribs could increase the accuracy.

For the simulations of the wing and the flaps (see Tab. 4.3), small errors occurred for the flap body (±2.5%) and the flap tracks (±3.2%). As the flap bodies are structures similar to the wing, a small error can be expected. But the flap tracks have a complex structural layout and the geometry of the flap tracks is automatically generated by ELWIS. Therefore, it is not an exact representation of the real geometry, which is an additional source of inaccuracy. However, the small error for the flap tracks clearly shows the high quality of the detailed track models that are generated by ELWIS. The high error in the computation of the carriage mass (±9.0%) can be explained by the applied method. For the mass computation of the carriages, the equations from Holert [124] are used. In his verification, errors of 36.7% for the A320 carriage and 18.7% for the A340 carriage occurred. As his method is the best available, it is used although the errors are relatively high. As the carriages of the A320 have an average mass of around 10kg while the total wing mass is almost 9t, 9.0% error at the carriage computation has no significant effect on the total wing mass.

The modeled spar mass of the A340 considerably increases, compared to the analysis without flaps. This can be explained by the additional load cases at the simulation with flaps and by the additional loads that are transferred from the flaps to the wing box. Therefore the spar mass at both reference aircraft increases, but the effect is larger at the A340.

For the third analysis case, the ailerons are also included in the analysis (see Tab. 4.4). The error for the aileron including its attachment is ±0.7%, which is a very good result. One uncer-

tainty for this computation is that the number and the positions of the attachment joints are unknown for both reference aircraft, wherefore assumptions had to be made.

Tab. 5.1: Computation time and percentage of physics-based mass estimation, relative to the wing mass, for different analysis cases (Intel Core i7-2600; 3.40GHz; 8GB RAM, ANSYS 13.0).

	Computation time [h:min]	Physics-based mass rel. to wing mass A320 [%]	Physics-based mass rel. to wing mass A340 [%]
Prim. struct. (w/o aeroelasticity)	ca. 0:45	62.0	68.9
Prim. struct.	ca. 1:30	62.0	68.9
Prim. struct. + flaps (w/o failure cases)	ca. 7:00	71.7	75.8
Prim. struct. + flaps	ca. 16:00	71.7	75.8
Prim. struct. + flaps + ailerons	ca. 24:00	72.5	77.0

For the evaluation of a new method for preliminary design, the trade-off between the benefit and the computational cost has to be considered. In Tab. 5.1, the computation time for five different analysis cases is compared with the ratio of the mass that is computed with the physics-based method relative to the total wing mass. It has to be considered, that the computation time greatly depends on the number of elements in the FE and the vortex-lattice model, the number of analyzed load cases and the number of necessary iterations until convergence is reached. If only the wing primary structure is computed, the wing mass estimation system needs around 1,5h. The computed primary structure represents 62.0% of the wing mass of the A320, respectively 68.9% at the A340. By turning the aeroelastic loop off, computation time can be reduced by a factor of two. If the flaps are included in the analysis, the analysis time increases to 7h (respectively 16h with consideration of failure cases). This higher analysis time is required to increase the share of the physics-based mass by 7% - 10% to 71.7% for the A320 and 75.8% for the A340. The additional consideration of the ailerons increases the share of physics-based mass by another 1%, but increases the computation time to 24h.

No general statement can be given, whether the increase in physics-based computed mass justifies the increase in computational time. The computation time for the primary structure is no issue for today's preliminary aircraft design tool chains. However, if the required computation time for the flaps and the ailerons can be accepted, depends on the specific aim of the study. Especially the high additional computation time for the ailerons, which leads to only 1% increase of the physics-based mass, has to be seen critical. If only the wing planform of a conventional wing should be varied slightly, a consideration of the movables might not be necessary. But if the focus of the study is on the movables, like in the WingOpt study in chapter 4.4, the additional effort pays off. Especially, if the analyzed wing geometry leaves the knowledge base of statistics-based methods, the physics-based WINGmass system is more reliable, wherefore the additional computation time can be justified.

Referring to the research question in chapter 1.3, it is demonstrated that the WINGmass system delivers reliably predictions of the wing mass, including the trailing edge devices. The calibration shows the accuracy of the physics-based method for conventional aircraft. However, the advantage of the WINGmass system is not the accurate recalculation of existing conventional aircraft. Due to its physical basis, its major advantage is the reliable applicability for sensitivity

studies and studies on novel configurations and structural layouts that are not captured by the knowledge base of existing statistical methods. This is clearly shown in the aircraft design study in chapter 4.4, where the flap design leaves the design space that is captured by statistical methods. Considering these advantages, the relatively high computation time of the WINGmass system is acceptable.

5.4 Discussion of the Aircraft Design Study

The capability of the WINGmass tool chain is demonstrated in the WingOpt aircraft design study in chapter 4.4. In this study, the wing area and the flap size is altered and their influence on the wing mass, the engine, the design masses and the 3000nm mission fuel analyzed. The results show the optimal combination of wing area and flap size for each required take-off field length. Additionally, the costs in terms of mission fuel for an increasing or decreasing take-off field length are computed.

According to the results of the WingOpt study, the fuel consumption of the reference configuration is 18.26t for a 3000nm mission. A small increase of the wing area, in combination with smaller flaps would lead to the optimal wing design for the same take-off field length. This optimal wing design would reduce the fuel consumption 0.2%, although the wing mass would increase around 5%. However, due to the better aerodynamic properties of this wing during take-off a lower engine thrust is required, wherefore the OEM keeps nearly constant.

The WingOpt study clearly shows the advantage of the WINGmass system, compared to classical statistics based methods to compute the secondary structures mass. It is shown that the change of the flap mass at changing flap sizes differs significantly, depending on whether the whole wing is scaled or the flap chord is modified. As it is shown in Fig. 4.14, a statistical method that computes the flap mass as function of the flap area is not able to take these effects into account.

The highest uncertainties of the results of the study are the aerodynamic computation of the high-lift characteristics and the zero lift drag. Both computations are based on simple handbook methods. For the zero lift drag high calibration factors were necessary for the initial calibration of the chain. The accuracy of the zero lift drag computation is crucial, as the ratio between zero lift drag and the induced drag determines the optimal wing area. Therefore the difference between the reference configuration and the optimal wing area for the same take-off field length might also be caused by the zero lift drag computations.

Due to issues, related to the instability of RCE and limited computational resources, no loop between the preliminary aircraft design tool VAMPzero and the wing mass estimation could be realized. Therefore, the influence of the varying design masses is not taken into account in the wing mass estimation. As the design masses are only changing within a small bandwidth, the influence of this simplification on the final wing mass is expected to be low. However it might slightly change the resulting optimum wing area and flap size.

5.5 Recommendations

This study demonstrates a reliable and applicable wing mass estimation method. However, further research is recommended to improve the future wing mass estimation process.

Modeling and Model Generation

The aim of this study is to develop a reliable wing mass estimation system for the total wing mass, including the major secondary structures. These secondary structures are all trailing edge devices, as they are the heaviest secondary structures. However, the chosen approach could be expanded for spoilers and slats. Spoilers can already be included in the ELWIS structural models. But as no method for the estimation of the aerodynamic loads is applicable, they are currently not used in the WINGmass system. Therefore, the next step should be the implementation of a higher-level aerodynamic model for the load estimation. To add an additional output in ELWIS for this aerodynamic model is simple. But first, research should focus on the selection of the aerodynamic method. For this selection, the opposing requirements of an accurate prediction of the wing including all movables and the numerical cost must be well balanced. The higher level aerodynamic modeling and the consideration of all movables would enable the consideration of load elevation systems that are currently neglected.

The track geometry is generated with respect to the cruise and the landing configuration of the flap. It is recommended to explore if the additional consideration of the take-off configuration would lead to an increased accuracy of the chain.

ELWIS generates the flap tracks based on implemented design rules. In order to analyze predefined flap track geometries, a method should be implemented, that ELWIS can generate FE models from geometries that are stored in CPACS. These geometries can result from a special flap track design tool (such as TEFLAMES [124]). Additionally, ELWIS should write back the generated geometries in CPACS, in order to enable such tools to analyze the ELWIS geometries.

The error in the estimation of the ribs is caused by the modeling of the ribs with shell elements. Therefore, it is recommended to analyze, whether the accuracy can be improved by modeling these ribs with struts that consist of struts in reality.

In the WINGmass system, the stringers are modeled in a smeared representation, which simplifies the modeling and allows the computation of the stringer pitch and stringer orientation during the normal sizing. However, it is recommended to add the possibility of an explicit stringer representation. It should be evaluated how the simplified smeared stringer modeling influences the wing behavior and sizing results. Also the possibility of a two level approach with a smeared stringer at the beginning and a explicit stringer representation afterwards should be examined.

The clamping of the wing model at the root is rather rough, compared to the real wing fuselage attachment. Therefore the coupling of the wing with a similar fuselage model is recommended to explore the influence of the simplified clamping. Therefore, focus has to lie on the correct modeling of the load-carrying structures in the center fuselage. Additionally, further analysis can be performed with global FEM model that include the fuselage, the wing and the tails. This work already started as can be seen in reference [151] and Fig. 5.1.
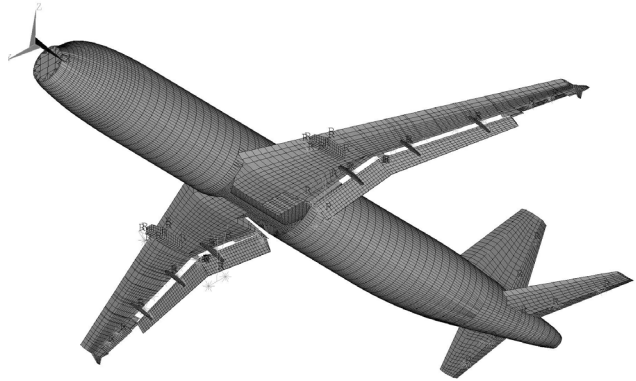

Fig. 5.1: A320 global FEM model with ELWIS wing and tail.

Structural Analysis and Sizing

The implemented structural sizing is able to handle composite as well as metallic materials. However, only composites having a balanced and symmetrical layup can be analyzed by using the implemented hand book sizing methods. This is sufficient for the majority of wing structures, but more advanced composite sizing methods are recommended in order to be able to perform an accurate sizing of a general layup. This method should also take manufacturing constrains into account (e.g. ramp-ups), as these constrains can significantly increase the mass of composite wings (see e.g. [72]).

The implemented handbook equations for the buckling computations are well known to be quite rough. It should be analyzed whether FEM-based buckling analysis can increase the reliability of the mass estimation. Using this method, it should be possible to consider the post-buckling behavior for the sizing of the structures.

In the WINGmass system, only static analyses are performed. However, the derivation of an equivalent beam model from the shell model and the dynamic flutter analyses of the beam model would increase the reliability of the mass estimation system. Especially the analysis of the wing-flap-configuration in early design stages would be a very interesting new research field. Usually, such flutter analyses are used to exclude fluttering wing configurations form the design space. However, a proper stiffening of the wing configuration might also lead to a good design. Therefore further research is required, to understand how a given wing configuration can be stiffened in an efficient and as light as possible way.

For wings with very high aspect ratios, the linear analysis in the WINGmass system might not be sufficient. Therefore the possibility of non-linear analysis should be implemented and the differences between both analysis modes studied.

The load-carrying structures of the landing gear and the engine pylon and the fixed trailing edge support structure is already included in the structural model. However, they are only used

to transform loads on the wing structure but are not sized. It should be analyzed how the mass of these additional structures can be included in the mass estimation process in an efficient way and which additional load cases and sizing criteria are necessary for that.

Application Aspects

The WINGmass system requires two main pieces of input: on the one hand the definition of the wing and on the other hand the load cases that should be analyzed. Both pieces of input must be provided by the user. Although the CPACS parameterization is very user-friendly, preparation of an analysis may take several hours. To reduce this time, a further support of the designer before the analysis starts would be preferable.
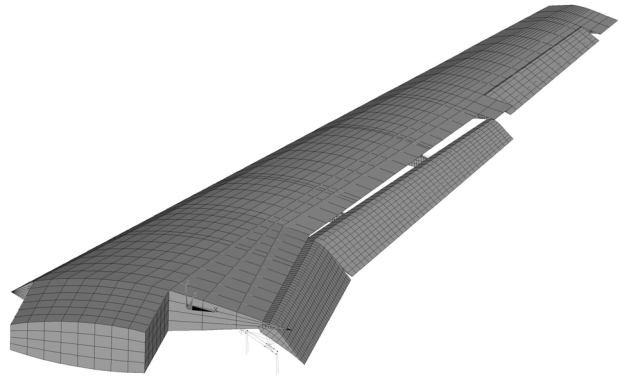

Fig. 5.2: ELWIS wing, generated from a VAMPzero CPACS input file.

For the wing related inputs, current research is ongoing how the preliminary aircraft design tool VAMPzero [149] can be enhanced in order to automatically generate the required wing geometry including the high-lift system. This automatically generated wing might not exactly be the wing, that should be analyzed, but it gives the designer a good starting point within a few minutes of work. In the next step, the designer can modify this wing according to his needs. First trials with an enhanced version of VAMPzero show, that a considerable time savings can be achieved. In Fig. 5.2, an ELWIS wing is shown that is created from a CPACS file that is generated by VAMPzero. To generate such wings, VAMPzero only requires a set of around 10 global aircraft design parameters, such as payload, range and cruise Mach number.

However, although the wing can be created very fast in CPACS, the load case definition still needs to be done by the user. Dependent on the number and type of load cases, this can be a time intensive process. First attempts to automate the load case generation have been undertaken in the project VAMP (Virtual Aircraft Multidisciplinary analysis and design Processes) [152]. However, the tool that is developed in VAMP is very simple and would need major improvements in order to be used together with the WINGmass system.

After load case generation is automated, a highly interesting research field would be the analysis of the influence of a wide range of different load cases on the wing. The knowledge and understanding of which load case has which impact at which wing geometry needs to be improved. This can reduce the number of required load cases for future wing studies and increase the reliability of the analysis, as only the important sizing load cases have to be analyzed. The analysis of the sizing load cases should include a detailed analysis of fatigue load cases, including their load spectra and corresponding material allowables (see e.g. [40]).

References

[1]   International Air Transport Association, *IATA Financial Forecast*, www.iata.org, 2011

[2]   European Commission, *The EU Emissions Trading Scheme*, ISBN 978-92-79-12255-2, 2009

[3]   *Luftverkehrsteuergesetz (LuftVStG)*, BGBI. I S. 1885, 9th December 2010

[4]   *Luftverkehrsteuer-Absenkungsverordnung 2012 (LuftVStAbsenkV 2012)*, BGBI. I S. 2732, 16th December 2011

[5]   Her Majesty's Revenue and Customs (HMRC), *Notice 550 Air Passenger Duty*, August 2010

[6]   Wikipedia contributors, *Airport improvement fee*, Wikipedia, The Free Encyclopedia, http://en.wikipedia.org/w/index.php?title=Airport_improvement_fee& oldid=469957810, 24th January 2012

[7]   Friese U., Peitsmeier H., Schwenn K., *Genervt vom Fluglärm*, Frankfurter Allgemeiner Zeitung, 12th December 2011

[8]   Washburn A., *NASA's Current Plans for ERA Airframe Technology*, 48th AIAA Aerospace Sciences Meeting, 2010

[9]   Airbus Deutschland, *VELA – Very Efficient Large Aircraft*, Final Technical Report, 2006

[10]   Ciampa P. D. et al., *A Functional Shape Parameterization Approach for Preliminary Optimization of Unconventional Aircraft*, 3rd CEAS Air & Space Conference, 2011

[11]   Frediani A. et al., *Development of an Innovative Configuration for Transport Aircraft; a Project of Five Italian Universities*, XVII Congresso Nazionale AIDAA, 2003

[12]   Frediani A., Oliviero F., *Conceptual Design of an Innovative Large PrandtlPlane Freighter*, 10th European Workshop on Aircraft Design Education, 2011

[13]   Kroo I., *Nonplanar Wing Concepts for Increased Aircraft Efficiency*, VKI lecture series on Innovative Configurations and Advanced Concepts for Future Civil Aircraft, 2005

[14]   Rossow C.-C., *Aerodynamics – A discipline swept away?*, The Aeronautical Journal, Volume 114, No 1160, Paper No. 3626, 2010

[15]   Hansen H., *Laminar Flow Technology - The Airbus View*, 27th International Congress of the Aeronautical Sciences (ICAS), 2010

[16]   Bertsch L., *Untersuchung von Hochauftriessystemen auf deren Anwendbarkeit im Projekt Q-STOL*, DLR Interner Bericht, IB 124-2006/08, 2006

[17]   Schneider O., Kreth S., Bertsch L., *Towards a Quiet Short Take-Off and Landing Transportation System : Concept Evaluation and ATM Integration*, International Powered Lift Conference, 2010

[18]   Lopez M. P. M., Dominguez F. J. C., Cediel J. D. C., *Integrated Multispar Torsion Box of Composite Material*, US Patent No.: 7,806,367 B2, 2010

[19] Ediger K., Zeumer C., Dugas M., *FAME-liA 4.00 F3 – Validation Document*, Technical Report, Airbus Deutschland GmbH, 2004

[20] Raymer D. P., *Aircraft Design: A Conceptual Approach*, AIAA Education Series, 4th edition, ISBN-13: 978-1563478291, 2006

[21] Torenbeek E., *Synthesis of Subsonic Airplane Design*, Springer Netherlands, ISBN-13: 978-9024727247, 1982

[22] Mechler H., *Synthese und Analyse im parametrischen Flugzeugvorentwurf*, PhD thesis, TU München, Dr. Hut Verlag, ISBN 3-934767-55-9, 2002

[23] Pardessus T., *Concurrent Engineering Development and Practices for Aircraft Design at Airbus*, 24th International Congress of the Aeronautical Sciences (ICAS), 2004

[24] Hürlimann F., *Mass Estimation of Transport Aircraft Wingbox Structures with a CAD/CAE-Based Multidisciplinary Process*, PhD thesis, ETH Zürich, Nr. 19458, ISBN 978-3-909386-46-8, 2010

[25] La Rocca G, *Knowledge Based Engineering Techniques to Support Aircraft Design and Optimization*, PhD thesis, TU Delft, ISBN 978-90-9026069-3, 2011

[26] Carreyette J. F., *Aircraft Wing Weight Estimation - A Brief Summary of the Accurace of Some Methods of Prediction and a Suggested 'First Approcimation' of Greater Accuracy*, Aircraft Engineering and Aerospace Technology, Volume 22, Issue 1, DOI: 10.1108/eb031848, 1950

[27] Howe D., *Initial Aircraft Weight Prediction*, College of Aeronautics Note No. 77, 1958

[28] Roskam J., *Airplane Design – Part V: Component Weight Estimation*, DARcorporation, ISBN: 1-884885-50-0, 2003

[29] Howe D., *The prediction of aircraft wing mass*, Journal of Aerospace Engineering, Volume 210, Issue 27, 1996

[30] Jenkinson L. R., Simpkin P., Rhodes D., *Civil Jet Aircraft Design*, Elsevier Science, ISBN 0-340-74152-X, 1999

[31] Sellner W., *Wing Mass Estimation for Trainer and Fighter Aircraft in the Predesign Phase based on more than 100 build Aircraft in the Period from 1935 to 2005*, SAWE Paper No. 3271, 61rd Annual Conference of the Society of Allied Weight Engineers (SAWE), 2002

[32] Shevell R. S., *Fundamentals of Flight – Second Edition*, Prentice Hall, ISBN-13: 978-0133390605, 1988

[33] McCullers L. A., *Aircraft Configuration Optimization Including Optimized Flight Profiles*, NASA N87-11743, 1984

[34] McCullers L. A., *Flight Optimization System*, Release 7.70, User's Guide, 2009

[35]   Udin S. V., Anderson W. J., *Wing Mass Formula for Subsonic Aircraft*, Journal of Aircraft, Vol. 29, No. 4, 1991

[36]   Dorbath F., Gaida U., *Large Civil Jet Transport (MTOM > 40t) – Statistical Mass Estimation*, Luftfahrttechnisches Handbuch, MA 401 12-01 B, 2013

[37]   Ripley E. L., *A Method of Wing Weight Prediction*, RAE Report, Report No. Structures 109, 1951

[38]   Burt M. E., *Weight Prediction for Wings of Box Construction*, RAE Report, Report No. Structures 186, 1955

[39]   Shanley F. R., Weight-Strength Analysis of Aircraft Structures, Dover Puplication Inc., New York, 1960

[40]   Schneider W., *A Procedure for Calculating the Weight of Wing Structures with Increased Service Life*, SAWE Paper No. 1021, 33rd Annual Conference of the Society of Allied Weight Engineers (SAWE), 1974

[41]   Torenbeek E., *Development and Application of a Comprehensive, Design-sensitive Weight Prediction Method for Wing Structures of Transport Category Aircraft,* Report LR-693, Delft University of Technology, 1992

[42]   Macci S. H., *Semi-Analytical Method for Predicting Wing Structural Mass,* SAWE Paper No. 2282, 54th Annual Conference of Society of Allied Weight Engineers (SAWE), 1995

[43]   Heinze W., *Ein Beitrag zur quantitativen Analyse der technischen und wirtschaftlichen Auslegungsgrenzen verschiedener Flugzeugkonzepte für den Transport großer Nutzlasten,* ZLR-Forschungsbericht 94-01, 1994

[44]   Koch A. et al., *Studies on the Climate Impact Mitigation Potential of Actual and Future Air Traffic*, 16th Air Transport Research Society (ATRS) World Conference, 2012

[45]   Kelm R., Läpple M., Grabietz M., *Wing Primary Structure Weight Estimation of Transport Aircraft in the Pre-Development Phase*, SAWE Paper No. 2283, 54th Annual Conference of Society of Allied Weight Engineers (SAWE), 1995

[46]   Kelm R., Grabietz M., *Aeroelastic Effects on the Weight of an Aircraft in the Pre-Design Phase*, SAWE Paper No. 2407, 56th Annual Conference of Society of Allied Weight Engineers (SAWE), 1997

[47]   Dugas M., Grabietz M., *Manual for FAME-W Release 4.00 F2*, Technical report, Airbus Deutschland GmbH, 2004

[48]   Dugas M., *Ein Beitrag zur Auslegung von Faserverbundtragflügeln im Vorentwurf*, PhD Thesis, University of Stuttgart, 2002

[49]   Anhalt C., *FAME-W Validation Document*, Technical Report, Airbus Deutschland GmbH, 2004

[50]   Ardema D. et al., *Analytical Fuselage and Wing Weight Estimation of Transport Aircraft*, NASA Technical Memorandum 110392, 1996

[51] Rizzi A., *Modeling and simulation aircraft stability and control – The SimSAC project*, Progress in Aerospace Sciences, Volume 47, Issue 8, p. 573-588, DOI: 10.1016/j.paerosci.2011.08.004, 2011

[52] Cavagna L., Ricci S., Travaglini L., *NeoCASS: An integrated tool for structural sizing, aeroelastic analysis and MDO at conceptual design level*, Progress in Aerospace Sciences, Volume 47, Issue 8, November 2011, Pages 621–635, DOI: 10.1016/j.paerosci.2011.08.006, 2011

[53] Cavagna L., Ricci S., Riccobene L., *Structural Sizing, Aeroelastic Analysis, and Optimization in Aircraft Conceptual Design*, Journal of Aircraft, Vol. 48, No. 6, 2011

[54] Bindolino G. et al., *Multilevel Structural Optimization for Preliminary Wing-Box Weight Estimation*, Journal of Aircraft, Vol. 47, No. 2, 2010

[55] Elham A., La Rocca G., van Tooren M.J.L., *Development and implementation of an advanced, design-sensitive method for wing weight estimation*, Aerospace Science and Technology, DOI: 10.1016/j.ast.2013.01.012, 2013

[56] Dorbath F., Nagel B., Gollnick V., *Comparison of Beam and Shell Theory for Mass Estimation in Preliminary Wing Design*, 2nd Aircraft Structural Design Conference, 2010

[57] Chaput A.J., Rizo-Patron S., *Vehicle Sketch Pad Structural Analysis Module Enhancements for Wing Design*, 50th AIAA Aerospace Sciences Meeting, 2012

[58] Österheld C. M., *Physikalisch begründete Analyseverfahren im integrierten multidisziplinären Flugzeugvorentwurf*, PhD Thesis, TU Braunschweig, 2003

[59] Werner-Westphal C., Heinze W., Horst P., *Structural sizing for an unconventional, environment-friendly aircraft configuration within integrated conceptual design*, Aerospace Science and Technology, 2008

[60] Rieke J., Heinze W., Horst P., *Benchmarking of CFRP Structures in the Preliminary Overall Design of Civil Transport Aircraft*, Deutscher Luft- und Raumfahrtkongress, 2008

[61] Rieke J., *Bewertung von CFK-Strukturen in einem mutlidisziplinären Entwurfsansatz für Verkehrsflugzeuge*, PhD Thesis, TU Braunschweig 2013

[62] Nagel B. et al., *An Alternative Procedure for FE-Wing Modelling*, Deutscher Luft- und Raumfahrtkonkress, 2006

[63] Laban M. et al., *A Computational Design Engine for Multi-Disciplinary Optimization with Application to a Blended Wing Body Configuration*, 9th AIAA/ISSMO Symposium on Multidisciplinary Analysis and Optimization, 2002

[64] Morris A. et al., *MOB – A European project on Multidisciplinary Design Optimization*, 24th International Congress of the Aeronautical Sciences (ICAS), 2004

[65] La Rocca G., van Tooren M. J. L., *Knowledge-Based Engineering Approach to Support Multidisciplinary Design and Optimization*, Journal of Aircraft, Vol. 46, No. 6, 2009

[66] Ledermann C., Ermanni P., Kelm R., *Dynamic CAD objects for structural optimization in preliminary aircraft design*, Aerospace Science and Technology, 2006

[67] Oltmann K. M., *Virtual Engineering Models for Aircraft Structure Weight Estimation*, 66th Annual Conference of Society of Allied Weight Engineers (SAWE), 2007

[68] Klemt T., Oltmann K. M., *Design Optimization in Aircraft Component Pre-Design*, 66th Annual Conference of Society of Allied Weight Engineers (SAWE), 2007

[69] Wenzel J., *Structural Sizing for Weight Estimation in Preliminary Aircraft Design*, 66th Annual Conference of Society of Allied Weight Engineers (SAWE), 2007

[70] Wenzel J., *Massenprognose der Primärsturktur mittels Finite-Elemente Methoden in frühen Phasen der Flugzeugentwicklung*, DLR Forschungsbericht 2010-16, 2010

[71] Hürlimann et al., *Mass estimation of transport aircraft wingbox structures with a CAD/CAE-based multidisciplinary process*, Aerospace Science and Technology, 2011

[72] Bes-Torres J. A., Rudsianto R., Kay E., *An Integrated and Rapid FEM-Based Weight Derivation Approach to Weight Estimation*, 71st Annual Conference of Society of Allied Weight Engineers (SAWE), 2012

[73] Schuhmacher G., Daoud F., Petersson O., *Multidisciplinary Airframe Design Optimization*, 28th International Congress of the Aeronautical Sciences (ICAS), 2012

[74] Dean S., *Aircraft Wing Design and Optimisation at QinetiQ using ModelCenter*, ModelCenter European Users Conference, 2008

[75] Ainsworth et al., *Airframe Wingbox Preliminary Design and Weight Prediction*, Society of Allied Weight Engineers (SAWE), 2010

[76] Funnell M., *Targeting Composite Wing Performance – Optimum Location of Laminate Boundaries*, Altair Engineering CAE Technology Conference, 2007

[77] Sanders K. L., *High-Lift Devices, a Weight and Performance Trade-Off Methodology*, 28th Annual Conference of Society of Allied Weight Engineers (SAWE), 1969

[78] Rudolph, P. K. C., *High-Lift Systems on Commercial Subsonic Airliners*, NASA Contractor Report 4746, 1996

[79] Patterson R. W., *Weight Estimates for Quite/STOL Aircraft*, 33rd Annual Conference of Society of Allied Weight Engineers (SAWE), 1974

[80] Gur O. et al., *Design Optimization of a Truss-Braced-Wing Transonic Transport Aircraft*, J. of Aircraft, Vol. 47, No. 6, 2010, DOI:10.2514/1.47546

[81] Kessler E., Laban M., Vankan W. J., *Multidisciplinary Wing Optimisation*, VIVACE Forum, 2005

[82] Perez R., Jansen P., Martins J., *Aero-Structural Optimization of Non-Planar Lifting Surface Configurations*, 12th AIAA/ISSMO Multidisciplinary Analysis and Optimization Conference, 2008

[83] Jansen P., Perez R., Martins J., *Aerostructural Optimization of Nonplanar Lifting Surfaces*, Journal of Aircraft, Vol. 47, No. 5, 2010, DOI: 10.2514/1.44727

[84] Dugas M., Schroeder K., *FAME-ACSS Documentation (Analytical Calculation of Secondary Wing Structure)*, Internal Report, Airbus Deutschland GmbH, 2004

[85] Dorbath F., van Veen L., Gaida U., *Wing Secondary Structure - Large Civil Jet Transport (MTOM > 40t) - Statistical Mass Estimation*, Luftfahrttechnisches Handbuch, MA 501 22 - 06 A, 2012

[86] van der Laan A. H., van Tooren M. J. L., *Parametric Modeling of Movables for Structural Analysis*, Journal of Aircraft, Vol. 42, No. 6, 2005

[87] van der Lann A. H., *Knowledge based engineering support for aircraft component design*, PhD Study, TU Delft, 2008

[88] Bayandor J. et al., *Parametric optimization of composite shell structures for an aircraft Krueger flap*, Composites Structures, Vol. 57, 2002

[89] Anhalt C., *Steigerung der aerodynamischen Effizienz von Hochauftriebsklappen – Vergleich adaptiver und passive Maßnahmen*, DLR Forschungsbericht 2004-14, 2004

[90] Schuhmacher G. et al., *Multidisciplinary Design Optimization Of A Regional Aircraft Wing Box*, 9th AIAA/ISSMO Symposium on Multidisciplinary Analysis and Optimization, 2002

[91] Nagel B., Kintscher M., Streit T., *Active and Passive Structural Measures for Aeroelastic Winglet Design*, 26th International Congress of the Aeronautical Sciences (ICAS), 2008

[92] Keye S., *Fluid-Structure Coupled Analysis of a Transport Aircraft and Flight-Test Validation*, Journal of Aircraft, Vol. 48, No. 2, 2011

[93] Heinrich R., *Development and Application of TAU–ANSYS Coupling Procedure*, Results of the Closing Symposium of the MEGADESIGN and MegaOpt Projects, Springer–Verlag, New York, 2009

[94] Drela M., Youngren H., *AVL V-3.30 user primer*, MIT Department of Aero & Astronautical Engineering, 2010

[95] White F. M., *Fluid Mechanics*, Seventh Edition in SI Units, Mc Graw Hill, Singapore, 2011, ISBN 978-007-131121-12

[96] Anderson J. D., *Fundamentals of Aerodynamics*, Third Edition, Mc Graw Hill, Singapore, 2001, ISBN 0-07-118146-6

[97] Schnerr G. H., *Gasdynamik*, Scriptum Technische Universität München, 2007

[98] Schnerr G. H., *Fluidmechanik II*, Scriptum Technische Universität München, 2006

[99] Binniger B., *Numerische Simulation von Strömungsvorgängen – 1. Teil*, Scriptum RWTH Aachen, 2012

[100] Karamcheti K., *Principles of Ideal Fluid Aerodynamics*, John Wiley & Sons, Inc., New York, 1966, ISBN: 978-0898741131

[101] Dieker S., Reimerdes H.-G., *Elementare Festigkeitslehre im Leichtbau*, Donat Verlag, 1992, ISBN 3-924444-58-7

[102] Cook R. D. et al., *Concepts and Application of Finite Element Analysis*, 4th edition, John Wiley & Sons. Inc., 2002, ISBN 0-471-35605-0

[103] Wall W. A., Bornemann B., *Finite Elemente*, Scriptum Technische Universität München, 2007

[104] Nagel B., *Methoden des Flugzeugentwurfs II*, Scriptum Technsiche Universität Hamburg-Harburg, 2012

[105] ANSYS® Mechanical APDL Release 13.0, *Theory Reference for the Mechanical APDL and Mechanical Applications*, ANSYS, Inc., 2010

[106] Dvorkin E. N., Bathe K. J., *A Continuum Mechanics Based Four-Node Shell Element for General Nonlinear Analysis*, Engineering Computations, Vol. 1, 1984.

[107] Nagel B. et al., *Communication in Aircraft Design: Can We Establish a Common Language?*, 28th Congress of the International Council of the Aeronautical Sciences (ICAS), 2012

[108] Liersch C., Hepperle M., *A Distributed Toolbox for Multidisciplinary Preliminary Aircraft Design*, CEAS Aeronautical Journal, Vol. 2, Numbers 1-4, 2011

[109] Böhnke D., et al., *An Integrated Method for Determination of the Oswald Factor in a Multi-Fidelity Design Environment*, 3rd CEAS Air & Space Conference, 2011

[110] Cooper D., La Rocca G., *Knowledge-based Techniques for Developing Engineering Applications in the 21st Century*, 7th AIAA ATIO Conference, 2007

[111] La Rocca, G., *Knowledge based engineering: Between AI and CAD. Review of a language based technology to support engineering design*, Advanced Engineering Informatics, Vol. 26, Issue 2, 2012

[112] Verhagen W. J. C. et al., *A critical review of Knowledge-Based Engineering: An identification of research challenges*, Advanced Engineering Informatics, Vol. 26, Issue 1, 2012

[113] Curran R. et al., *A multidisciplinary implementation methodology for knowledge based engineering: KNOMAD*, Expert Systems with Applications, Vol. 37, Issue 11, 2010

[114] MATLAB 7.4.0 (R2007a), The MathWorks Inc., Natick, MA, 2007

[115] Hutchins C., Missoum S., Takahashi T., *Fully Parameterized Wing Model for Preliminary Design*, 13th AIAA/ISSMO Multidisciplinary Analysis Optimization Conference, 2010

[116] Dubovikov E., *Novel Approach and Algorithm for Searching Rational Nonconventional Airframe Concepts of New Generation Aircraft*, 28th Congress of the International Council of the Aeronautical Sciences (ICAS), 2012

[117] Klatt F., *Erstellung eines Finite Elemente Fahrwerksersatzmodells*, Student Thesis, TU Hamburg-Harburg, 2012

[118] Deutsches Zentrum für Luft- und Raumfahrt (DLR), *CPACS 2.0 Documentation*, 2012, download: http://code.google.com/p/cpacs/

[119] Deinert S., Petersson Ö., Daoud F., Baier H., *Aircraft Loft Optimization With Respect to Aeroelastic Lift and Induced Drag Loads*, 10th World Congress on Structural and Multidisciplinary Optimization, 2013

[120] La Rocca G., Langen T. H. M., Brouwers Y. H. A., *The Design and Engineering Engine. Towards a Modular System for Collaborative Aircraft Design*, 28th Congress of the International Council of the Aeronautical Sciences (ICAS), 2012

[121] Rizze A., et al., *Towards a Unified Framework using CPACS for Geometry Management in Aircraft Design*, 50th AIAA Aerospace Sciences Meeting, 2012

[122] Thielecke F., *Vorlesung Flugzeugsysteme I – Teil 3a Hochauftriebssysteme*, Lecture Notes, TU Hamburg-Harburg, 2007

[123] Staub A., Damage Modelling of Integral Composite Flaps under Bird Strike, DLR Internal Report, DLR - IB 435 - 2012/24, 2012

[124] Holert B., *Eine Methode zum mehrkriteriellen Entwurf der Führungsmechanismen in Hochauftriebssystemen von Transportflugzeugen*, PhD Thesis, TU Hamburg-Harburg, 2006

[125] Pletschacher P., *Technologien für niedrigere Kosten*, Luft- und Raumfahrt, Heft 4, 2009

[126] Niu M. C.-Y., *Airframe Structural Design – Practical Design Information and Data on Aircraft Structures*, Conmilit Press LTD., 1995, ISBN 962-7128-04-X

[127] *www.attach.high-g.net*, downloaded on 2011/07/04

[128] Klatt F., *Erstellung eines Finite Elemente Fahrwerksersatzmodells*, DLR Internal Report, IB-328-2012-16, 2012

[129] Moerland E., *Development of an aeroelastic analysis tool for structural sizing of high-lift devices during preliminary design*, Master Thesis, TU Delft, 2011

[130] Werner-Spatz C., *Flugzeuggesamtentwurf mit Zirkulationskontrolle am Hochauftriebssystem*, PhD Thesis, TU Braunschweig, 2010

[131] Werner-Spatz C., Heinze W., Horst P., *Improved Representation of High-Lift Devices for a Multidisciplinary Conceptual Aircraft Design Process*, Journal of Aircraft, Vol. 46, No. 6, 2009

[132] von Mises R., *Mechanik der festen Körper im plastisch-deformablen Zustand*, Nachrichten von der Gesellschaft der Wissenschaften zu Göttingen, p 582-592, 1913

[133] Gürdal Z., Haftka R., Hajela P., *Design and Optimization of Laminated Composite Materials*, John Wilex & Sons. Inc, ISBN 0-471-25276-X, 1999

[134] Puck A., *Festigkeitsanalyse von Faser-Matrix-Laminaten – Modelle für die Praxis*, Carl Hanser Verlag, München, ISBN 3-446-18194-6, 1996

[135] Bruhn E.F., *Analysis & Design of Flight Vehicle Structures*, Jacobs Publishing Inc., 1973

[136] Ramberg W., Osgood W. R., *Description of Stress-Strain Curves by Three Parameters*, NACA Technical Note No. 902, 1943

[137] *Metallic Materials and Elements for Aerospace Vehicles Structures*, Military Handbook MIL-HDBK-5H, Department of Defense, United States of America, 1998

[138] Hill H. N., *Determination of Stress-Strain Relations from "Offset" Yield Strength Values*, NACA Technical Note No. 927, 1944

[139] *Luftfahrt-Technisches Handbuch; HSB – Handbuch Struktur Berechnung,* Industrieausschuss Strukturberechnungsunterlage, PDF Handbook Version 1.0.0, 2009

[140] Carl U., Holert B., *Rechnerunterstütze Synthese von Klappenführungsmechanismen – TEFLAMES*, Technische Universität Hamburg Harburg, Projektbericht Nr.: 04-158, v. 1.08, 2005

[141] Rajeswari B., Dutt H. N. V., *Analysis of Wing Flap Configurations by a Nonplanar Vortex Lattice Method*, Journal of Aircraft, Vol. 25, No. 2, 1988

[142] Heilmann L., *Nutzung eines einfachen aerodynamischen Verfahrens zur Modellierung von Hochauftriebssystemen im Flugzeugvorentwurf*, Bachelor Thesis, TU Berlin, 2011

[143] Dargel, G., Hansen, H., Wild, J., Streit, T., Rosemann, H., *Aerodynamische flügelauslegung mit multifunktionalen steuerflächen (aerodynamic design of wings with multifunctional control devices)*, DGLR Jahrbuch 2002, DGLR-2002-096, Vol I, DGLR, 2002.

[144] Hövelmann A., *Aerodynamic Investigations of Noise-Reducing High-Lift Systems for Passenger Transport Aircraft*, Diploma Thesis, TU München, 2011

[145] Pincha P. J., *Algorithmic Mass-Factoring of Finite Element Model Analyses*, 41st Annual Conference of Society of Allied Weight Engineers (SAWE), 1982

[146] *A320 - Airplane Characteristics*, Airbus S.A.S., Customer Service, Technical Data and Services, Blagnac, France, 2010

[147] *A340-200/-300 - Airplane Characteristics*, Airbus S.A.S., Customer Service, Technical Data and Services, Blagnac, France, 2010

[148] Seider D., Fischer P.M., Litz M., Schreiber A., Gerndt A., *Open Source Software Framework for Applications in Aeronautics and Space*, IEEE Aerospace Conference, 2012

[149] Böhnke D., Nagel B., Gollnick V., *An Approach to Multi-fidelity in Conceptual Aircraft Design in Distributed Design Environments*, IEEE Aerospace Conference, 2011

[150] Roskam J., *Airplane Design – Part VI: Preliminary Calculation of Aerodynamic, Thrust and Power Characteristics*, DARcorporation, ISBN: 1-884885-52-7, 2004

[151] Scherer J., Kohlgrüber D., Dorbath F., Sorour M., *A Finite Element Based Tool Chain for Structural Sizing of Transport Aircraft in Preliminary Aircraft Design*, 62. Deutscher Luft- und Raumfahrtkongress, 2013

[152] Zill T., Ciampa P.D., Nagel B., *Multidisciplinary Design Optimization in a Collaborative Distributed Aircraft Design System*, 50th AIAA Aerospace Sciences Meeting including the New Horizons Forum and Aerospace Exposition, AIAA 2012-0553, 2012